Scuola di Dottorato in Scienze di base "Galileo Galilei"
Dottorato di Ricerca in Fisica

Graduate Course in Physics
University of Pisa

The School of Graduate Studies in Basic Siences "GALILEO GALILEI"

PhD Thesis

Aspects of LHC phenomenology

Candidate:
Pier Paolo Giardino

Supervisor:
prof. Alessandro Strumia

2013

Contents

Introduction

Identifying the mechanism of the electroweak symmetry breaking is one of the main goal of the Large Hadron Collider. In the Standard Model the electroweak symmetry is broken due to the existence of an elementary scalar particle: the Higgs boson.

The Higgs boson was for a long time the missing piece of the Standard Model puzzle. Furthermore in the absence of direct signal of new physics, the Higgs boson couplings might indirectly indicate a portal to Beyond Standard Model theories. In this context, the discovery made at LHC of a new particle with a mass of 125.66 ± 0.34 GeV and the characteristics of the Higgs boson is of great importance: it could be the conclusive achievement of the Standard Model, or it could give a renewed impulse to the search for new physics. The discovery of this new particle was announced by the ATLAS and CMS collaborations during 2012. After that, all LHC and TeVatron collaborations presented at the Moriond 2013 conference the results based on the full collected data.

First of all, one must make sure that the new resonance is, indeed, the Higgs boson that induces the electroweak symmetry breaking and gives masses to both the SM vector bosons and to fermions. The SM has definite predictions for the gauge boson and fermion couplings with the Higgs boson. Those affect both the Higgs boson production mechanism at the LHC as well as its dominant decay modes. Fortunately for a Higgs boson mass of 125.5 GeV the LHC experiments do have sensitivity to test these couplings in all interesting final states $\gamma\gamma$, ZZ^*, WW^*, $b\bar{b}$ and $\tau\bar{\tau}$, taking into account different Higgs boson productions mechanisms.

Therefore, it is possible to thoroughly examine the couplings of this particle to the other SM particles. If those were incompatible with the ones the SM predicts, the amount of the deviation could give us hints of what kind of new physics we should expect and its scale of energy and it could outline a convenient line of research. This possibility is motivated by numerous multi-Higgs, supersymmetric, composite Higgs, dark matter, exotic scalar, etc. models. Otherwise, if the new particle is indeed the Standard Model Higgs, although that would not exclude the possibilities for new physics, we should try explaining fundamental topics (like naturalness or vacuum stability) only in terms of the SM.

Higgs couplings

Motivated by this, we have performed a state-of-the-art global fit to Higgs boson data, including all sub-categories studied by the experimental collaborations.

As pointed out in chapter 1 $m_h \approx 125$ GeV is a particularly fortunate value for the LHC since various Higgs boson search channels are measurable. This gave us the opportunity to study several new physics scenarios beyond the SM: new scalars, 2HDM, supersymmetry, dilaton, composite Higgs, invisible Higgs decays, possibly into Dark Matter particles, anomalous couplings of the top, etc.

We determined from data the production cross sections (assuming standard Higgs decays) and the Higgs decays widths (assuming standard productions), finding that they lie along the SM predictions. In a more general context, we allowed the Higgs boson gauge and Yukawa couplings to be free param-

eters and accordingly modify the Higgs tree level couplings hWW, hZZ, $hf\bar{f}$ as well as the loop level processes such as the Higgs production in gluon-gluon fusion $gg \to h$ and Higgs decays to $h \to \gamma\gamma, gg$. We also allow for an invisible branching fraction.

While our fits are in general model independent, we demonstrate usefulness of our results for constraining new physics beyond the SM using some well known models as examples. These examples show that in the present stage of accuracy the LHC data constrains models severely. Qualitatively all the studies reach the same conclusion, that the best fit regions lie along SM predictions, supporting the SM Higgs boson hypothesis.

Electro-weak potential stability

Thus, although the discovery of the Higgs boson was expected to be the herald of new physics soon to be found at the TeV scale, so far no signal of new physics nor any clear deviation from the SM Higgs properties have been detected at the LHC. Moreover, the Higgs mass has not provided unambiguous indications for new physics. The measured value $M_h = 125.66 \pm 0.34$ GeV is a bit high for supersymmetry and a bit low for composite models, making theoretical interpretations rather uncomfortable. Neither option is unequivocally preferred, although neither option is excluded.

In any case, the measurement of the Higgs mass M_h has determined the last unknown parameter of the SM, fixing the Higgs quartic coupling λ. Thus we can try is to extrapolate λ to high energy in search for clues. Indeed, $M_h = 125.66 \pm 0.34$ GeV lies well within the parameter window in which the SM can be extrapolated all the way up to the Planck mass $M_{\rm Pl}$, with no problem of consistency other than remaining in the dark about naturalness. Just as high-energy extrapolations of the gauge coupling constants gave us hints about a possible grand unification of fundamental forces, so the extrapolation of λ has revealed an unexpected feature of the SM that opens new avenues for theoretical speculation. The intriguing result is that, assuming the validity of the SM up to very high energy scales, the measured value of M_h is near-critical, in the sense that it places the EW vacuum right at the border between absolute stability and metastability.

The critical condition for stability is defined as the vanishing of the effective coupling $\lambda_{\rm eff}$, see equation 2.11, at some energy scale Λ_I. We find $\Lambda_I = 10^{10}$–10^{12} GeV, see equation 2.15, suggesting that the instability is reached well below the Planck mass. The presence of an instability at an intermediate scale could be interpreted as a sign of a new-physics threshold around Λ_I. It is suggestive that neutrino masses, axion, and inflation give independent indications for new dynamics at roughly similar energy scales. The hypothetical new physics could be responsible for a matching condition $\lambda \approx 0$ at a scale near Λ_I. The vanishing of λ could be the result of special dynamics occurring above Λ_I.

Another peculiarity found in the extrapolation of λ is its slow running at high energy. This is due to a combination of two factors: the reduction of all SM couplings at high energy and an accidental zero of β_λ at a scale of about 10^{17}–10^{18} GeV. It is the slow running of λ at high energy that saves the EW vacuum from premature collapse, in a situation where $\Lambda_I \ll M_{\rm Pl}$. Were β_λ large and negative above Λ_I, we could not live with an instability scale much smaller than the cutoff scale, without being confronted with early vacuum decay. Unfortunately, for the moment we have no way to tell whether this special condition allowing for a prolonged vacuum lifetime is just a numerical coincidence or an important feature of the SM.

At any rate, the smallness of β_λ at high energy makes it possible to assume that there is no new-physics threshold around Λ_I and that the SM continues to be valid up to the quantum-gravity scale, since the tunnelling probability remains small. In this context, the value of $\lambda(M_{\rm Pl})$ may be regarded

as 'normal' for a SM coupling. Indeed, as discussed in section 2.2.1, the ratios $\sqrt{4|\lambda|}/y_t$ and $\sqrt{8|\lambda|}/g_2$ (which, at low energy, correspond to M_h/M_t and M_h/M_W, respectively) are of order unity both at the Fermi and Planck scales. The vanishing of λ at an intermediate scale could then be purely accidental. After all, the Higgs quartic is the only SM coupling that can cross zero during its RG evolution, since $\lambda = 0$ is not a point of enhanced symmetry.

So, in the context of the SM, the measured value of M_h is special because it corresponds to a near-critical situation in which the Higgs vacuum does not reside in the configuration of minimal energy, but in a metastable state close to a phase transition.

It is possible that this condition of near-criticality of the SM vacuum is the most important message we have learnt so far from experimental data on the Higgs boson. Near-criticality gives us a unique opportunity to obtain information about physics taking place at energy scales well beyond the reach of any collider experiment. Its consequences are so intriguing and potentially so revolutionary that they deserve accurate calculations and dedicated studies.

Chapters 2 ad 3 are dedicated to continue the programme of investigating the status and implications of near-criticality. In particular in chapter 2 we explore the significance of near-criticality in terms of high-energy SM parameters, while in chapter 3 we improve the calculation of the large-field extrapolation of the Higgs potential and of the critical value of M_h for absolute stability.

SM parameters at NNLO

The main new calculations presented here are the results for the $\overline{\text{MS}}$ quartic Higgs coupling $\lambda(\bar{\mu})$ and the top Yukawa coupling $y_t(\bar{\mu})$ at NNLO precision (two loops) in terms of physical observables: the pole masses of the Higgs (M_h), of the top (M_t), of the Z (M_Z), of the W (M_W), the $\overline{\text{MS}}$ strong coupling $\alpha_3(M_Z)$, and the Fermi constant G_μ. We improve the previous studies where 2-loop threshold corrections to $\lambda(\bar{\mu})$ had been computed in the limit of vanishing weak gauge couplings, and 2-loop electroweak threshold corrections to $y_t(\bar{\mu})$ had been neglected. As a byproduct of our two-loop calculation of $\lambda(\bar{\mu})$ we also obtain the $\overline{\text{MS}}$ quadratic Higgs coupling $m^2(\bar{\mu})$ at the NNLO level.

Recently, many authors have contributed towards the completion of the calculation of the renormalisation-group (RG) evolution (β-functions and thresholds) of the sizeable SM couplings at NNLO precision. Our new calculation of threshold corrections, together with these results, allows us to refine the determination of the critical value of M_h that ensures absolute vacuum stability within the Standard Model (SM) up to the Planck scale. Furthermore, our precision extrapolation of the SM to high energy scales is relevant for testing any new physics scenario able of making predictions, such as unification of gauge couplings constants, or high-scale supersymmetric models that restrict or predict the quartic Higgs coupling.

Large Extra Dimensions

In any case, although the data seem point to a standard Higgs and we did not find any proof of new physics, we can not exclude the existence of some not standard physics at energies reachable at LHC. An intriguing possibilities is that of Larger Extra Dimensions.

Since the start of the LHC program, experiments have tested directly some of the theoretical ideas about new physics at the electroweak scale. In one popular scenario, which will be considered here, Standard Model fields are confined on a 3-dimensional brane, while gravity propagates in the full D-dimensional space, with δ flat and compactified extra spatial dimensions ($D = 4+\delta$). This scenario

allows for quantum gravity at the weak scale and could therefore be a solution to the Higgs mass hierarchy problem.

Chapter 4 is dedicated to the study of theories of this kind. In particular we will see how we can use the LHC data in order to test Large Extra Dimensions.

Chapter 1

Higgs boson at LHC

As stated in the introduction the discovery of a new particle at LHC could have enormous consequences. We are interested in knowing if this particle is the long-waited Standard Model (SM) Higgs boson [1–4]. On one side, the experimental collaborations are measuring its discrete quantum numbers to check if it is a scalar. On the other side, various theoretical groups [5–7] started to approximatively reconstruct from data its production cross section and its decay modes and consequently its couplings to check if they agree with the SM predictions or with other models beyond the SM. Clearly, this is a more significant test that can be precisely done only by the experimental collaborations, which indeed started to present analyses along these lines.

Accidentally, $m_h \approx 126$ GeV is a particularly fortunate value for the LHC, because, according to the SM predictions, various Higgs boson search channels are measurable.

There are four main production modes for Higgs boson from pp collisions at $\sqrt{s} \sim 8$ TeV. The gluon-gluon fusion production mode has the largest cross section, followed in turn by vector boson fusion (VBF), associated Wh and Zh production, and production in association with top quarks, $t\bar{t}h$. The cross sections for the Higgs boson production modes and the decay branching fractions, together with their uncertainties, are taken from [8].

Because different search categories are sensitive to different Higgs boson couplings, the LHC can study the properties of a Higgs boson with $m_h \approx 126\,\text{GeV}$ and test if it follows the SM predictions or is affected by new physics.

Here we present the "universal fit" analysis introduced in [9]. The main feature of this "universal fitting" procedure is the assumtion that new physics can be approximated as a first-order perturbation with respect to the SM predictions. This assumption is increasingly supported by data, that agree with the SM with precisions around the 20% level.

Such results, obtained after two years of LHC operation and with only 25/fb data per experiment, implies severe constraints on models where the Higgs boson is a portal to new physics. We analyse several models and rule out alternative scenarios to the Higgs boson.

In section (1.1) we present the data and the fitting procedure. In section (1.2) we present the characteristics of the "universal fit". In section (1.4) we derive the first measurement of the Higgs mass from the rates, rather than from the position of the peaks in the $\gamma\gamma$ and ZZ invariant mass distributions. Next, in section (1.5) we present fits in various specific models, updating our previous results and comparing the full fit to the simplified 'universal' fit to verify that it is a good approximation. We fit Higgs cross sections in section (1.5.1), Higgs couplings in (1.5.2), composite Higgs models in (1.5.3), new physics in loops in (1.5.4), two Higgs doublet models in (1.5.5), the MSSM in (1.5.6), the dilaton in (1.5.7), the Higgs invisible width in (1.5.8) and models where DM couples to the Higgs in (1.5.9).

1.1 The data

Searches for the SM Higgs boson have been carried out in proton-proton collisions at $\sqrt{s} = 7$ (2011 data) and 8 TeV (2012 data) with about 25/fb of total integrated luminosity.

Our updated analysis uses the new data presented at the Moriond 2013 conference by the CMS, ATLAS and TeVatron collaborations [10–13] in the following five decay modes: $\gamma\gamma$ [14], ZZ^* (followed by ZZ^* decays to $4\ell, 2\ell 2\nu, 2\ell 2q, 2\ell 2\tau$) [15], WW^* (followed by WW^* decays to $\ell\nu\ell\nu, \ell\nu qq$) [11, 16], $\tau^+\tau^-$ (followed by leptonic and hadronic decays of the τ-leptons) [17] and $b\bar{b}$ [18] (the ATLAS $b\bar{b}$ result was updated at the EPS HEP 2013 [19]), and the first tentative measurements in the $\mu^+\mu^-$ [20], $Z\gamma$ [21] and WWW [22] channels, as well as their combination [23]. Here and throughout, ℓ stands for electrons or muons and q for quarks.

For a given Higgs boson mass, the search sensitivity depends on the production cross section of the Higgs boson, its decay branching fraction into the chosen final state, the signal selection efficiency, the mass resolution, and the level of standard model backgrounds in the same or a similar final state. For low values of the Higgs boson mass, the $h \to \gamma\gamma$ and $h \to ZZ^* \to 4\ell$ channels play a special role due to the excellent mass resolution for the reconstructed diphoton and four-lepton final states, respectively. The $h \to WW^* \to \ell\nu\ell\nu$ channel provides high sensitivity but has relatively poor mass resolution due to the presence of neutrinos in the final state. The sensitivity in the $b\bar{b}$ and $\tau^+\tau^-$ decay modes is reduced due to the large backgrounds and poor mass resolutions.

We include in our data-set all exclusive $\gamma\gamma$ and $\tau\tau$ sub-categories described by the experimental collaborations by telling how much each Higgs production channel in the SM contributes to the various rates. Such information is fully included in our analysis. We adopt the MultiVariate Analysis (MVA) $\gamma\gamma$ analysis from CMS and we combine all experiments, such that we find an average $\gamma\gamma$ rate very close to the SM prediction. Consequently our results differ from previous analyses performed without including the latest CMS $\gamma\gamma$ data [5].

This is an important issue because, while most of the presented LHC results are well consistent with the SM predictions within experimental errors, there are few unexpected new developments that need commenting. The most important of them is the discrepancy between the ATLAS and CMS results in the $h \to \gamma\gamma$ channels. With full luminosity, ATLAS finds an overall rate of 1.65 ± 0.34, higher than the SM prediction of 1, and higher than the CMS result of 0.80 ± 0.30. The two measurements are compatible within 2σ. In addition, the two CMS $\gamma\gamma$ analyses (MVA and cut based) show different signal rates. Finally, the two Higgs boson mass determinations in ATLAS, from the peaks in the $\gamma\gamma$ and ZZ channels, differ by 2σ. Both experiments have cross checked their analyses and reached conclusions that those deviations are due to statistical fluctuations of both signal and background. This conclusion implies that: (i) combining all data in a global fit is meaningful and increases the precision; (ii) selecting instead any single measurement, for example the ATLAS excess in $\gamma\gamma$, is not justified and introduces a bias in the data.

The experimental collaborations report Higgs boson rates R in units of the central value of the SM prediction. Their results could be fully encoded in a likelihood $\mathcal{L}(R, M_h)$, but only a limited amount of information is reported by the experiments. Often the experimental collaborations report the measured rates as $R^{\rm exp} \pm R^{\rm err}$: we use the results in this form whenever available. Sometimes collaborations only report the upper bounds on rates at 95% C.L., $R^{\rm limit}_{\rm observed}$, and the expected upper bound at 95% C.L. in absence of a Higgs boson signal, $R^{\rm limit}_{\rm expected}$, as function of the Higgs boson mass m_h. Assuming that the $\chi^2 = -2\ln\mathcal{L}$ has a Gaussian form in R, these two experimental informations allow one to extract the mean $R^{\rm exp}$ and the standard deviation $R^{\rm err}$ as $R^{\rm exp} = R^{\rm limit}_{\rm observed} - R^{\rm limit}_{\rm expected}$ and $R^{\rm err} = R^{\rm limit}_{\rm expected}/1.96$, where 1.96 arises because 95% confidence level corresponds to about 2 standard

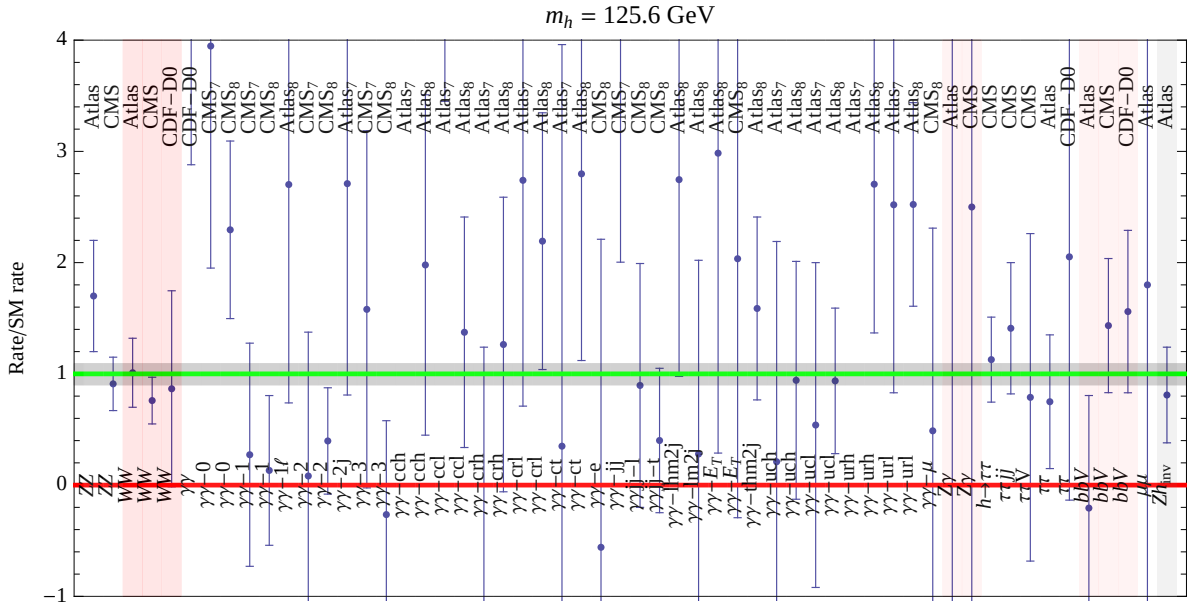

Figure 1.1: *Measured Higgs boson rates at ATLAS, CMS, CDF, D0 and their average (horizontal gray band at $\pm 1\sigma$). Here 0 (red line) corresponds to no Higgs boson, 1 (green line) to the SM Higgs boson (including the latest data point, which describes the invisible Higgs rate).*

deviations [6].[1] The χ^2 is approximated as

$$\chi^2 = \sum_I \frac{(R_I^{\rm exp} - 1)^2}{(R_I^{\rm err})^2}, \tag{1.1}$$

where the sum runs over all measured Higgs boson rates I.

The theoretical uncertainties on the Higgs production cross sections σ_j start to be non-negligible and affect the observed rates in a correlated way. We take into account such correlations in the following way. We subtract from the total uncertainty $R_I^{\rm err}$ the theoretical component due to the uncertainty in the production cross sections, obtaining the purely experimental uncertainty, $R_I^{\rm err-exp}$. The theoretical error is reinserted by defining a χ^2 which depends on the production cross sections σ_j,

$$\chi^2 = \sum_I \frac{(R_I^{\rm exp} - R_I^{\rm th}(\sigma_j))^2}{(R_I^{\rm err-exp})^2} + \sum_j \frac{(\sigma_j - \sigma_j^{\rm th})^2}{(\sigma_j^{\rm err})^2}, \tag{1.2}$$

and marginalising it with respect to the free parameters σ_j, constrained to have a central value $\sigma_j^{\rm th}$ and an uncertainty $\sigma_j^{\rm err}$ given by

$$\begin{aligned}
&\sigma(pp \to h)_{\rm th} = (19.4 \pm 2.8)\,{\rm pb}, && \sigma(pp \to jjh)_{\rm th} = (1.55 \pm 0.04)\,{\rm pb},\\
&\sigma(pp \to Wh)_{\rm th} = (0.68 \pm 0.03)\,{\rm pb}, && \sigma(pp \to Zh)_{\rm th} = (0.39 \pm 0.02)\,{\rm pb},\\
&\sigma(pp \to t\bar{t}h)_{\rm th} = (0.128 \pm 0.018)\,{\rm pb} && \text{at } \sqrt{s} = 8\,{\rm TeV}.
\end{aligned} \tag{1.3}$$

See also [24]. We neglect the relatively small uncertainties on the SM theoretical predictions for Higgs branching ratios, dominated by a 4% uncertainty on the $h \to b\bar{b}$ width.

[1] A similar procedure was described by Azatov et al. in [5].

We summarise all data in fig. 1.1 together with their 1σ error-bars. The grey band shows the $\pm 1\sigma$ range for the naive weighted average of all rates: 0.98 ± 0.10. It lies along the SM prediction of 1 (horizontal green line) and is almost 10 σ away from 0 (the horizontal red line is the background-only rate expected in the absence of a Higgs boson).

1.2 The universal Higgs fit

We perform the most generic fit in terms of a particle h with couplings to pairs of $t, b, \tau, W, Z, g, \gamma$ equal to $r_t, r_b, r_\tau, r_W, r_Z, r_g, r_\gamma$ in units of the SM Higgs coupling. This means, for example, that the coupling to the top is given by $r_t(m_t/V)h\bar{t}t$, where $r_t = 1$ in the SM and $V = 246\,\text{GeV}$ is the Higgs vacuum expectation value. Similarly, the $h\gamma\gamma$ coupling is assumed to be r_γ times its SM prediction. In the SM this couplings first arises at one loop level. Experiments are starting to probe also the $h\bar{\mu}\mu$ and the $hZ\gamma$ effective couplings, so that also the corresponding r_μ and $r_{Z\gamma}$ parameters will start to be measured. This discussion can be summarized by the following effective Lagrangian:

$$\begin{aligned}\mathscr{L}_h \;=\; & r_t \frac{m_t}{V} h\bar{t}t + r_b \frac{m_b}{V} h\bar{b}b + r_\tau \frac{m_\tau}{V} h\bar{\tau}\tau + r_\mu \frac{m_\tau}{V} h\bar{\mu}\mu + r_Z \frac{M_Z^2}{V} h Z_\mu^2 + r_W \frac{2M_W^2}{V} h W_\mu^+ W_\mu^- + \\ & + r_\gamma c_{\text{SM}}^{\gamma\gamma} \frac{\alpha}{\pi V} h F_{\mu\nu} F_{\mu\nu} + r_g c_{\text{SM}}^{gg} \frac{\alpha_s}{12\pi V} h G^a_{\mu\nu} G^a_{\mu\nu} + r_{Z\gamma} c_{\text{SM}}^{Z\gamma} \frac{\alpha}{\pi V} h F_{\mu\nu} Z_{\mu\nu}. \end{aligned} \tag{1.4}$$

The various SM loop coefficients c_{SM} are summarised in appendix 1.A.1. This Lagrangian is often written in a less intuitive but practically equivalent form by either using $\text{SU}(2)_L \otimes \text{U}(1)_Y$-invariant effective operators, or assuming that the Higgs is the pseudo-Goldstone boson of a spontaneously broken global symmetry and writing its chiral effective theory [5]. We do not consider a modified Higgs coupling to charm quarks, given that $h \to c\bar{c}$ decays at LHC are hidden by the QCD background. While we cannot exclude that new physics affects $h \to c\bar{c}$ much more than all other Higgs properties, for simplicity we proceed by discarding this possibility.

Furthermore, we take into account the possibility of Higgs decays into invisible particles X (such as Dark Matter or neutrinos [27]) with branching ratio BR_{inv}. In almost all measured rates BR_{inv} is equivalent to a common reduction r of all the other Higgs couplings, $\text{BR}_{\text{inv}} \simeq 1 - r^2$, such that BR_{inv} is indirectly probed by data [6]. The only observable that directly probes an invisible Higgs width is the $pp \to Zh \to \ell^+\ell^-\, \bar{X}X$ rate measured by ATLAS [28], which implies

$$\text{BR}_{\text{inv}} = -0.19 \pm 0.43. \tag{1.5}$$

Any possible new-physics model can be described as specific values of the r_i parameters. Several examples are provided in section 1.5.

Following the procedure described in the previous section, we approximatively extract from data the function

$$\chi^2(r_t, r_b, r_\tau, r_W, r_Z, r_g, r_\gamma, r_{Z\gamma}, r_\mu, \text{BR}_{\text{inv}}), \tag{1.6}$$

which describes all the information contained in Higgs data. We find $\chi^2 = 58.8$ at the best fit (56 data points, 10 free parameters), marginally better than the SM fit, $\chi^2_{\text{SM}} = 61.7$ (no free parameters).

1.3 Universal fit to small new physics effects

The universal χ^2 of equation (1.6) has a too complicated form to be reported analytically, and depends on too many variables to be reported in numerical form, like plots or tables. For these reasons, previous

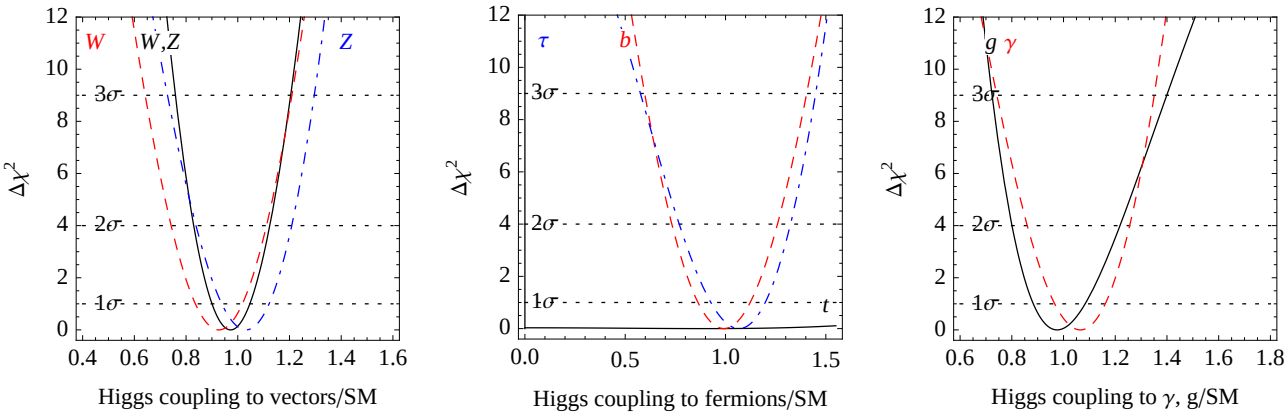

Figure 1.2: χ^2 *as function of the model-independent Higgs couplings* r_i *to the various SM particles, varying them one-by-one.*

analyses [5–7] focused on particular BSM models with a reduced number of parameters. For example, fig. 1.2 shows the fit as function of each r_i, setting all others to their SM values of unity: we see that the χ^2 are approximately parabolic.

We here observe that Higgs data are converging towards the SM predictions with small errors, thereby it is time to start making the approximation

$$r_i = 1 + \epsilon_i \qquad \text{with} \qquad \epsilon_i \ll 1 \tag{1.7}$$

and $\text{BR}_{\text{inv}} = \epsilon_{\text{inv}}$. The observable rates R_I are computed at first order in ϵ_i, and consequently the χ^2 is expanded up to second order in ϵ_i. As well known, this Gaussian approximation is a great simplification; for example marginalisations over nuisance parameters just becomes minimisation, which preserves the Gaussian form. Fig. 1.2 suggests that this approximation already seems reasonably good.

For LHC at 8 TeV the main observables are approximated as

$$\begin{aligned}
R_{h\to WW} &= 1 - 1.14\epsilon_b + 1.58\epsilon_g - \epsilon_{\text{inv}} - 0.04\epsilon_t + 1.72\epsilon_W + 0.02\epsilon_Z - 0.13\epsilon_\tau \\
R_{h\to ZZ} &= 1 - 1.14\epsilon_b + 1.58\epsilon_g - \epsilon_{\text{inv}} - 0.04\epsilon_t - 0.28\epsilon_W + 2.02\epsilon_Z - 0.13\epsilon_\tau \\
R_{h\to\tau\tau} &= 1 - 1.14\epsilon_b + 1.58\epsilon_g - \epsilon_{\text{inv}} - 0.04\epsilon_t - 0.28\epsilon_W + 0.02\epsilon_Z + 1.87\epsilon_\tau \\
R_{h\to\gamma\gamma} &= 1 - 1.14\epsilon_b + 1.58\epsilon_g - \epsilon_{\text{inv}} - 0.04\epsilon_t - 0.45\epsilon_W - 0.06\epsilon_Z - 0.13\epsilon_\tau + 2\epsilon_\gamma \\
R_{h\to bb} &= 1 + 0.86\epsilon_b + 1.58\epsilon_g - \epsilon_{\text{inv}} - 0.04\epsilon_t - 0.28\epsilon_W + 0.02\epsilon_Z - 0.13\epsilon_\tau \\
R_{V(h\to bb)} &= 1 + 0.86\epsilon_b - 0.17\epsilon_g - \epsilon_{\text{inv}} - 0.05\epsilon_t + 0.83\epsilon_W + 0.67\epsilon_Z - 0.13\epsilon_\tau,
\end{aligned} \tag{1.8}$$

where these expressions have been obtained by performing a first-order Taylor expansion in all the ϵ parameters of the full non-linear expressions. For all observables but the last one, we have assumed the total Higgs production cross section. When fitting the many real observables, we take into account the relative contribution of each production cross section, as determined by experimental cuts. The full χ^2 can now be reported in a simple form. Indeed the χ^2 is a quadratic function of the ϵ_i, and it is usually written as

$$\chi^2 = \sum_{i,j} (\epsilon_i - \mu_i)(\sigma^2)^{-1}_{ij}(\epsilon_j - \mu_j), \qquad \text{where} \qquad (\sigma^2)_{ij} = \sigma_i \rho_{ij} \sigma_j \tag{1.9}$$

Process X	$h \to WW$	$h \to ZZ$	$h \to \gamma\gamma$	$Vh \to Vbb$	$h \to \tau\tau$
Sensitivity c_X	6.4%/ GeV	7.8%/ GeV	−1.5%/ GeV	−5.4%/ GeV	−4.1%/ GeV
Measured rate/SM	0.82 ± 0.16	1.08 ± 0.20	1.07 ± 0.19	0.93 ± 0.36	1.13 ± 0.28
Higgs mass in GeV	122.8 ± 2.5	126.5 ± 2.5	121 ± 12	127 ± 7	123 ± 7

Table 1.1: *Determinations of the Higgs mass from the measured Higgs rates, assuming the SM predictions for such rates. We do not use here the independent determination of the Higgs mass from the peak positions in the $\gamma\gamma$ and ZZ energy spectra.*

in terms of the mean values μ_i of each parameter ϵ_i, of its error σ_i and in terms of the correlation matrix ρ_{ij}. We believe that this is the most useful form in which experimental collaborations could report their results. From our approximated analysis of LHC and TeVatron [13] data we obtain:

$$\begin{array}{rcl} \epsilon_b &=& -0.23 \pm 0.31 \\ \epsilon_g &=& -0.25 \pm 0.25 \\ \epsilon_{\rm inv} &=& -0.20 \pm 0.26 \\ \epsilon_W &=& -0.14 \pm 0.14 \\ \epsilon_Z &=& +0.00 \pm 0.13 \\ \epsilon_\gamma &=& -0.02 \pm 0.16 \\ \epsilon_\tau &=& +0.00 \pm 0.19 \end{array} \qquad \rho = \begin{pmatrix} 1 & 0.75 & 0.17 & 0.45 & 0.39 & 0.53 & 0.45 \\ 0.75 & 1 & 0.52 & 0.32 & 0.19 & 0.39 & 0.32 \\ 0.17 & 0.52 & 1 & 0.55 & 0.41 & 0.51 & 0.40 \\ 0.45 & 0.32 & 0.55 & 1 & 0.67 & 0.69 & 0.60 \\ 0.39 & 0.19 & 0.41 & 0.67 & 1 & 0.60 & 0.54 \\ 0.53 & 0.39 & 0.51 & 0.69 & 0.60 & 1 & 0.58 \\ 0.45 & 0.32 & 0.40 & 0.60 & 0.54 & 0.58 & 1 \end{pmatrix} \tag{1.10}$$

We have not reported the central value of $r_t = 1 + \epsilon_t$, of $\epsilon_{Z\gamma}$ and of ϵ_μ because they presently are known only up to uncertainties much larger than 1. Future searches for $t\bar{t}h$ production, for $h \to Z\gamma$ and for $h \to \mu^+\mu^-$ will improve the situation.

In many models the Higgs couplings to vectors satisfy $\epsilon_W = \epsilon_Z$, because of $\mathrm{SU}(2)_L$ invariance. Furthermore, in many models LEP precision data force ϵ_W and ϵ_Z to be very close to 0. This restriction can of course be implemented by just setting these parameters to be equal or vanishing in the quadratic χ^2.

Since the uncertainties on the ϵ_i parameters are now smaller then 1, the universal approximation starts to be accurate. In the next sections, where we analyze several specific models, we will systematically compare our full numerical fit (plotting best fit regions in yellow with continuous contours at the 90 and 99% C.L.) with the universal approximation (best fit ellipsoidal regions in gray with dotted contours, at the same confidence levels).

1.4 Reconstructing the Higgs mass

The CMS and ATLAS collaborations reported measurements of the pole Higgs mass M_h obtained as the position of the peaks observed in the invariant mass of the $h \to \gamma\gamma$ and $h \to ZZ \to 4\ell$ distributions:

$$M_h = 125.7 \pm 0.4 \ \text{GeV} = \begin{cases} 125.4 \pm 0.5_{\rm stat} \pm 0.6_{\rm syst} \ \text{GeV} & \text{CMS } \gamma\gamma \\ 125.8 \pm 0.5_{\rm stat} \pm 0.2_{\rm syst} \ \text{GeV} & \text{CMS } ZZ \\ 126.8 \pm 0.2_{\rm stat} \pm 0.7_{\rm syst} \ \text{GeV} & \text{ATLAS } \gamma\gamma \\ 124.3 \pm 0.6_{\rm stat} \pm 0.4_{\rm syst} \ \text{GeV} & \text{ATLAS } ZZ \end{cases} . \tag{1.11}$$

These measurements are mutually compatible, and the uncertainty is so small that in the subsequent fits to rates we can fix M_h to its combined best-fit value. We combined all uncertainties in quadrature, using the standard Gaussian error propagation and neglecting correlations among systematic uncertainties. The averages within each experiment agree with those reported by the experiments.

The ATLAS collaboration reports the combined value for the Higgs mass, based on the $\gamma\gamma$ and ZZ channels, as $M_h = 125.5 \pm 0.2_{\rm stat}{}^{+0.5}_{-0.6{\rm syst}}$ (best fit signal strength $R = 1.43 \pm 0.16_{\rm stat} \pm 0.14_{\rm syst}$) [25], whereas CMS gives $M_h = 125.7 \pm 0.3_{\rm stat} \pm 0.3_{\rm syst}$ based on $\gamma\gamma$, ZZ, WW, $\tau\tau$ and bb (best fit signal strength $R = 0.80 \pm 0.14$) [26].

We here discuss how the Higgs mass can be independently measured, with a bigger uncertainty, by requiring that the measured rates agree with their SM predictions. Such predictions have a dependence on the Higgs mass that, around 125 GeV, can be approximated as

$$\sigma(pp \to X) \approx \sigma(pp \to X)_{M_h=125\,\rm GeV} \times [1 + c_X \times (M_h - 125\,\rm GeV)]. \tag{1.12}$$

In table 1.1 we list the values of the coefficients c_X and of the measured rates for the various processes averaging all experiments, as well as the Higgs mass indirectly derived from such rates. We see that the single best indirect determination of M_h comes from the $h \to WW$ rates, that presently have no sensitivity to M_h if one wants to measure it from a mass peak. On the other hand, the $h \to \gamma\gamma$ signal that offers the best peak measurement of M_h has very little indirect sensitivity to M_h, because the $\gamma\gamma$ rate happens to have a weak dependence on M_h. Averaging over all channels we find

$$M_h = 124.5 \pm 1.7 \ \text{GeV} \qquad \text{(Higgs mass extracted from the rates, assuming the SM)} \tag{1.13}$$

which is compatible with the determination of the pole Higgs mass obtained in a model-independent way from the positions of the peaks.

1.5 Model-dependent Higgs fits

1.5.1 Higgs production cross sections

Assuming the SM predictions for the Higgs decays, we extract from the data the Higgs production cross sections. Given that measured rates of various exclusive and inclusive Higgs channels agree with their SM preditctions, we find that production cross sections too agree with SM predictions, as shown in fig. 1.3a. As expected, the most precisely probed cross section is the dominant one, $\sigma(pp \to h)$. At the opposite extremum $\sigma(pp \to jjh)$ is still largely unknown. The uncertainties on the reconstructed cross sections are correlated, altought we do not report the correlation matrix.

1.5.2 Higgs couplings

We here extract from data the Higgs boson couplings to vectors and fermions, assuming that only the SM particles contribute to the $h \to gg, \gamma\gamma, \gamma Z$ loops. This amounts to restrict the universal fit in terms of the r_i parameters by setting the parameters for loop couplings to

$$r_g = r_t, \qquad r_\gamma \approx 1.282 r_W - 0.282 r_t \qquad r_{Z\gamma} \approx 1.057 r_W - 0.057 r_t \tag{1.14}$$

These numerical expressions are obtained by rescaling the expressions for the SM loops summarised in appendix 1.A.1. In particular, the W loop (rescaled by r_W) and the top loop (rescaled by r_t) contribute to $h \to \gamma\gamma$ with a negative interference.

Under this assumption the top coupling of the Higgs, r_t, becomes indirectly probed via the loop effects. The fit to the couplings is shown in fig. 1.3b and agrees with the SM predictions (diagonal line), signalling that the new boson really is the Higgs. The correlation matrix can be immediately obtained by inserting equation (1.14) into the universal χ^2 of equation (1.9).

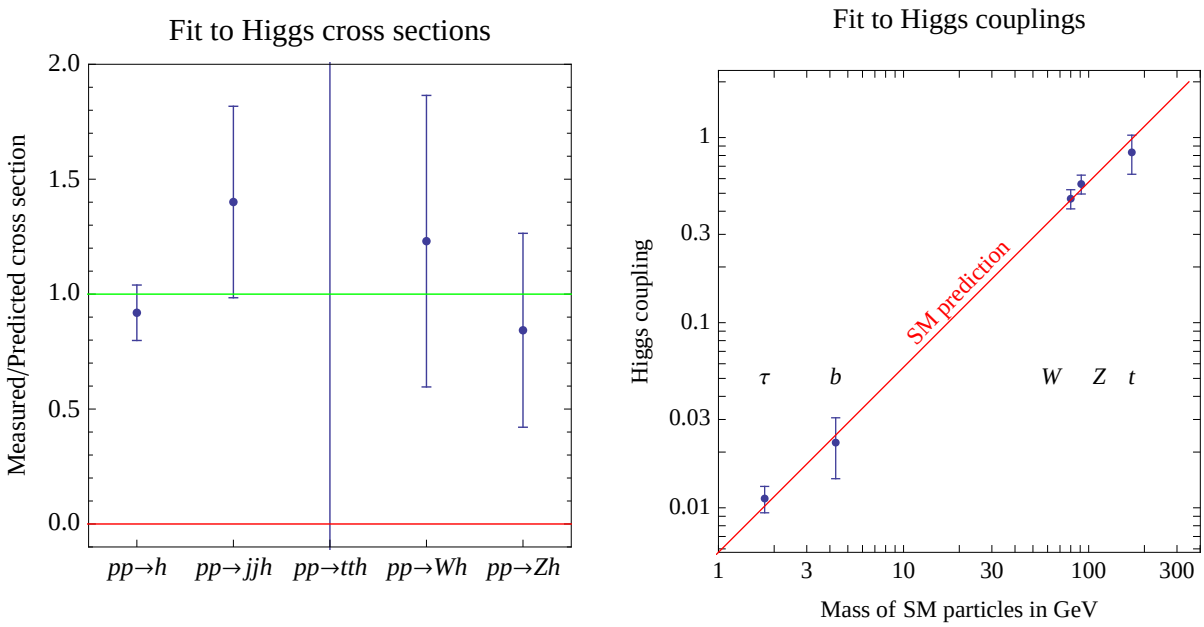

Figure 1.3: **Left**: *reconstruction of the Higgs production cross sections in units of the SM prediction.* **Right**: *reconstruction of the Higgs couplings to the* t, Z, W, b, τ*, assuming that no new particles exist. The SM predicts that Higgs couplings are proportional to particle masses (diagonal line).*

We allow the SM prediction to vary in position and slope by assuming that the Higgs couplings to particles with mass m are given by $(m/v')^p$. Taking into account all correlations, we find that data imply parameters p and v' close to the SM prediction of m/v (diagonal line in fig. 1.3b):

$$p = 0.99 \pm 0.03, \qquad v' = v(1.00 \pm 0.07) \tag{1.15}$$

with a 27% correlation.

1.5.3 Composite Higgs models

Models where the Higgs is composite often assume the further restriction, in addition to equation (1.14), of a common rescaling with respect to their SM values of the Higgs boson couplings to the W, Z bosons and a common rescaling of the Higgs boson couplings to all fermions. These rescalings are usually denoted as a and c, respectively:

$$r_t = r_b = r_\tau = r_\mu = c, \qquad r_W = r_Z = a. \tag{1.16}$$

The resulting fit is shown in fig. 1.4a. We see that our approximated universal fit (dotted contours) reproduces very well our full fit (continuous contours). The best fit converged towards the SM; in particular data now disfavour the solution with $c < 0$ which appeared in previous fits. Similar fits by the ATLAS and CMS collaborations are given in [29]. The CMS result is similar to ours, while ATLAS has $c/a = 0.85^{+0.23}_{-0.13}$, due to their larger $h \to VV$ rates, which is compatible with our result at 1σ level.

The reason is visualised in fig. 1.4b, where we show the bands favoured by the overall rates for Higgs decay into heavy vectors (WW and ZZ, that get affected in the same way within the model assumptions), into fermions (bb and $\tau\tau$, that get affected in the same way within the model

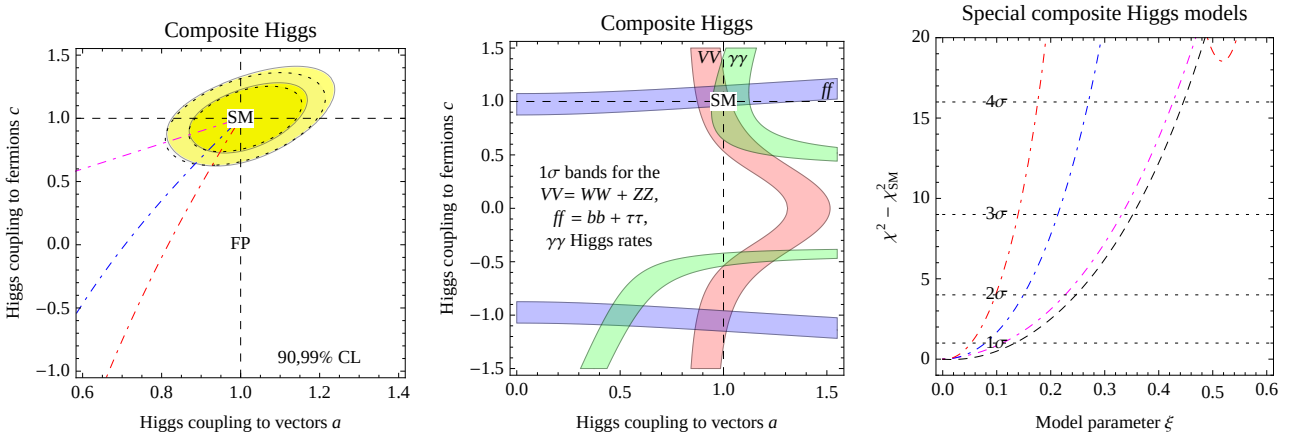

Figure 1.4: **Left**: *fit of the Higgs boson couplings assuming common rescaling factors a and c with respect to the SM prediction for couplings to vector bosons and fermions, respectively. The two sets of contour lines are our full fit (continuous) and our approximated 'universal' fit (dotted).* **Middle**: *1σ bands preferred by the three independent overall rates within the model.* **Right**: *values of the χ^2 along the trajectories in the (a, c) plane shown in the left panel, and given by $a = \sqrt{1-\xi}$ and $c = a$ (magenta) $c = (1-2\xi)/a$ (blue) $c = (1-3\xi)/a$ (red), as motivated by composite Higgs models [30]. The black dashed curve corresponds to $a = 1$ and $c = 1-\xi$.*

assumptions) and into $\gamma\gamma$. We see that these bands only cross around the SM point, $a = c = 1$. The full fit to all exclusive rates contains more information than this simplified fit.

In fig. 1.4c we show the full χ^2 restricted along the trajectories in the (a, c) plane (plotted in the left panel) predicted by simple composite pseudo-Goldstone Higgs models in terms of the parameter $\xi = (V/F_\pi)^2$, where F_π is the scale of global symmetry breaking.

1.5.4 New physics only in the loop processes

We here assume that only the loop processes are modified with respect to the SM predictions, summarized in appendix 1.A.1. This amounts to restrict our universal fit setting

$$r_t = r_b = r_\tau = r_\mu = r_W = r_Z = 1, \qquad \frac{\Gamma(h \leftrightarrow gg)}{\Gamma(h \leftrightarrow gg)_{\rm SM}} = r_g^2, \qquad \frac{\Gamma(h \to \gamma\gamma)}{\Gamma(h \to \gamma\gamma)_{\rm SM}} = r_\gamma^2 \tag{1.17}$$

with $\mathrm{BR}_{\rm inv} = 0$ and $r_{Z\gamma} = 1$. The latter assumption is at present justified because of the large experimental error in the $h \to Z\gamma$ rate, even though in general new physics in the loop processes would induce deviation from unity in both $r_{Z\gamma}$ and r_γ. The result is shown in the left panel of fig. 1.5, under the form of a fit to the ratios of $\mathrm{BR}(h \to gg)$ and $\mathrm{BR}(h \to \gamma\gamma)$ with respect to the SM. One can see that the SM is well within the 1σ contour. The analogous ATLAS result [29] is instead barely compatible with the SM at 2σ level because they only fit ATLAS data, where $h \to VV$ rates have a central value above the SM. The universal fit approximates well the full fit. The dashed trajectories show the loop effect due to extra scalar particles with the same quantum numbers of the top (red), of the bottom (blue), of the tau (vertical black line). The explicit expressions for the contribution of scalar, fermion and vector particles running in the loop can be found in appendix 1.A.1. Note that any additional color-less but electrically charged particle would lead to the same trajectory obtained for the scalar partner of the τ.

To better investigate the constraints on a possible new scalar S, in the right panel of fig. 1.5 we

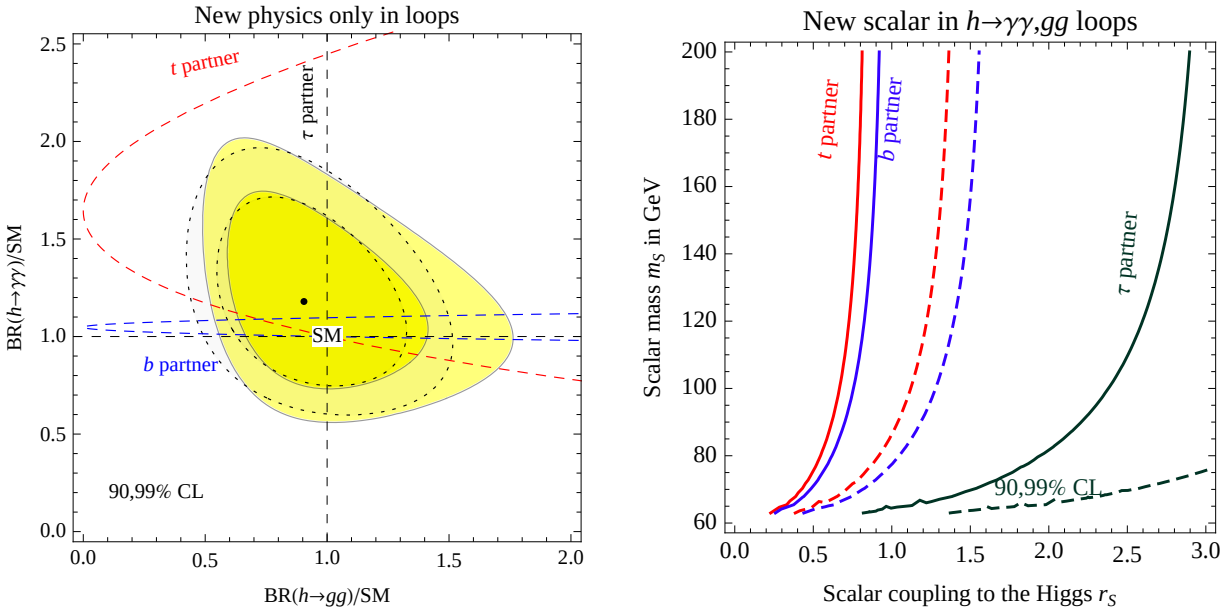

Figure 1.5: **Left**: *fit for the Higgs boson branching fraction to photons and gluons, with* 1 *and* 2σ *contours. The dashed curves shows the possible effect of extra scalar partners of the top (red), of the bottom (blue), of the tau (black). Dotted lines show the Gaussian approximation.* **Right**: *Upper bound at* 90% *(solid) and* 99% *(dashed) C.L. on the new scalar coupling* r_S *to the Higgs as a function of the new scalar mass* m_S*.*

show the upper bound, as function of the scalar mass m_S, on the scalar coupling r_S to the Higgs boson, defined by the coupling

$$r_S \frac{2m_S^2}{V} hSS. \tag{1.18}$$

The resulting loop effects are summarised in appendix 1.A.1. The solid and dashed curves in fig. 1.5b are respectively the upper bounds at 90% (solid) and 99% (dashed) C.L. More stringent limits are obtained on the top and bottom partners than on the τ partner.

One can also use the universal fit with the assumption of eq. (1.17) to derive indirect constraints on the top quark magnetic and chromomagnetic dipole moments [31, 32], which in the SM are expected to be respectively $g_t \approx 2$ and $k_t \approx 2$. Allowing g_t and k_t to vary freely, the $h \to \gamma\gamma$ and $h \to gg$ amplitudes are modified with respect to the SM as:

$$r_\gamma = \frac{c_\gamma^{(W)} + c_\gamma^{(t)} \left(\frac{3}{8} g_t^2 - \frac{1}{2}\right)}{c_\gamma^{(W)} + c_\gamma^{(t)}}, \qquad r_g = \frac{3}{8} k_t^2 - \frac{1}{2} \ , \tag{1.19}$$

where the quantities $c_\gamma^{(W)}$ and $c_\gamma^{(t)}$ are defined in eq. (1.35) of the Appendix. Numerically we have $c_\gamma^{(W)} = -1.043$ and $c_\gamma^{(t)} = 0.223$. Fig. 1.6 shows the 90% and 99% C.L. allowed regions for g_t and k_t. The uncertainty on k_t is comparable to the one from its direct measurement, while the one for g_t is even smaller [33].

Eq. (1.19) was computed by [31, 32] at the weak scale, in the phase with broken electroweak symmetry. An analogous computation was performed in [34], promoting the dipoles to full $\mathrm{SU}(2)_L \otimes \mathrm{U}(1)_Y$-invariant effective operators with a non-renormalizable dimension $d > 4$, suppressed by a factor $1/\Lambda^{d-4}$, Λ being the cutoff of the theory. The result [34] is that the dipole operators before electroweak

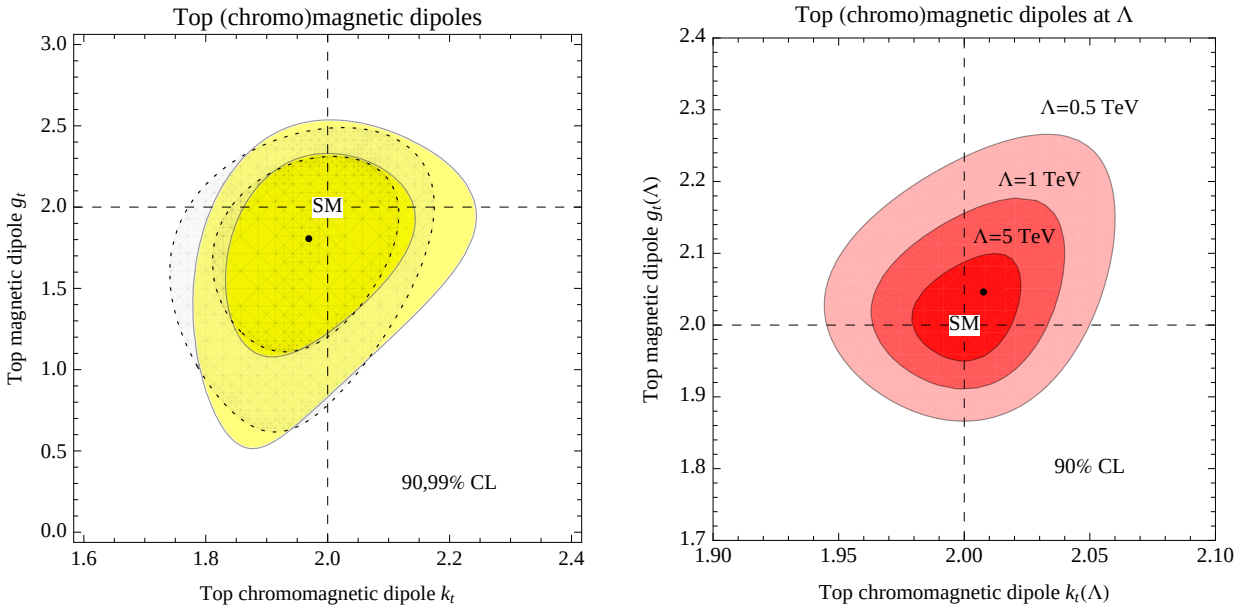

Figure 1.6: *Best fit regions for the (chromo)magnetic dipole moments of the top quark.* **Left***: as defined at m_h according to the computation of [31, 32].* **Right***: as defined at a cutoff scale Λ according to the computation of [34].*

symmetry breaking contribute, via RGE mixing, to other one-loop suppressed operators affecting the $h \to \gamma\gamma$ and $h \to gg$ decay rates [35]. Finite parts are not computed. Because of the RGE running from Λ down to m_h, the effect is proportional to $\ln \Lambda/m_h$, differently from equation (1.19). Using the operator mixing result of [34] and parametrizing the $d = 6$ dipole operators at Λ via quantities analogous to g_t and k_t but defined at Λ, the decay rates [35] can be written as

$$r_\gamma = 1 - \frac{4/3}{c_\gamma^{(W)} + c_\gamma^{(t)}} \left(\frac{g_t(\Lambda)}{2} - 1 \right) \log \frac{\Lambda}{m_h}\,, \qquad r_g = 1 - \frac{6}{c_g^{(t)}} \left(\frac{k_t(\Lambda)}{2} - 1 \right) \log \frac{\Lambda}{m_h}\,, \tag{1.20}$$

where the quantity $c_g^{(t)}$ is defined in eq. (1.35) of the Appendix. Numerically $c_g^{(t)} = 1.03$. Repeating our fit, we obtain similar constraints as illustrated in the right panel of fig. 1.6, for representative values of the cutoff.

1.5.5 Models with two Higgs doublets

There are four types of two Higgs doublets models (2HDM) where tree level flavour-changing neutral currents (FCNCs) are forbidden by a Z_2 symmetry [36] and both doublets H_1 and H_2 get a vacuum expectation value:

- type I [37, 38] where only one doublet couples to all quarks and leptons;
- type II [38, 39], where up-type quarks couple to H_2 and H_1 couples to down-type quarks and leptons. The Higgs sector of the MSSM is a type II 2HDM;
- type X (lepton-specific or leptophilic) where H_2 couples only to quarks and H_1 couples only to leptons;

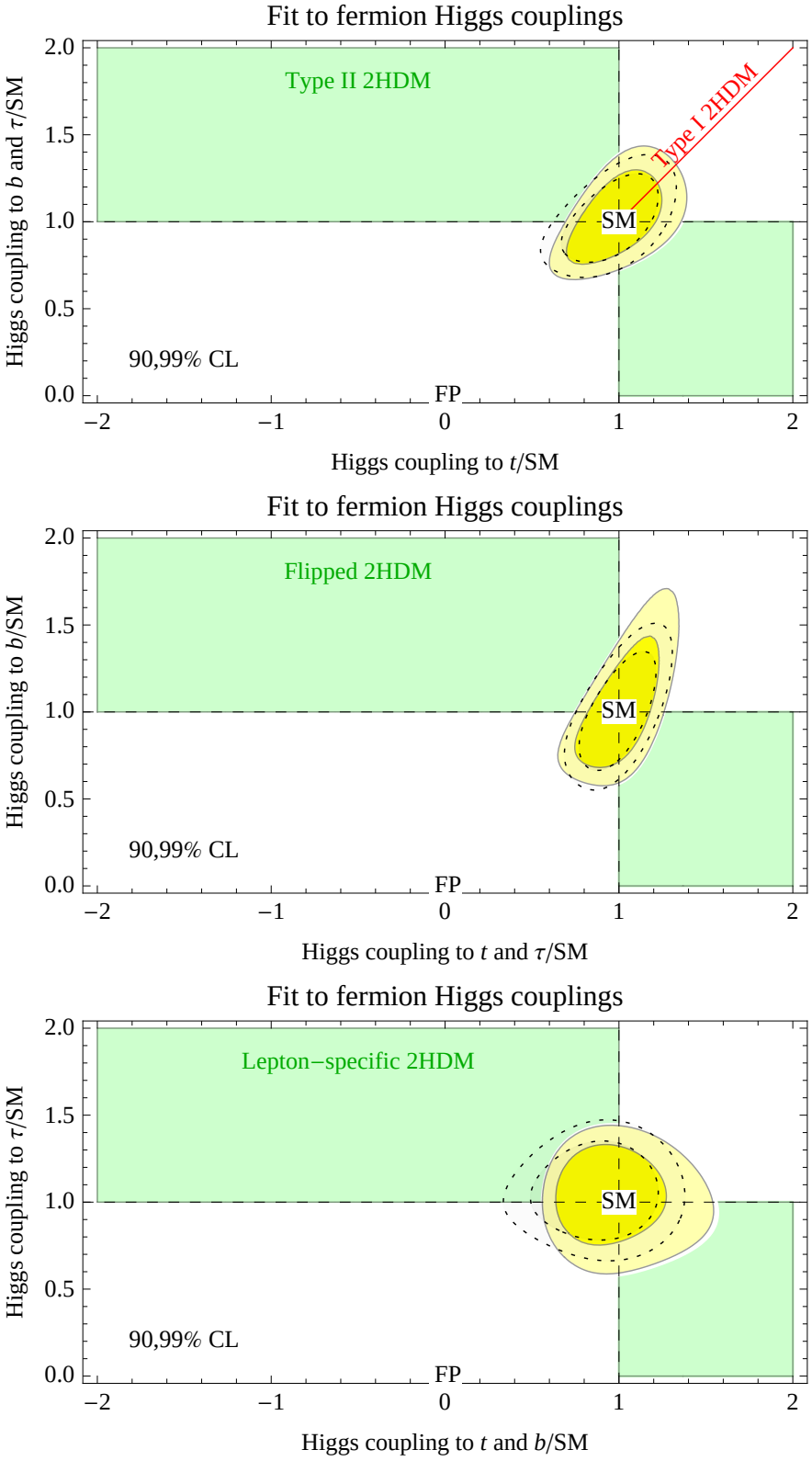

Figure 1.7: *Fit to the t-quark and to b-quark and τ-lepton Yukawa couplings assuming the structure predicted by the various types of two Higgs doublet models. The point marked as 'SM' is the Standard Model; the point marked as 'FP' is the fermiophobic case.*

- type Y (flipped) [40], where H_2 couples to up-type quarks and H_2 to down-type quarks, and (contrary to the type II HDM) leptons couple to H_2.

For an extensive review see [41] and for some previous fits see [42]. The modification to Yukawa couplings to up-type and down-type quarks and leptons in the four 2HDMs are:

	Type I	Type II	Type X (lepton-specific)	Type Y (flipped)
r_t	$\cos\alpha/\sin\beta$	$\cos\alpha/\sin\beta$	$\cos\alpha/\sin\beta$	$\cos\alpha/\sin\beta$
r_b	$\cos\alpha/\sin\beta$	$-\sin\alpha/\cos\beta$	$\cos\alpha/\sin\beta$	$-\sin\alpha/\cos\beta$
r_τ	$\cos\alpha/\sin\beta$	$-\sin\alpha/\cos\beta$	$-\sin\alpha/\cos\beta$	$\cos\alpha/\sin\beta$

As usual, $\tan\beta = v_2/v_1$ is the ratio of the VEVs of the two doublets and α is the mixing angle of the CP-even mass eigenstates. The SM limit corresponds to $\beta - \alpha = \pi/2$. In all of the models the vector couplings are also modified as

$$r_W = r_Z = \sin(\beta - \alpha). \tag{1.21}$$

The results of our fits are presented in fig. 1.7 in terms of the fermion couplings r_t, r_b, r_τ, restricted by the 2HDM models to lie within the green regions. We find that in each case, it is r_t that dominates the fit and the bottom contributions to gluon fusion and $h \to \gamma\gamma$ are negligible.

The type II 2HDM (upper panel) allows for independent modification of the t coupling r_t, and for a common modification of the b and τ couplings, $r_b = r_\tau$. The former is predicted be reduced and the latter enhanced by the model. The modification of equation (1.21) of the vector couplings can be equivalently written as $r_W = r_Z = (1 + r_t r_b)/(r_t + r_b) \simeq 1 + \epsilon_t\epsilon_b/2$, showing that it is a small second order effect. In this model a negative t Yukawa coupling is still allowed at slightly more than 99% CL. The red line in the same panel shows the parameter space allowed by type I 2HDM, where all the couplings scale uniformly.

In the flipped 2HDM (middle panel) the τ Yukawa coupling changes in the same way as the t coupling and the region with negative coupling is disfavoured by data. Finally, in the leptophilic 2HDM (lower panel) the t and b couplings vary in the same way, while the τ coupling is independent.

The universal fit provides a good approximation to the full fit in all 2HD models.

1.5.6 Supersymmetry

Supersymmetry can affect Higgs physics in many different ways, such that it is difficult to make general statements. We here focus on the two most plausible effects:

- The stop squark loop affect the $h \leftrightarrow gg, \gamma\gamma, Z\gamma$ rates. Given that the stop has the same gauge quantum numbers of the top, such effects are correlated and equivalent to a modification of the Higgs coupling to the top (as long as it is not directly measured via the $t\bar{t}h$ production cross section) by an amount given by

$$R_{\tilde{t}} = 1 + \frac{m_t^2}{4}\left[\frac{1}{m_{\tilde{t}_1}^2} + \frac{1}{m_{\tilde{t}_2}^2} - \frac{(A_t - \mu/\tan\beta)^2}{m_{\tilde{t}_1}^2\, m_{\tilde{t}_2}^2}\right] \tag{1.22}$$

  in the limit of heavy stop masses, $m_{\tilde{t}_{1,2}} \gg m_t$. Notice that $R_{\tilde{t}}$ can be enhanced or reduced with respect to one, depending on the latter mixing term.

- The type II 2HDM structure of supersymmetric models modifies at tree level the Higgs couplings, as already discussed in section 1.5.5.

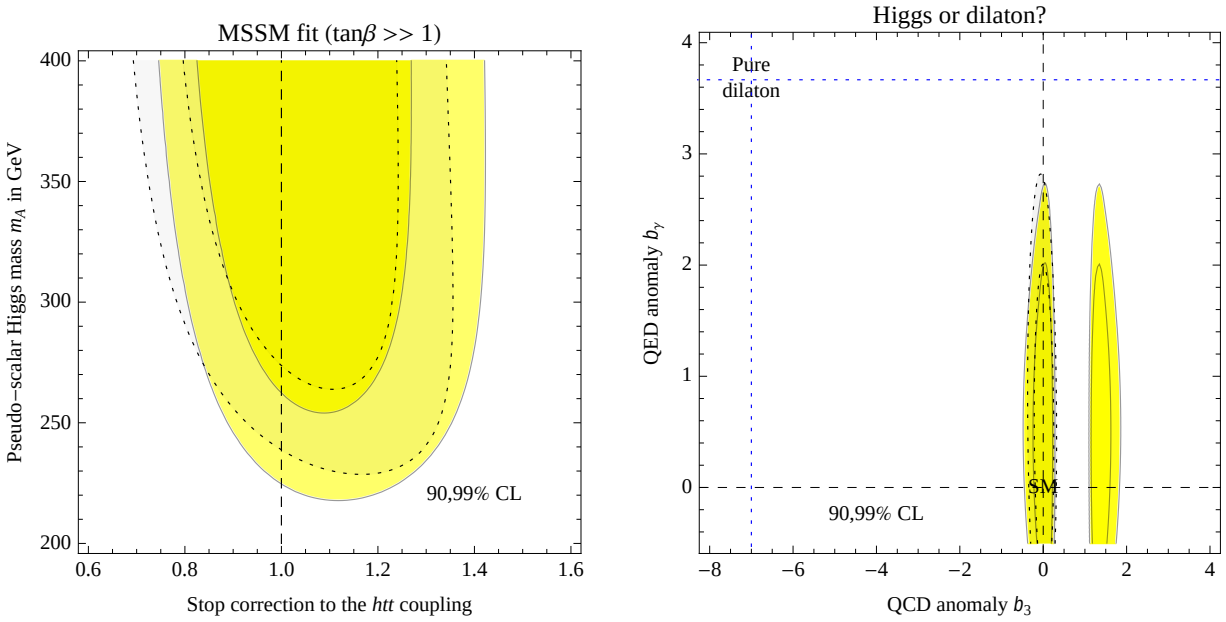

Figure 1.8: **Left**: *Fit to the two main effects present in supersymmetry: stop loop correction to the $ht\bar{t}$ coupling and tree-level modification of the Higgs couplings due to the two-Higgs doublet structure.* **Right**: *fit as function of the β-function coefficients $b_3 = b_\gamma$ that parameterise dilaton models. The SM Higgs is reproduced at the experimentally favored point $b_3 = b_\gamma = 0$, while the pure dilaton is excluded at more than 5σ.*

All of this amounts to specialise the universal χ^2 inserting the following values of its parameters

$$r_t = R_{\tilde{t}} \frac{\cos\alpha}{\sin\beta}, \qquad r_b = r_\tau = r_\mu = -\frac{\sin\alpha}{\cos\beta}, \qquad r_W = r_Z = \sin(\beta - \alpha). \tag{1.23}$$

Furthermore, the parameters $r_g, r_\gamma, r_{Z\gamma}$ relative to loop processes are fixed as in equation (1.14). We trade the α parameter (mass mixing between Higgses) for the pseudo-scalar Higgs mass m_A using

$$\tan 2\alpha = \frac{m_A^2 + M_Z^2}{m_A^2 - M_Z^2} \tan 2\beta. \tag{1.24}$$

Finally, we assume a large $\tan\beta$, as motivated by the observed value of the Higgs mass. Fig. 1.8a shows the resulting fit. Once again, the universal fit approximates well the full fit. Of course, supersymmetry can manifest in extra ways not considered here, e.g. very light staus or charginos could enhance $h \to \gamma\gamma$ [43].

1.5.7 Data prefer the Higgs to the dilaton

As another example of a model where both the tree level and the loop level Higgs couplings are modified, we consider the dilaton. The dilaton is an hypothetical particle φ, that, like the Higgs, couples to SM particles with strength proportional to their masses [44]. More precisely the dilaton has a coupling to the trace of the energy-momentum tensor $T_{\mu\nu}$, suppressed by some unknown scale Λ:

$$\frac{\varphi}{\Lambda} T^\mu_\mu = \frac{\varphi}{\Lambda} \left(\sum_f m_f \bar{f} f - M_Z^2 Z_\mu^2 - 2M_W^2 W_\mu^2 + b_3 \frac{\alpha_3}{8\pi} G^a_{\mu\nu} G^a_{\mu\nu} + b_\gamma \frac{\alpha_{\text{em}}}{8\pi} F_{\mu\nu} F_{\mu\nu} \right). \tag{1.25}$$

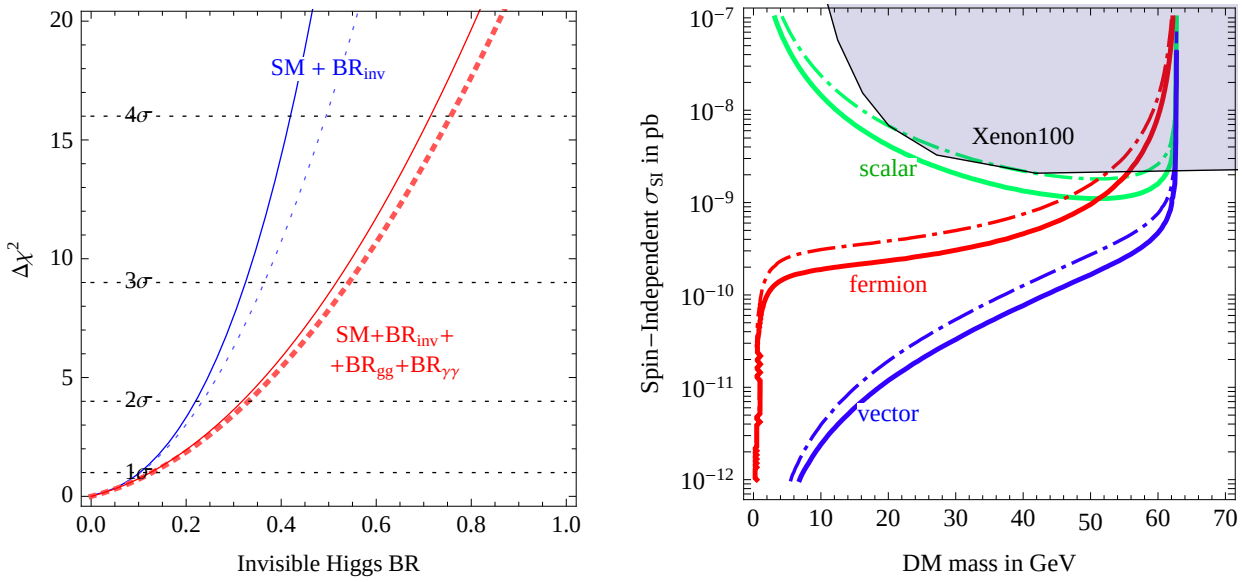

Figure 1.9: **Left:** *fits to the invisible Higgs boson branching fraction under the two different assumptions described in section 1.5.8. The full fit (continuos curves) is well approximated by the universal fit (dotted curves).* **Right***: upper limit on the spin-independent DM cross section on nucleons as a function of the DM mass for scalar (green), Majorana fermion (red) and vector (blue) DM. We adopted the 95% C.L. bounds* $\mathrm{BR}_{\mathrm{inv}} < 0.24$ *(solid,* equation (1.28)*) and* < 0.34 *(dot-dashed,* equation (1.29)*). The shaded region is excluded at* 90% *C.L. by* XENON*100 [46].*

The dilaton couplings to gg and $\gamma\gamma$ differ from the corresponding Higgs boson couplings, because equation (1.25) contains the latter two quantum terms, that are present in T^μ_μ because scale invariance is anomalous and broken at quantum level by the running of the couplings. Indeed b_3 and b_γ are the β-function coefficients of the strong and electromagnetic gauge couplings. In the SM they have the explicit values $b_3 = -7$ and $b_\gamma = 11/3$: we call 'pure dilaton' this special model, which gives a significant enhancement of $h \leftrightarrow gg$.

Models where a dilaton arises usually often contain also new light particles, such that b_3 and b_γ can differ from their SM values. Thereby we perform a generic fit where b_3 and b_γ are free parameters in addition to Λ. Then, our universal fit is adapted to the case of the generic dilaton by setting

$$r \equiv r_W = r_Z = r_t = r_b = r_\tau = \frac{V}{\Lambda}, \qquad r_g \approx r(1 - 1.45 b_3), \qquad r_\gamma \approx r(1 + 0.15 b_\gamma) \tag{1.26}$$

where $V = 246\,\mathrm{GeV}$.

In our previous analyses [6, 7], the dilaton gave fits of comparable quality to the SM Higgs, despite the significantly different predictions of the dilaton: enhanced $\gamma\gamma$ rates and reduced vector boson fusion rates. The first feature is no longer favoured by data, and the second feature is now disfavoured: so we find that present data prefer the Higgs to the 'pure dilaton' at about 5σ level. We then consider the generic dilaton, showing in fig. 1.8b that the allowed part of its parameters space is the one where it mimics the Higgs, possibly up to a sign difference in r_g and/or r_γ. The linear couplings of the dilaton in equation (1.25) become identical to those of the SM Higgs in the limit $b_3 = b_\gamma = 0$ and $\Lambda = V$. This situation is not easily realisable in models, given that adding extra charged particles increases b_γ rather than reducing it; one needs to subtract particles by e.g. assuming that that 3rd generation particles are composite [45].

1.5.8 Higgs boson invisible width

New physics can easily give a large effect providing an extra invisible [47] Higgs boson decay channel, for example into dark matter particles [48,49]. Alternatively, the effective operator $|\partial_\mu H^\dagger H|^2$ similarly has the effect of rescaling all rates by a common factor [50].

In the SM total Higgs boson width is predicted to be $\Gamma(h)_{\rm SM} \approx 4.0\,{\rm MeV}$ at $m_h = 125\,{\rm GeV}$. It is well known that measuring the Higgs boson total width at the LHC requires additional assumptions [51]. Let us explain how present data can probe the Higgs boson width, without directly measuring it. In view of CP invariance we can assume the equality of $gg \to h$ and $h \to gg$ amplitudes, that we collectively denote as $h \leftrightarrow gg$. The gluon fusion production rate is then proportional to $\Gamma(gg \to h)$ as given by the well known Breit-Wigner formula

$$\sigma(gg \to h) = \frac{\pi}{8}\frac{\Gamma(h \to gg)\Gamma(h)}{(s-m_h^2)^2 + m_h^2\Gamma(h)^2} \overset{\Gamma(h)\ll m_h}{\simeq} \frac{\pi^2}{8m_h}\Gamma(h \to gg)\delta(s-m_h^2). \tag{1.27}$$

Then, one partial decay width can be reconstructed by data. By performing a global fit to the Higgs boson branching ratios in the context of theories where the decay widths are related we can reconstruct the total Higgs boson width. Of course this is based on theoretical assumptions, but the result gets significantly different only in highly deviant models, e.g. in models where the Higgs boson predominantly decays into light quarks (a decay mode not probed by present data).

We perform two fits.

1. In the first fit, the invisible Higgs width is the only new physics. We find (blue curves in fig. 1.9a) that present data imply $\mathrm{BR}_{\rm inv} = -0.07 \pm 0.15$. The one-sided upper bound, computed restricting to $0 \le \mathrm{BR}_{\rm inv} \le 1$, is
$$\mathrm{BR}_{\rm inv} < 0.24 \text{ at } 95\% \text{ C.L.} \tag{1.28}$$

2. In addition to the invisible width we also allow for non-standard values of $h \to \gamma\gamma$ and $h \leftrightarrow gg$, finding a weaker constraint on $\mathrm{BR}_{\rm inv}$ (red curves in fig. 1.9a)
$$\mathrm{BR}_{\rm inv} < 0.34 \text{ at } 95\% \text{ C.L.} \tag{1.29}$$
The reason is that an enhanced $gg \to h$ production rate can partially compensate for an invisible Higgs width, but a full compensation would be possible only by enhancing all production rates by the same amount. The Higgs coupling to vectors is independently measured to agree with SM predictions from electroweak precision data.

Notice that the main constraint con $\mathrm{BR}_{\rm inv}$ does not come from the direct search for $pp \to Zh \to \ell\ell\not{E}_T$ (included in our data-set) but from the global fit [6, 52].

1.5.9 Dark Matter models

The invisible Higgs boson decay width [52] constrains Dark Matter (DM) candidates with mass below $M_h/2$. The Higgs sector of the SM allows for a direct coupling to particles of a hidden sector. If the latter are stable and interact weakly with the SM sector, they could represent viable Dark Matter (DM) candidates. If DM particles have mass below $M_h/2$, the Higgs boson can thus decay into a couple of DM particles, which would escape detection. Invisible Higgs decays are constrained by the fact that the ATLAS and CMS Higgs rates are compatible with the predictions of the SM Higgs boson. The experimental bound on $\mathrm{BR}_{\rm inv}$ can be used to constrain the DM mass and its elastic cross section

on nucleons probed in direct detection experiments, as illustrated for instance in [53], where DM is assumed to be either a scalar S, or a Majorana fermion f or a vector V coupled to the Higgs as

$$r_S \frac{2m_S^2}{V} hSS + r_f \frac{m_f}{V} h\bar{f}f + r_V \frac{2m_V^2}{V} hV_\mu V_\mu \ . \tag{1.30}$$

The partial Higgs decay width into dark matter $\Gamma(h \to \mathrm{DM\,DM})$ and the spin-independent DM-proton elastic cross section σ_{SI} can be calculated in terms of the parameters of the above Lagrangian. Both are proportional to the square of the DM-Higgs coupling, so that the ratio $\mu \equiv \sigma_{\mathrm{SI}}/\Gamma(h \to \mathrm{DM\,DM})$ depends only on the the unknown DM mass and on the known masses and couplings of the relevant SM particles (see for instance the expressions provided in [53]).

This allows us to relate the invisible Higgs branching fraction to the DM direct detection cross section:

$$\mathrm{BR}_{\mathrm{inv}} \equiv \frac{\Gamma(h \to \mathrm{DM\,DM})}{\Gamma_h^{\mathrm{SM}} + \Gamma(h \to \mathrm{DM\,DM})} = \frac{\sigma_{\mathrm{SI}}}{\mu \Gamma_h^{\mathrm{SM}} + \sigma_{\mathrm{SI}}} \tag{1.31}$$

where $\Gamma_h^{\mathrm{SM}} = 4.1\,\mathrm{MeV}$ is the total Higgs decay width into all SM particles, that we fix to its SM prediction. For a given DM mass, an upper bound on the Higgs invisible branching fraction implies an upper bound on the DM scattering cross section on nucleons. The relation between the invisible branching fraction and the direct detection cross section strongly depends on the spinorial nature of the DM particle, in particular, the strongest (weakest) bound is derived in the vectorial (scalar) case.

Imposing the upper bounds on $\mathrm{BR}_{\mathrm{inv}}$ derived in section 1.5.8, fig. 1.9 shows the corresponding upper limits on the spin-independent DM cross section on nucleons as a function of the DM mass, in the case of scalar (green), Majorana fermion (red) and vector (blue) DM candidates.

In all cases, the derived bounds are stronger than the direct one from XENON100 as long as the mass of DM is lighter than $M_h/2$. This conclusion does not rely on the assumption that DM is a thermal relic that reproduces the observed cosmological DM abundance. The limit on σ_{SI} crucially depends on the assumption that DM directly couples to the Higgs. Larger values of σ_{SI} remain possible in different models, where DM couples to the Z or directly to nucleons via loops of supersymmetric or other particles.

1.A Appendix

1.A.1 New physics contributions to loop processes

The coefficients in the second line of equation (1.4) arise at one-loop. They are obtained by summing the contributions of all scalars (S) fermions (f) and vectors (V) that couple to the Higgs as in equation (1.30). The explicit expressions for the loop effects are [54]:

$$c_g^{(S)} = \frac{C_2^S}{2} r_S A_S(\tau_S) \qquad c_g^{(f)} = 2C_2^f r_f A_f(\tau_f) \tag{1.32}$$
$$c_\gamma^{(S)} = \frac{N_S Q_S^2}{24} r_S A_S(\tau_S) \qquad c_\gamma^{(f)} = \frac{N_f Q_f^2}{6} r_f A_f(\tau_f) \qquad c_\gamma^{(V)} = -\frac{7Q_V^2}{8} r_V A_V(\tau_V)$$

where for each particle $p = S, f, V$, $\tau_p = m_h^2/4m_p^2$, N_p is the number of colors, C_2^p is the Casimir of the color representation ($\mathrm{Tr}(T^a T^b) = C_2 \delta^{ab}$), and the loop functions are

$$A_S(\tau) = \frac{3}{\tau^2}\left[f(\tau) - \tau\right] \ , \ A_f(\tau) = \frac{3}{2\tau^2}\left[(\tau-1)f(\tau) + \tau\right] \tag{1.33}$$
$$A_V(\tau) = \frac{1}{7\tau^2}\left[3(2\tau-1)f(\tau) + 3\tau + 2\tau^2\right] \tag{1.34}$$

with $f(\tau) = \arcsin^2(\sqrt{\tau})$ for $\tau \leq 1$ such that $A_p(\tau_p) \to 1$ in the limit $\tau_p \to 0$ (heavy p-particle).

In particular, in the SM, the hgg coupling is dominated by the top loop, and the $h\gamma\gamma$ coupling arise from the sum of the top and W boson loops:

$$c_{\mathrm{SM}}^{gg} = c_g^{(t)} = A_f(\tau_t) \qquad c_{\mathrm{SM}}^{\gamma\gamma} = c_\gamma^{(t)} + c_\gamma^{(W)} = \frac{2}{9} A_f(\tau_t) - \frac{7}{8} A_V(\tau_W) \ . \tag{1.35}$$

Beyond the SM (BSM) physics affects the parameters r_g and r_γ as

$$r_g = 1 + \frac{c_{\mathrm{BSM}}^{gg}}{c_{\mathrm{SM}}^{gg}}, \qquad r_\gamma = 1 + \frac{c_{\mathrm{BSM}}^{\gamma\gamma}}{c_{\mathrm{SM}}^{\gamma\gamma}}. \tag{1.36}$$

For example, additional scalar particles with the same quantum numbers of a stop, sbottom and stau respectively contribute to c_{BSM}^{gg} and to $c_{\mathrm{BSM}}^{\gamma\gamma}$ as:

$$\begin{aligned} c_g^{(\tilde{t})} &= \frac{1}{4} r_{\tilde{t}} A_S(\tau_{\tilde{t}}) \quad c_g^{(\tilde{b})} = \frac{1}{4} r_{\tilde{b}} A_S(\tau_{\tilde{b}}) \quad c_g^{(\tilde{\tau})} = 0 \\ c_\gamma^{(\tilde{t})} &= \tfrac{1}{18} r_{\tilde{t}} A_S(\tau_{\tilde{t}}) \quad c_\gamma^{(\tilde{b})} = \frac{1}{72} r_{\tilde{b}} A_S(\tau_{\tilde{b}}) \quad c_\gamma^{(\tilde{\tau})} = \frac{1}{24} r_{\tilde{\tau}} A_S(\tau_{\tilde{\tau}}). \end{aligned} \tag{1.37}$$

Bibliography

[1] F. Englert and R. Brout, Phys. Rev. Lett. 13, 321 (1964).

[2] P. W. Higgs, Phys. Lett. 12 (1964) 132.

[3] P. W. Higgs, Phys. Rev. Lett. 13, 508 (1964).

[4] G. S. Guralnik, C. R. Hagen and T. W. B. Kibble, Phys. Rev. Lett. 13, 585 (1964).

[5] D. Carmi, A. Falkowski, E. Kuflik and T. Volansky, arXiv:1202.3144. A. Azatov, R. Contino and J. Galloway, arXiv:1202.3415. J. R. Espinosa, C. Grojean, M. Muhlleitner and M. Trott, arXiv:1202.3697. T. Li, X. Wan, Y. Wang and S. Zhu, arXiv:1203.5083. J. Ellis and T. You, arXiv:1204.0464. A. Azatov, R. Contino, D. Del Re, J. Galloway, M. Grassi and S. Rahatlou, JHEP 1206 (2012) 134 [arXiv:1204.4817]. M. Klute, R. Lafaye, T. Plehn, M. Rauch and D. Zerwas, arXiv:1205.2699; A. Azatov, S. Chang, N. Craig and J. Galloway, Phys. Rev. D 86 (2012) 075033 [arXiv:1206.1058]. I. Low, J. Lykken and G. Shaughnessy, Phys. Rev. D 86 (2012) 093012 [arXiv:1207.1093]. T. Corbett, O. J. P. Eboli, J. Gonzalez-Fraile and M. C. Gonzalez-Garcia, Phys. Rev. D 86 (2012) 075013 [arXiv:1207.1344]. M. R. Buckley and D. Hooper, Phys. Rev. D 86 (2012) 075008 [arXiv:1207.1445]. M. Montull and F. Riva, JHEP 1211 (2012) 018 [arXiv:1207.1716]. J. R. Espinosa, C. Grojean, M. Muhlleitner and M. Trott, arXiv:1207.1717. D. Carmi, A. Falkowski, E. Kuflik, T. Volansky and J. Zupan, JHEP 1210 (2012) 196 [arXiv:1207.1718]. S. Banerjee, S. Mukhopadhyay and B. Mukhopadhyaya, JHEP 1210 (2012) 062 [arXiv:1207.3588]. D. Bertolini and M. McCullough, JHEP 1212 (2012) 118 [arXiv:1207.4209]. F. Bonnet, T. Ota, M. Rauch and W. Winter, Phys. Rev. D 86 (2012) 093014 [arXiv:1207.4599]. T. Plehn and M. Rauch, Europhys. Lett. 100 (2012) 11002 [arXiv:1207.6108]. J. R. Espinosa, C. Grojean, V. Sanz and M. Trott, arXiv:1207.7355. A. Djouadi, arXiv:1208.3436. L. Maiani, A. D. Polosa, V. Riquer, arXiv:1209.4816. G. Cacciapaglia, A. Deandrea, G. D. La Rochelle and J. -B. Flament, arXiv:1210.8120. G. Moreau, arXiv:1210.3977. G. Belanger, B. Dumont, U. Ellwanger, J. F. Gunion and S. Kraml, JHEP 1302 (2013) 053 E. Masso and V. Sanz, arXiv:1211.1320. T. Corbett, O. J. P. Eboli, J. Gonzalez-Fraile and M. C. Gonzalez-Garcia, Phys. Rev. D 87 (2013) 015022 [arXiv:1211.4580]. [arXiv:1212.5244]. C. Cheung, S. D. McDermott and K. M. Zurek, arXiv:1302.0314. K. Cheung, J. S. Lee and P. -Y. Tseng, arXiv:1302.3794. A. Falkowski, F. Riva and A. Urbano, arXiv:1303.1812.

[6] P. P. Giardino, K. Kannike, M. Raidal and A. Strumia, JHEP 1206 (2012) 117 [arXiv:1203.4254].

[7] P. P. Giardino, K. Kannike, M. Raidal and A. Strumia, [arXiv:1207.1347].

[8] LHC Higgs Cross Section Working Group, arXiv:1101.0593 (Recommended values on SM Higgs XS at 7 TeV and SM Higgs production cross sections at $\sqrt{s} = 8$ TeV (2012 update)), arXiv:1201.3084, arXiv:1307.1347 [hep-ph]. (Branching Ratios and Partial-Decay Widths).

[9] P. P. Giardino, K. Kannike, I. Masina, M. Raidal and A. Strumia, arXiv:1303.3570 [hep-ph].

[10] Guillelmo Gomez-Ceballos, CMS Collaboration, Talk at the Moriond 2013 EW session.

[11] Fabrice Hubaut, ATLAS Collaboration, Talk at the Moriond 2013 EW session. Eleni Mountricha, ATLAS Collaboration, Talk at the Moriond 2013 QCD session.

[12] Valentina Dutta, CMS Collaboration, Talk at the Moriond 2013 EW session. Victoria Martin, ATLAS Collaboration, Talk at the Moriond 2013 EW session.

[13] Lidija Živković, CDF and DO Collaborations, Talk at the Moriond 2013 EW session.

[14] CMS Collaboration, CMS-PAS-HIG-13-001. ATLAS Collaboration, ATLAS-CONF-2013-012.

[15] CMS Collaboration, CMS-PAS-HIG-13-002. ATLAS Collaboration, ATLAS-CONF-2013-013.

[16] CMS Collaboration, CMS-PAS-HIG-13-003. ATLAS Collaboration, ATLAS-CONF-2013-030.

[17] CMS Collaboration, CMS-PAS-HIG-13-004. ATLAS Collaboration, ATLAS-CONF-2012-160.

[18] ATLAS Collaboration, ATLAS-CONF-2012-161.

[19] David Lopez Mateos, ATLAS Collaboration, talk given at the EPS HEP 2013 conference.

[20] ATLAS Collaboration, ATLAS-CONF-2013-010.

[21] CMS Collaboration, CMS-PAS-HIG-13-006. ATLAS Collaboration, ATLAS-CONF-2013-009.

[22] CMS Collaboration, CMS-PAS-HIG-13-009.

[23] Mingshui Shen, CMS Collaboration, Talk at the Moriond 2013 EW session. Bruno Mansoulie, CMS Collaboration, Talk at the Moriond 2013 EW session. ATLAS Collaboration, ATLAS-CONF-2013-014.

[24] M. Duhrssen, S. Heinemeyer, H. Logan, D. Rainwater, G. Weiglein and D. Zeppenfeld, Phys. Rev. D **70** (2004) 113009 [hep-ph/0406323].

[25] ATLAS Collaboration, ATLAS-CONF-2013-014.

[26] CMS Collaboration, CMS-PAS-HIG-13-005.

[27] K. Belotsky, D. Fargion, M. Khlopov, R. Konoplich and K. Shibaev, Phys. Rev. D 68 (2003) 054027 [hep-ph/0210153].

[28] ATLAS Collaboration, ATLAS-CONF-2013-011 See also reference [53]

[29] ATLAS Collaboration, ATLAS-CONF-2013-034. CMS Collaboration, CMS-PAS-HIG-13-005.

[30] G. F. Giudice, C. Grojean, A. Pomarol and R. Rattazzi, JHEP 0706 (2007) 045 [hep-ph/0703164]. A. Pomarol and F. Riva, JHEP 1208 (2012) 135 [arXiv:1205.6434].

[31] L. Labun and J. Rafelski, arXiv:1209.1046.

[32] L. Labun and J. Rafelski, arXiv:1210.3150.

[33] J. F. Kamenik, M. Papucci and A. Weiler, Phys. Rev. D 85 (2012) 071501 [arXiv:1107.3143].

[34] J. Elias-Miro, J. R. Espinosa, E. Masso, A. Pomarol and , arXiv:1302.5661 [hep-ph]. See also: C. Degrande, J. M. Gerard, C. Grojean, F. Maltoni, G. Servant and , JHEP **1207** (2012) 036 [Erratum-ibid. **1303** (2013) 032] [arXiv:1205.1065 [hep-ph]]. R. Contino, M. Ghezzi, C. Grojean, M. Muhlleitner and M. Spira, arXiv:1303.3876 [hep-ph].

[35] A. V. Manohar and M. B. Wise, Phys. Lett. B **636** (2006) 107 [hep-ph/0601212].

[36] S. L. Glashow and S. Weinberg, Phys. Rev. D 15 (1977) 1958.

[37] H. E. Haber, G. L. Kane and T. Sterling, Nucl. Phys. B 161 (1979) 493.

[38] L. J. Hall and M. B. Wise, Nucl. Phys. B 187 (1981) 397.

[39] J. F. Donoghue and L. F. Li, Phys. Rev. D 19 (1979) 945.

[40] V. D. Barger, J. L. Hewett and R. J. N. Phillips, Phys. Rev. D 41 (1990) 3421. Y. Grossman, Nucl. Phys. B 426 (1994) 355 [hep-ph/9401311]. A. G. Akeroyd and W. J. Stirling, Nucl. Phys. B 447 (1995) 3. A. G. Akeroyd, Phys. Lett. B 377 (1996) 95 [hep-ph/9603445]. A. G. Akeroyd, J. Phys. G 24 (1998) 1983 [J. Phys. G G 24 (1998) 1983] [hep-ph/9803324]. M. Aoki, S. Kanemura, K. Tsumura and K. Yagyu, Phys. Rev. D 80 (2009) 015017 [arXiv:0902.4665].

[41] G. C. Branco, P. M. Ferreira, L. Lavoura, M. N. Rebelo, M. Sher and J. P. Silva, Phys. Rept. 516 (2012) 1 [arXiv:1106.0034].

[42] R. T. D'Agnolo, E. Kuflik and M. Zanetti, arXiv:1212.1165. A. Celis, V. Ilisie and A. Pich, arXiv:1302.4022.

[43] M. Carena, I. Low and C. E. M. Wagner, arXiv:1206.1082. L. Wang and X. -F. Han, arXiv:1206.1673. W. -F. Chang, J. N. Ng and J. M. S. Wu, arXiv:1206.5047. N. Bonne and G. Moreau, arXiv:1206.3360. B. Bellazzini, C. Petersson and R. Torre, arXiv:1207.0803. J. Baglio, A. Djouadi and R. M. Godbole, arXiv:1207.1451. G. F. Giudice, P. Paradisi, A. Strumia and A. Strumia, JHEP 1210 (2012) 186 [arXiv:1207.6393].

[44] L. Randall and R. Sundrum, Phys. Rev. Lett. 83 (1999) 3370. Y. Eshel, S. J. Lee, G. Perez and Y. Soreq, JHEP 1110 (2011) 015 [arXiv:1106.6218]; V. Barger and M. Ishida, arXiv:1110.6452. K. Cheung and T. -C. Yuan, Phys. Rev. Lett. 108 (2012) 141602 [arXiv:1112.4146].

[45] B. Bellazzini, C. Csaki, J. Hubisz, J. Serra and J. Terning, Eur. Phys. J. C **73** (2013) 2333 [arXiv:1209.3299 [hep-ph]].

[46] XENON100 Collaboration, Phys. Rev. Lett. 109 (2012) 181301 [arXiv:1207.5988].

[47] O. J. P. Eboli and D. Zeppenfeld, Phys. Lett. B 495, 147 (2000) [arXiv:hep-ph/0009158]. R. M. Godbole, M. Guchait, K. Mazumdar, S. Moretti and D. P. Roy, Phys. Lett. B 571, 184 (2003) [arXiv:hep-ph/0304137]. J.F. Kamenik and C. Smith, arXiv:1201.4814.

[48] M. Raidal and A. Strumia, Phys. Rev. D 84 (2011) 077701 [arXiv:1108.4903]. Y. Mambrini, Phys. Rev. D 84 (2011) 115017 [arXiv:1108.0671]. A. Arhrib, R. Benbrik and N. Gaur, arXiv:1201.2644. X.G. He, B. Ren and J. Tandean, arXiv:1112.6364. C. Cheung and Y. Nomura, arXiv:1112.3043. X. Chu, T. Hambye and M. H. G. Tytgat, 1112.0493. O. Lebedev, H. M. Lee and Y. Mambrini, Phys. Lett. B 707 (2012) 570 [arXiv:1111.4482]. C. Englert, J. Jaeckel, E. Re and M. Spannowsky, Phys. Rev. D 85 (2012) 035008 [arXiv:1111.1719]. I. Low, P. Schwaller, G. Shaughnessy and C. E. M. Wagner, Phys. Rev. D 85 (2012) 015009 [arXiv:1110.4405]. M. Pospelov and A. Ritz, Phys. Rev. D 84 (2011) 113001 [arXiv:1109.4872]. T. Cohen, J. Kearney, A. Pierce and D. Tucker-Smith, arXiv:1109.2604. X. -G. He and J. Tandean, Phys. Rev. D 84 (2011) 075018 [arXiv:1109.1277]. C. -S. Chen and Y. Tang, arXiv:1202.5717. V. Barger, M. Ishida and W. -Y. Keung, arXiv:1203.3456. J. Cao, Z. Heng, J. M. Yang and J. Zhu, arXiv:1203.0694.

[49] A. Djouadi, O. Lebedev, Y. Mambrini and J. Quevillon, Phys. Lett. B 709 (2012) 65 [arXiv:1112.3299].

[50] R. Contino, C. Grojean, M. Moretti, F. Piccinini and R. Rattazzi, JHEP 1005, 089 (2010) [arXiv:1002.1011]. R. Grober and M. Muhlleitner, JHEP 1106, 020 (2011) [arXiv:1012.1562]. S. De Curtis, M. Redi and A. Tesi, arXiv:1110.1613.

[51] M. Duhrssen, S. Heinemeyer, H. Logan, D. Rainwater, G. Weiglein and D. Zeppenfeld, Phys. Rev. D 70, 113009 (2004) [arXiv:hep-ph/0406323]. R. Lafaye, T. Plehn, M. Rauch, D. Zerwas and M. Duhrssen, JHEP 0908 (2009) 009 [arXiv:0904.3866].

[52] J. R. Espinosa, M. Muhlleitner, C. Grojean and M. Trott, arXiv:1205.6790.

[53] A. Djouadi, A. Falkowski, Y. Mambrini and J. Quevillon, arXiv:1205.3169 [hep-ph].

[54] For a recent review see A. Djouadi, Phys. Rept. 457 (2008) 1 [hep-ph/0503172].

Chapter 2

(Meta-)Stability of the Electro-Weak Potential

As stated in the introduction the measured values of the top and Higgs masses suggest a near-critical electro-weak vacuum. Near-criticality gives us a unique opportunity to obtain information about physics taking place at energy scales well beyond the reach of any collider experiment. Its consequences are so intriguing and potentially so revolutionary that they deserve accurate calculations and dedicated studies.

Recently, many authors have contributed towards the completion of the calculation of the renormalisation - group (RG) evolution (β-functions and thresholds) of the sizeable SM couplings at NNLO precision. We summarise the present status of these calculations in table 2.1. Furthermore, our precision extrapolation of the SM to high energy scales is relevant for testing any new physics scenario able of making predictions, such as unification of gauge couplings constants, or high-scale supersymmetric models that restrict or predict the quartic Higgs coupling.

In section 2.1 we present numerical results for the $\overline{\text{MS}}$ couplings at the weak scale. The implications of these results for Planck scale physics are discussed in sections 2.2–2.3. The results are summarised in the the last section.

2.1 SM couplings at the electroweak scale

In this section we give practical results for the SM parameters $\theta = \{\lambda, m^2, y_t, g_2, g_Y\}$, computed in terms of the observables $M_h, M_t, M_W, M_Z, G_\mu$ and $\alpha_3(M_Z)$, whose measured values are listed in table 2.2. In the next chapter we will give the complete calculation of the NNLO threshold correction of the Higgs quartic coupling and of the yukawa coupling of the top as done in [1]. We notice that the weak-scale values for the $\overline{\text{MS}}$ gauge couplings at the scale $\bar{\mu}$ are given in terms of G_μ, M_W and M_Z and not in terms of the fine structure constant and the weak mixing angle at the M_Z scale as usually done. Each $\overline{\text{MS}}$ parameter θ is expanded in loops as

$$\theta = \theta^{(0)} + \theta^{(1)} + \theta^{(2)} + \cdots \tag{2.1}$$

where the tree-level values $\theta^{(0)}$ are listed in table 2.1, the one-loop corrections $\theta^{(1)}$ are analytically given in appendix 2.A.1 and the two-loop corrections $\theta^{(2)}$ are computed in the next chapter. After combining these corrections, we give in the following the numerical values for the SM parameters renormalised at the top pole mass M_t in the $\overline{\text{MS}}$ scheme.

Renormalisation Group Equations

	LO 1 loop	NLO 2 loop	NNLO 3 loop	NNNLO 4 loop
g_3	full [2,3]	$\mathcal{O}(\alpha_3^2)$ [4,5] $\mathcal{O}(\alpha_3\alpha_{1,2})$ [6] full [12]	$\mathcal{O}(\alpha_3^3)$ [7,8] $\mathcal{O}(\alpha_3^2\alpha_t)$ [9] full [13,14]	$\mathcal{O}(\alpha_3^4)$ [10,11]
$g_{1,2}$	full [2,3]	full [12]	full [13,14]	—
y_t	full [15]	$\mathcal{O}(\alpha_t^2, \alpha_3\alpha_t)$ [16] full [17]	full [18,19]	—
λ, m^2	full [15]	full [20,21]	full [22,23]	—

Threshold corrections at the weak scale

	LO 0 loop	NLO 1 loop	NNLO 2 loop	NNNLO 3 loop
g_2	$2M_W/V$	full [24,25]	full [1]	—
g_Y	$2\sqrt{M_Z^2 - M_W^2}/V$	full [24,25]	full [1]	—
y_t	$\sqrt{2}M_t/V$	$\mathcal{O}(\alpha_3)$ [26] $\mathcal{O}(\alpha)$ [27]	$\mathcal{O}(\alpha_3^2, \alpha_3\alpha_{1,2})$ [28] full [1]	$\mathcal{O}(\alpha_3^3)$ [29–31]
λ	$M_h^2/2V^2$	full [32]	for $g_{1,2} = 0$ [33] full [1]	—
m^2	M_h^2	full [32]	full [1]	—

Table 2.1: *Present status of higher-order computations included in our code. Here we have defined* $V \equiv (\sqrt{2}G_\mu)^{-1/2}$ *and* $g_1 = \sqrt{5/3}g_Y$.

M_W	=	80.384 ± 0.014 GeV	Pole mass of the W boson	[35]
M_Z	=	91.1876 ± 0.0021 GeV	Pole mass of the Z boson	[36]
M_h	=	125.66 ± 0.34 GeV	Pole mass of the higgs	[37]
M_t	=	$173.36 \pm 0.65 \pm 0.3$ GeV	Pole mass of the top quark	[38]
$V \equiv (\sqrt{2}G_\mu)^{-1/2}$	=	246.21971 ± 0.00006 GeV	Fermi constant for μ decay	[39]
$\alpha_3(M_Z)$	=	0.1184 ± 0.0007	$\overline{\text{MS}}$ gauge SU(3)$_c$ coupling (5 flavours)	[40]

Table 2.2: *Input values of the SM observables used to fix the SM fundamental parameters* $\lambda, m, y_t, g_2, g_Y$. *The pole top mass,* M_t, *is a naive average of TeVatron, CMS, ATLAS measurements, all extracted from difficult MonteCarlo modellings of top decay and production in hadronic collisions. Furthermore,* M_t *is also affected by a non-perturbative theoretical uncertainty of order* Λ_{QCD}, *that we quantify as* $\pm 0.3\,\text{GeV}$.

$\bar{\mu} = M_t$	λ	y_t	g_2	g_Y	$m/\,\text{GeV}$
LO	0.13023	0.99571	0.65294	0.34972	125.66
NLO	0.12879	0.95096	0.64754	0.35940	132.85
NNLO	0.12710	0.93989	0.6483	0.3587	132.03

Table 2.3: *Values of the fundamental SM parameters computed at tree level, one loop, two loops in the* $\overline{\text{MS}}$ *scheme and renormalised at* $\bar{\mu} = M_t$ *for the central values of the measurements listed in table 2.2.*

2.1.1 The Higgs quartic coupling

For the Higgs quartic coupling, defined by writing the SM potential as $V = -\frac{1}{2}m^2|H|^2 + \lambda|H|^4$, we find

$$\lambda(\bar{\mu} = M_t) = 0.12710 + 0.00206\left(\frac{M_h}{\text{GeV}} - 125.66\right) - 0.00004\left(\frac{M_t}{\text{GeV}} - 173.35\right) \pm 0.00030_{\text{th}}\ . \quad (2.2)$$

The dependence on M_t is small because λ is renormalised at M_t itself. Here and below the theoretical uncertainty is estimated from the dependence on $\bar{\mu}$ (varied around M_t by one order of magnitude) of the higher-order unknown 3 loop corrections. Such dependence is extracted from the known SM RGE at 3 loops (as summarized in appendix 2.A.2).

2.1.2 The Higgs mass term

For the mass term of the Higgs doublet in the SM Lagrangian (normalised such that $m = M_h$ at tree level) we find

$$\frac{m(\bar{\mu} = M_t)}{\text{GeV}} = 132.03 + 0.94\left(\frac{M_h}{\text{GeV}} - 125.66\right) + 0.17\left(\frac{M_t}{\text{GeV}} - 173.35\right) \pm 0.15_{\text{th}}. \quad (2.3)$$

2.1.3 The top Yukawa coupling

For the top Yukawa coupling we get

$$y_t(\bar{\mu} = M_t) = 0.93697 + 0.00550\left(\frac{M_t}{\text{GeV}} - 173.35\right) - 0.00042\,\frac{\alpha_3(M_Z) - 0.1184}{0.0007} \pm 0.00050_{\text{th}}\ . \quad (2.4)$$

The central value differs from the NNLO value in table 2.3 because we include here also the NNNLO (3 loop) pure QCD effect [29–31]. The theoretical uncertainty is estimated accordingly, and does not take into account the non-perturbative theoretical uncertainty of order Λ_{QCD} in the definition of M_t.

2.1.4 The weak gauge couplings

The best-fit values from [34] is

$$\alpha_Y^{-1}(M_Z) = 98.35 \pm 0.013, \qquad \alpha_2^{-1}(M_Z) = 29.587 \pm 0.008. \quad (2.5)$$

Table 2.3 reports their central values extrapolated at the renormalisation scale $\bar{\mu} = M_t$ using the SM two-loop RGE equations.

2.1.5 The strong gauge coupling

Table 2.2 contains the value of $\alpha_3(M_Z)$, as extracted from the global fit of [40] in the effective SM with 5 flavours. Including RG running from M_Z to M_t at 4 loops in QCD and at 2 loops in the electroweak gauge interactions, and 3 loop QCD matching at M_t to the full SM with 6 flavours, we get

$$g_3(\bar{\mu} = M_t) = 1.1666 + 0.00314\,\frac{\alpha_3(M_Z) - 0.1184}{0.0007} - 0.00046\left(\frac{M_t}{\text{GeV}} - 173.35\right). \quad (2.6)$$

The SM parameters can be renormalised to any other desired energy by solving the SM renormalisation group equations summarised in appendix 2.A.2. For completeness, we include in the one- and two-loop RG equations the contributions of the small bottom and tau Yukawa couplings, as computed

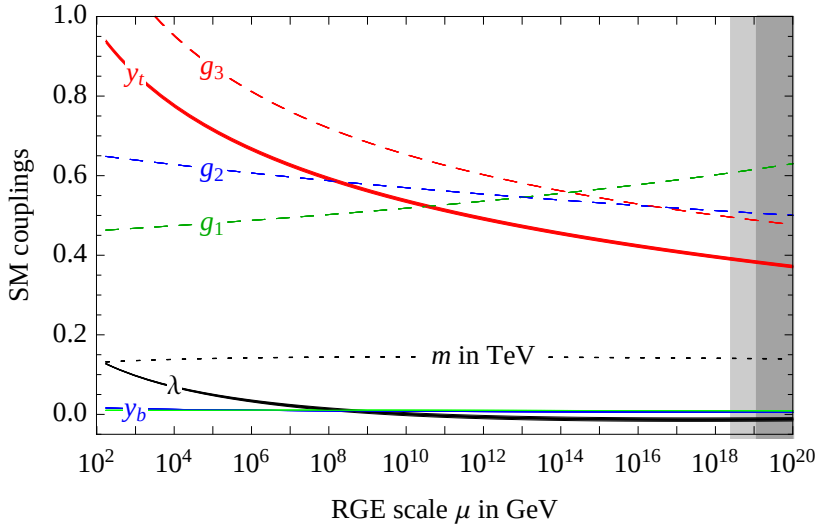

Figure 2.1: *Renormalisation of the SM gauge couplings* $g_1 = \sqrt{5/3}g_Y, g_2$, g_3, *of the top, bottom and* τ *couplings* (y_t, y_b, y_τ), *of the Higgs quartic coupling* λ *and of the Higgs mass parameter* m. *All parameters are defined in the* $\overline{\text{MS}}$ *scheme. We include two-loop thresholds at the weak scale and three-loop RG equations. The thickness indicates the* $\pm 1\sigma$ *uncertainties in* M_t, M_h, α_3.

from the $\overline{\text{MS}}$ b-quark mass, $m_b(m_b) = 4.2\,\text{GeV}$, and from $M_\tau = 1.777\,\text{GeV}$. Within the $\overline{\text{MS}}$ scheme β functions are gauge-independent [41]; similarly the $\overline{\text{MS}}$ parameters are gauge independent too.

2.2 Extrapolation of the SM up to the Planck scale

The most puzzling and intriguing outcome of the Higgs discovery has been the finding that M_h lies very close to the boundary between stability and metastability regions. This result is the main motivation for our refined NNLO calculation of the SM Higgs potential at large field values. Indeed, the special Higgs mass found by ATLAS and CMS is so close to criticality that any statement about stability or metastability of the EW vacuum requires a careful analysis of theoretical and experimental errors. The discovered proximity to criticality also naturally stimulates many theoretical speculations on its possible hidden significance or on special matching conditions at very high energy scales. Here, we will explore the implications of our improved computation of the Higgs quartic coupling extrapolated to very high scales.

2.2.1 SM couplings at the Planck scale

The first issue we want to address concerns the size of the SM coupling constants. When we try to extract information from the values of the coupling constants, it is reasonable to analyse their values not at the weak scale, but at some high-energy scale where we believe the SM matches onto some extended theory. So, using our NNLO results, we extrapolate the SM couplings from their weak-scale values (as determined in section 2.1) to higher energies.

The evolution of the SM couplings up to a large cut-off scale is shown in fig. 2.1. At the Planck

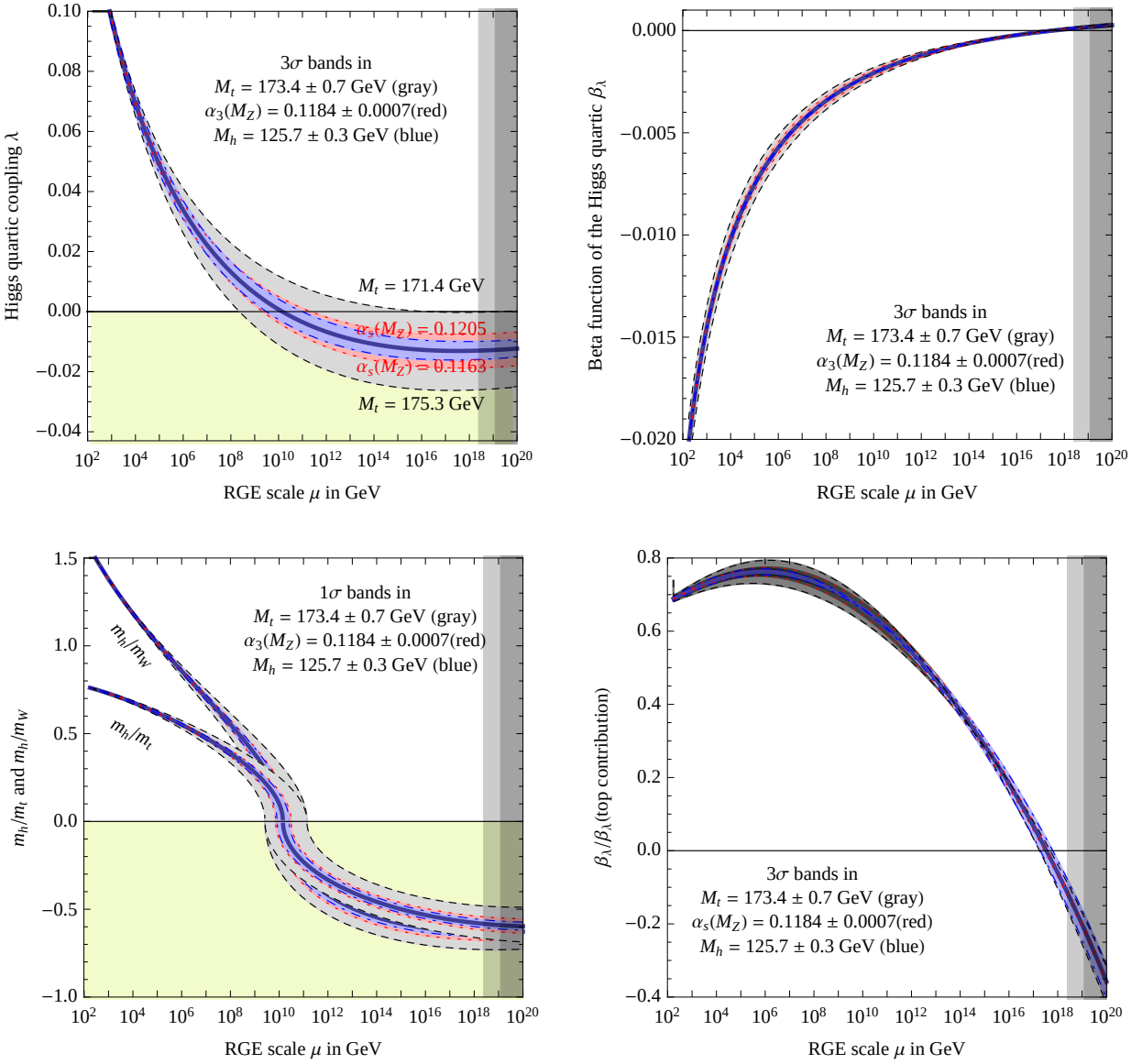

Figure 2.2: **Upper**: *RG evolution of* λ (**left**) *and of* β_λ (**right**) *varying* M_t, $\alpha_3(M_Z)$, M_h *by* $\pm 3\sigma$. **Lower**: *Same as above, with more "physical" normalisations. The Higgs quartic coupling is compared with the top Yukawa and weak gauge coupling through the ratios* $\mathrm{sign}(\lambda)\sqrt{4|\lambda|}/y_t$ *and* $\mathrm{sign}(\lambda)\sqrt{8|\lambda|}/g_2$, *which correspond to the ratios of running masses* m_h/m_t *and* m_h/m_W, *respectively* (**left**). *The Higgs quartic* β*-function is shown in units of its top contribution,* $\beta_\lambda(\text{top contribution}) = -3y_t^4/8\pi^2$ (**right**). *The grey shadings cover values of the RG scale above the Planck mass* $M_{\mathrm{Pl}} \approx 1.2 \times 10^{19}\,\mathrm{GeV}$, *and above the reduced Planck mass* $\bar{M}_{\mathrm{Pl}} = M_{\mathrm{Pl}}/\sqrt{8\pi}$.

mass, we find the following values of the SM parameters:

$$g_1(M_{\rm Pl}) = 0.6168 \tag{2.7a}$$

$$g_2(M_{\rm Pl}) = 0.5057 \tag{2.7b}$$

$$g_3(M_{\rm Pl}) = 0.4873 + 0.0002\,\frac{\alpha_3(M_Z) - 0.1184}{0.0007} \tag{2.7c}$$

$$y_t(M_{\rm Pl}) = 0.3823 + 0.0051\left(\frac{M_t}{\rm GeV} - 173.35\right) - 0.0021\,\frac{\alpha_3(M_Z) - 0.1184}{0.0007} \tag{2.7d}$$

$$\begin{aligned}\lambda(M_{\rm Pl}) = {} & -0.0128 - 0.0065\left(\frac{M_t}{\rm GeV} - 173.35\right) + \\ & +0.0018\,\frac{\alpha_3(M_Z) - 0.1184}{0.0007} + 0.0029\left(\frac{M_h}{\rm GeV} - 125.66\right)\end{aligned} \tag{2.7e}$$

$$\begin{aligned}m(M_{\rm Pl}) = {} & 140.2\,{\rm GeV} + 1.6\,{\rm GeV}\left(\frac{M_h}{\rm GeV} - 125.66\right) + \\ & -0.25\,{\rm GeV}\left(\frac{M_t}{\rm GeV} - 173.35\right) + 0.05\,{\rm GeV}\,\frac{\alpha_3(M_Z) - 0.1184}{0.0007}\end{aligned} \tag{2.7f}$$

All Yukawa couplings, other than the one of the top quark, are very small. This is the well-known flavour problem of the SM, that we will not investigate here.

The three gauge couplings and the top Yukawa coupling remain perturbative and are fairly weak at high energy, becoming roughly equal in the vicinity of the Planck mass. The near equality of the gauge couplings may be viewed as an indicator of an underlying grand unification even within the simple SM, once we allow for threshold corrections of the order of 10% around a scale of about 10^{16} GeV (of course, in the spirit of this paper, we are disregarding the acute naturalness problem). The (properly normalised) hypercharge coupling g_1 becomes the largest coupling in the SM already at scales of about 10^{14} GeV, and the weak coupling g_2 overcomes the strong coupling at about 10^{16} GeV. The top Yukawa becomes smaller than any of the gauge couplings at scales larger than about 10^{10} GeV.

The Higgs quartic coupling remains weak in the entire energy domain below $M_{\rm Pl}$. It decreases with energy crossing $\lambda = 0$ at a scale of about 10^{10} GeV, see fig. 2.2 (upper left). Indeed, λ is the only SM coupling that is allowed to change sign during the RG evolution because it is not multiplicatively renormalised. For all other SM couplings, the β functions are proportional to their respective couplings and crossing zero is not possible. This corresponds to the fact that $\lambda = 0$ is not a point of enhanced symmetry.

In fig. 2.2 (lower left) we compare the size of λ with the top Yukawa coupling y_t and the gauge coupling g_2, choosing a normalisation such that each coupling is equal to the corresponding particle mass, up to the same proportionality constant. In other words, we are plotting the ratios

$$\text{sign}(\lambda) \times \sqrt{4|\lambda|}/y_t \qquad \text{and} \qquad \text{sign}(\lambda) \times \sqrt{8|\lambda|}/g_2\ , \tag{2.8}$$

equal to the ratios of running masses m_h/m_t and m_h/m_W, respectively. Except for the region in which λ vanishes, the Higgs quartic coupling looks fairly "normal" with respect to the other SM couplings. Nonetheless, the RG effect reduces significantly the overall size of λ in its evolution from low to high energy. Although the central values of Higgs and top masses do not favour a scenario with vanishing Higgs self coupling at the Planck scale ($M_{\rm Pl}$) — a possibility originally proposed in ref. [42, 43] and discussed more recently in ref. [33, 44–47] — the smallness of λ around $M_{\rm Pl}$ offers reasons for speculation, as we will discuss later.

Another important feature of the RG evolution of λ is the slowing down of the running at high

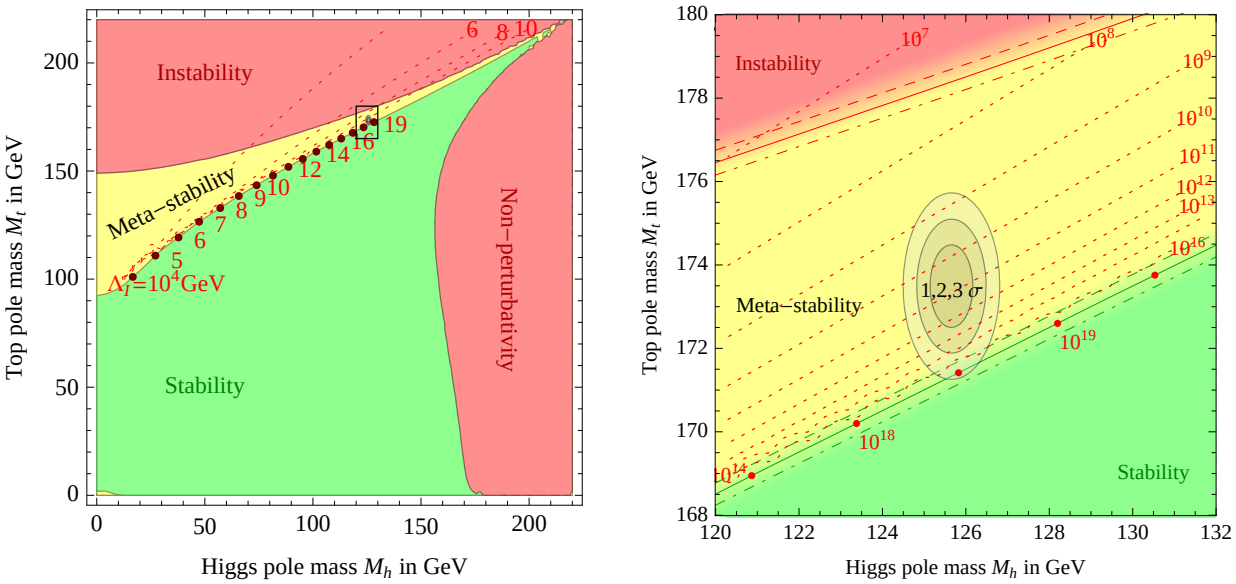

Figure 2.3: **Left**: *SM phase diagram in terms of Higgs and top pole masses. The plane is divided into regions of absolute stability, meta-stability, instability of the SM vacuum, and non-perturbativity of the Higgs quartic coupling. The top Yukawa coupling becomes non-perturbative for* $M_t > 230$ GeV. *The dotted contour-lines show the instability scale* Λ_I *in* GeV *assuming* $\alpha_3(M_Z) = 0.1184$. **Right**: *Zoom in the region of the preferred experimental range of* M_h *and* M_t *(the grey areas denote the allowed region at 1, 2, and 3*σ*). The three boundary lines correspond to 1-*σ *variations of* $\alpha_3(M_Z) = 0.1184 \pm 0.0007$, *and the grading of the colours indicates the size of the theoretical error.*

energy. As shown in fig. 2.2 (upper right), the corresponding Higgs quartic β-function vanishes at a scale of about 10^{17}–10^{18} GeV. In order to quantify the degree of cancellation in the β-function, we plot in fig. 2.2 (lower right) β_λ in units of its pure top contribution. The vanishing of β_λ looks more like an accidental cancellation between various large contributions, rather than an asymptotic approach to zero. Given that the β-functions of the other SM couplings are all different than zero, it is not evident to find valid symmetry or dynamical reasons for the vanishing of β_λ alone near $M_{\rm Pl}$. However, the smallness of β_λ (and λ) at high energy implies that tiny variations of the input values of the couplings at $M_{\rm Pl}$ lead to wide fluctuations of the instability scale, thus justifying our refined calculation.

2.2.2 Derivation of the stability bound

In order to compute the stability bound on the Higgs mass one has to study the full effective potential and identify the critical Higgs field above which the potential becomes smaller than the value at the EW vacuum. We will refer to such critical energy as the instability scale Λ_I.

A first estimate of the instability scale can be obtained by approximating the effective potential with its RG-improved tree level expression.

The SM effective potential is known up to two-loops [12] and for large field values ($h \gg v$), it can be approximated as,

$$V_{\rm eff}^{\rm tree}(h) = \frac{\lambda(\mu)}{4} h^4 \,, \tag{2.9}$$

with $\mu = \mathcal{O}(h)$. In this way the condition of absolute stability of the potential is

$$\lambda(\Lambda) \geq 0$$

for any value Λ up to the Planck scale (as for instance done in [49]). Also, as discussed in [28], the minimum Higgs mass ensuring vacuum stability corresponds to the initial value of λ such that at some scale Λ_0

$$\lambda(\Lambda_0) = \beta_\lambda(\Lambda_0) = 0 \ , \qquad \beta_\lambda = \frac{d}{d\ln\mu}\lambda(\mu) \ . \tag{2.10}$$

Actually a more accurate determination of the minimal M_h is obtained taking into account the full structure of the Higgs potential at the two-loop level. In practice, as pointed out in [33], the determination of M_h obtained by the condition (2.10) differs by about 0.1 GeV from the one determined by the absolute stability of the RG-improved two-loop potential.

One the other hand, if we are also interested in analyzing the shape of the Higgs potential close to the Planck scale and in the scale where the instability occurs (as a function of M_h and M_t), the study of the RG evolution of λ is not sufficient and we need the complete structure of the effective potential at the two-loop level. We can always define an effective coupling $\lambda_{\rm eff}(h)$ such that for $h \gg v$ the two-loop effective potential assumes the form

$$V_{\rm eff}(h) = \lambda_{\rm eff}(h)\frac{h^4}{4}. \tag{2.11}$$

The quantity $\lambda_{\rm eff}$ can be extracted from the effective potential at two loops [12] and is explicitly given in appendix 2.A.3.

2.2.3 The SM phase diagram in terms of Higgs and top masses

The two most important parameters that determine the various EW phases of the SM are the Higgs and top-quark masses. In fig. 2.3 we update the phase diagram given in ref. [33] with our improved calculation of the evolution of the Higgs quartic coupling. The regions of stability, metastability, and instability of the EW vacuum are shown both for a broad range of M_h and M_t, and after zooming into the region corresponding to the measured values. The uncertainty from α_3 and from theoretical errors are indicated by the dashed lines and the colour shading along the borders. Also shown are contour lines of the instability scale Λ_I.

As previously noticed in ref. [33], the measured values of M_h and M_t appear to be rather special, in the sense that they place the SM vacuum in a near-critical condition, at the border between stability and metastability. In the neighbourhood of the measured values of M_h and M_t, the stability condition is well approximated by

$$M_h > 129.6\,\text{GeV} + 2.0(M_t - 173.35\,\text{GeV}) - 0.5\,\text{GeV}\,\frac{\alpha_3(M_Z) - 0.1184}{0.0007} \pm 0.3\,\text{GeV} \ . \tag{2.12}$$

The quoted uncertainty comes only from higher order perturbative corrections. Other non-perturbative uncertainties associated with the relation between the measured value of the top mass and the actual definition of the top pole mass used here (presumably of the order of $\Lambda_{\rm QCD}$) are buried inside the parameter M_t in equation (2.12). For this reason we include a theoretical error in the top pole mass and take $M_t = (173.35 \pm 0.65_{\rm exp} \pm 0.3_{\rm th})\,\text{GeV}$. Combining in quadrature theoretical uncertainties with experimental errors, we find

$$M_h > (129.6 \pm 1.5)\,\text{GeV} \qquad \text{(stability condition)}. \tag{2.13}$$

From this result we conclude that vacuum stability of the SM up to the Planck scale is excluded at 2.5σ (99.3% C.L. one-sided). Since the main source of uncertainty in equation (2.12) comes from M_t,

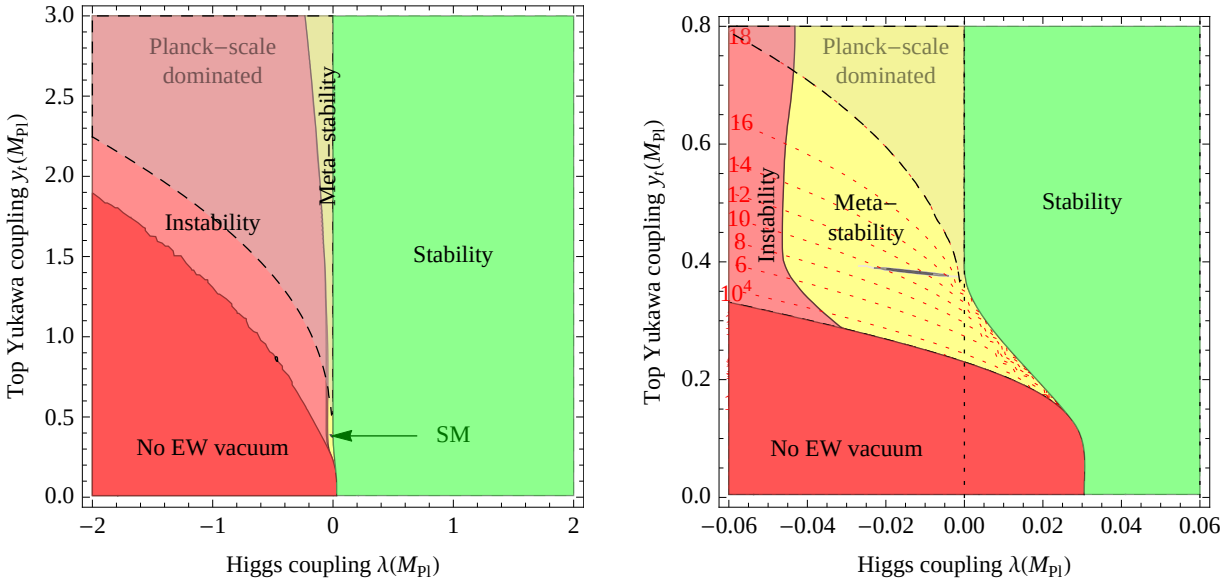

Figure 2.4: **Left**: *SM phase diagram in terms of quartic Higgs coupling λ and top Yukawa coupling y_t renormalised at the Planck scale. The region where the instability scale Λ_I is larger than 10^{18} GeV is indicated as 'Planck-scale dominated'.* **Right**: *Zoom around the experimentally measured values of the couplings, which correspond to the thin ellipse roughly at the centre of the panel. The dotted lines show contours of Λ_I in* GeV.

any refinement in the measurement of the top mass is of great importance for the question of EW vacuum stability.

Since the experimental error on the Higgs mass is already fairly small and will be further reduced by future LHC analyses, it is becoming more appropriate to express the stability condition in terms of the pole top mass. We can express the stability condition of equation (2.12) as

$$M_t < (171.36 \pm 0.15 \pm 0.25_{\alpha_3} \pm 0.17_{M_h})\,\text{GeV} = (171.36 \pm 0.46)\,\text{GeV} \tag{2.14}$$

In the latter equation we combined in quadrature the theoretical uncertainty with the experimental uncertainties on M_h and α_3.

Notice that the stability bound is scheme and gauge independent. While intermediate steps of the computation (threshold corrections, higher-order RG equations, and the effective potential) are scheme-dependent, the values of the effective potential at its local minima are scheme-independent physical observables, and thus the stability condition has the same property.

We find that the instability scale (defined as the scale at which $\lambda_{\rm eff}$ vanishes) is

$$\log_{10}\frac{\Lambda_I}{\text{GeV}} = 11.0 + 0.8\left(\frac{M_h}{\text{GeV}} - 125.66\right) - 1.4\left(\frac{M_t}{\text{GeV}} - 173.35\right) + 0.3\,\frac{\alpha_3(M_Z) - 0.1184}{0.0007} \tag{2.15}$$

The scale Λ_0 at which the $\overline{\rm MS}$ running coupling λ vanishes is a scheme-dependent quantity and is slightly smaller than the scale Λ_I. We find $\Lambda_0 \approx 0.15\Lambda_I$, with the same dependence on the SM parameters as in equation (2.15).

2.2.4 The SM phase diagram in terms Planck-scale couplings

The discovery of the SM near-criticality has led to many theoretical speculations [28,33,46,47,50–71]. In order to address such speculations and to investigate if the measured value of M_h is really special in the SM, it is more appropriate to study the phase diagram in terms of the Higgs quartic and the top Yukawa coupling evaluated at some high-energy scale, rather than at the weak scale. This is because of our theoretical bias that the SM is eventually embedded into a new framework at short distances, possibly as short as the Planck length. Therefore, it is more likely that information about the underlying theory is directly encoded in the high-energy coupling constants. For this reason in fig. 2.4 we recast the phase diagram of fig. 2.3 in terms of $\lambda(M_{\rm Pl})$ and $y_t(M_{\rm Pl})$. The diagram is shown in a broad range of couplings allowed by perturbativity, and also after zooming into the interesting region. The new area denoted as 'no EW vacuum' corresponds to a situation in which λ is negative at the weak scale, and therefore the usual Higgs vacuum does not exist. In the region denoted as 'Planck-scale dominated' the instability scale Λ_I is larger than 10^{18} GeV. In this situation we expect that both the Higgs potential and the tunnelling rate receive large gravitational corrections and any assessment about vacuum stability becomes unreliable.

From the left panel of fig. 2.4 it is evident that, even when we consider the situation in terms of high-energy couplings, our universe appears to live under very special conditions. The interesting theoretical question is to understand if the apparent peculiarity of $\lambda(M_{\rm Pl})$ and $y_t(M_{\rm Pl})$ carry any important information about phenomena well beyond the reach of any collider experiment. Of course this result could be just an accidental coincidence, because in reality the SM potential is significantly modified by new physics at low or intermediate scales. Indeed, the Higgs naturalness problem corroborates this possibility. However, both the reputed violation of naturalness in the cosmological constant and the present lack of new physics at the LHC cast doubts on the validity of the naturalness criterion for the Higgs boson. Of course, even without a natural EW sector, there are good reasons to believe in the existence of new degrees of freedom at intermediate energies. Neutrino masses, dark matter, axion, inflation, baryon asymmetry provide good motivations for the existence of new dynamics below the Planck mass. However, for each of these problems we can imagine solutions that either involve physics well above the instability scale or do not significantly modify the shape of the Higgs potential. As a typical example, take the see-saw mechanism. As shown in ref. [51], for neutrino masses smaller than 0.1 eV (as suggested by neutrino-oscillation data without mass degeneracies), either neutrino Yukawa couplings are too small to modify the running of λ or the right-handed neutrino masses are larger than the instability scale. In other words, a see-saw neutrino does not modify our conclusions about stability of the EW vacuum. Couplings of weak-scale dark matter to the Higgs boson are constrained to be small by WIMP direct searches (although dark-matter particles with weak interactions would modify the running of the weak gauge couplings, making the Higgs potential more stable).

Thus, it is not inconceivable that the special values of $\lambda(M_{\rm Pl})$ and $y_t(M_{\rm Pl})$ carry a significance and it is worth to investigate their consequences. In the next section we discuss several possible classes of solutions that explain the apparent peculiarity of the SM parameters.

2.3 More on SM phase diagrams

2.3.1 The SM phase diagram in terms of gauge couplings

So far we have been studying the phase diagram in terms of Higgs and top masses or couplings, keeping the other SM parameters fixed. This is reasonable, since the EW vacuum is mostly influenced by the Higgs and top quark. However it is interesting to study how the scan of other parameters can affect

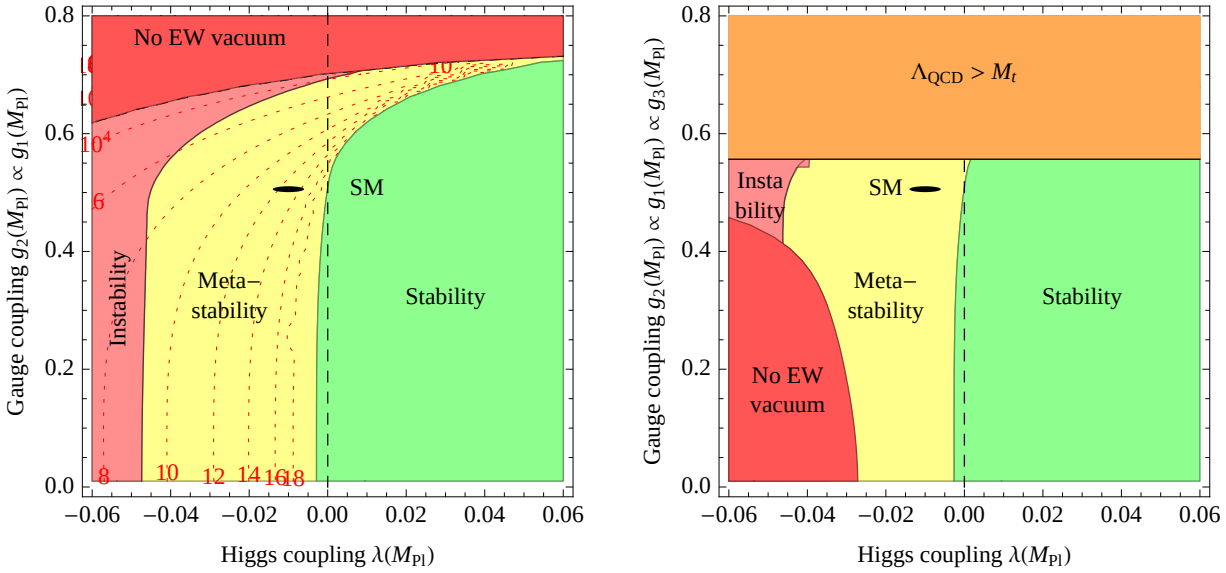

Figure 2.5: *SM phase diagram in terms of the Higgs quartic coupling $\lambda(M_{\rm Pl})$ and of the gauge coupling $g_2(M_{\rm Pl})$.* **Left***: A common rescaling factor is applied to the electro-weak gauge couplings g_1 and g_2, while g_3 is kept constant.* **Right***: A common rescaling factor is applied to all SM gauge couplings g_1, g_2, g_3, such that a 10% increase in the strong gauge coupling at the Planck scale makes $\Lambda_{\rm QCD}$ larger than the weak scale. The measured values of the couplings correspond to the small ellipse marked as 'SM'.*

our results.

We start by considering the scanning of weak couplings defined at some high-energy scale, which we identify with $M_{\rm Pl}$. The impact of the gauge couplings g_1 and g_2 can be understood from the leading terms of the RG equation for the Higgs quartic coupling

$$(4\pi)^2 \frac{d\lambda}{d\ln\bar{\mu}^2} = -3y_t^4 + 6y_t^2\lambda + 12\lambda^2 + \frac{9}{16}\left(g_2^4 + \frac{2}{5}g_2^2g_1^2 + \frac{3}{25}g_1^4\right) - \frac{9}{2}\lambda\left(g_2^2 + \frac{g_1^2}{5}\right) + \cdots . \qquad (2.16)$$

For small $\lambda(M_{\rm Pl})$, the weak gauge couplings have the effect of reducing even further the Higgs quartic coupling in its evolution towards lower energies, thus contributing to destabilise the potential. For large $\lambda(M_{\rm Pl})$, they tend to make λ grow at lower energy.

We quantify the situation by plotting in fig. 2.5 (left) the SM phase diagram in terms of $\lambda(M_{\rm Pl})$ and $g_2(M_{\rm Pl})$. For simplicity, we scan over the hypercharge coupling $g_1(M_{\rm Pl})$ by keeping fixed the ratio $g_1(M_{\rm Pl})/g_2(M_{\rm Pl}) = 1.22$ as in the SM, while $y_t(M_{\rm Pl})$ and $g_3(M_{\rm Pl})$ are held to their SM values. As in previous cases, also the phase diagram in terms of weak gauge couplings shows the peculiar characteristic of the SM parameters to live close to the phase boundary. (Note that the figure is zoomed around the region of the physical values, so that the proximity to the boundary is not emphasised.)

Figure 2.5 (left) shows that the weak gauge couplings in the SM lie near the maximum possible values that do not lead to a premature decay of the EW vacuum. Were g_2 and g_1 50% larger than their actual values, we wouldn't be here speculating on the peculiarity of the Higgs mass.

Next, we discuss the impact of scanning the strong gauge coupling constant. In fig. 2.5 (right) we show the phase diagram in the plane $\lambda(M_{\rm Pl})$, $g_2(M_{\rm Pl})$, obtained by varying all three gauge couplings by a common rescaling factor. The top Yukawa coupling $y_t(M_{\rm Pl})$ is held fixed at its SM value and so, as the other couplings scan, the top mass does not correspond to the measured value.

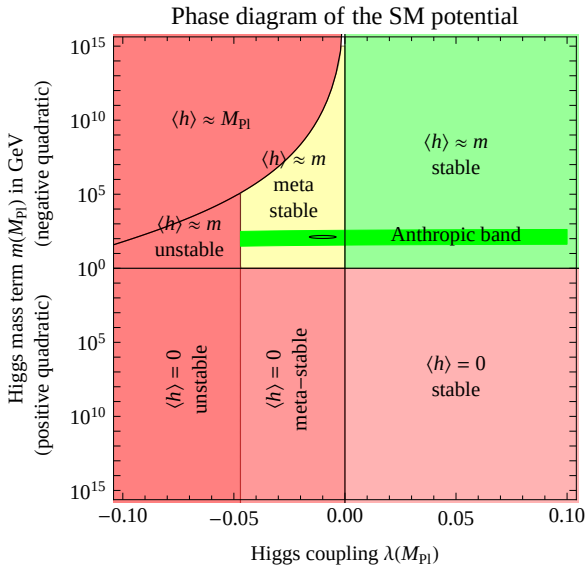

Figure 2.6: *Phase diagram of the SM in terms of the parameters of the Higgs potential evaluated at the Planck scale. In the metastability region, there is an upper bound on m from the requirement of a Higgs vacuum at a finite field value. The green region is simple thanks to the fact that* $\beta(\lambda) = 0$ *at* $M_{\rm Pl}$*. On the vertical axis we plot* $|m(M_{\rm Pl})|$*, in the case of negative (above) and positive (below) Higgs quadratic term.*

The coupling g_3 affects β_λ only at two loops, but it has a more important role in the RG evolution of the top Yukawa coupling, whose leading terms are given by

$$(4\pi)^2 \frac{dy_t^2}{d\ln\bar{\mu}^2} = y_t^2\left(\frac{9}{2}y_t^2 - 8g_3^2 - \frac{9}{4}g_2^2 - \frac{17}{20}g_1^2\right) + \cdots . \tag{2.17}$$

When the value of g_3 is reduced at fixed $y_t(M_{\rm Pl})$, the low-energy top Yukawa coupling becomes smaller. This reduces the stabilising effect of the top for a given $\lambda(M_{\rm Pl})$ and explains the appearance in fig. 2.5 (right) at small gauge couplings of a 'No EW vacuum' region (where λ is negative at the weak scale).

On the other hand, when g_3 is increased, the value of $\Lambda_{\rm QCD}$ grows rapidly. Whenever

$$\alpha_3(M_{\rm Pl}) > \frac{6\pi}{21\ln(M_{\rm Pl}/M_t)}, \tag{2.18}$$

which corresponds to $g_3(M_{\rm Pl}) > 0.54$, the value of $\Lambda_{\rm QCD}$ becomes larger than M_t, preventing a perturbative extrapolation from the Planck to the weak scale. As shown in fig. 2.5 (right), this region is reached as soon as the SM gauge couplings are increased by only 11%. Once again, the SM gauge couplings live near the top of the range allowed by simple extrapolations of the minimal theory.

2.3.2 The SM phase diagram in terms of Higgs potential parameters

The Higgs mass parameter m in the Higgs potential is the origin of the well-known naturalness problem. Here we show that the simple requirement of the existence of a non-trivial EW vacuum sets an upper bound on m, which is completely independent of any naturalness argument.

Let us start by considering the tree-level Higgs potential

$$V_0 = -\frac{m_0^2}{2}|H_0|^2 + \lambda_0|H_0|^4 . \tag{2.19}$$

For $m^2 > 0$ and $\lambda > 0$, the potential has the usual non-trivial vacuum at $\langle h \rangle = v = m/\sqrt{2\lambda}$. However, since v is proportional to m and λ is negative above the instability scale Λ_I, the Higgs vacuum at finite field value no longer exists when m^2 is too large. The upper bound on m^2 can be estimated by considering the minimisation condition of the potential, including only the logarithmic running of λ, but neglecting the evolution of m (which is a good approximation, as shown in fig. 2.1):

$$\left[2\lambda(v) + \frac{\beta_\lambda(v)}{2}\right] v^2 = m^2. \tag{2.20}$$

For values of v in the neighbourhood of Λ_I, we can approximate[1] $\lambda(v) \approx \beta_\lambda(\Lambda_I) \ln v/\Lambda_I$ and $\beta_\lambda(v) \approx \beta_\lambda(\Lambda_I)$. Then we see that equation (2.20) has a solution only if

$$m^2 < -\beta_\lambda(\Lambda_I)\, e^{-3/2} \Lambda_I^2. \tag{2.21}$$

Note that $\beta_\lambda(\Lambda_I)$ is negative in the SM.

Figure 2.6 shows the SM phase diagram in terms of the parameters $\lambda(M_{\rm Pl})$ and $m(M_{\rm Pl})$. The sign of each one of these parameters corresponds to different phases of the theory, such that $\lambda(M_{\rm Pl}) = m(M_{\rm Pl}) = 0$ is a tri-critical point.

The region denoted by '$\langle h \rangle \approx M_{\rm Pl}$' corresponds to the case in which equation (2.21) is not satisfied and there is no SM-like vacuum, while the Higgs field slides to large values. In the region of practical interest, the upper limit on m is rather far from its actual physical value $m = M_h$, although it is much stronger than $M_{\rm Pl}$, the ultimate ultraviolet cutoff of the SM. A much more stringent bound on m can be derived from anthropic considerations [72] and the corresponding band in parameter space is shown in fig. 2.6. We find it remarkable that the simple request of the existence of a non-trivial Higgs vacuum, without any reference to naturalness considerations, gives a bound on the Higgs bilinear parameter m. Unfortunately, for the physical value of λ, the actual numerical value of the upper bound is not of great practical importance.

2.3.3 Lifetime of the SM vacuum

The measured values of M_h and M_t indicate that the SM Higgs vacuum is not the true vacuum of the theory and that our universe is potentially unstable. The rate of quantum tunnelling out of the EW vacuum is given by the probability $d\wp/dV\, dt$ of nucleating a bubble of true vacuum within a space volume dV and time interval dt [73–75]

$$d\wp = dt\, dV\ \Lambda_B^4\, e^{-S(\Lambda_B)}\,. \tag{2.22}$$

In equation (2.22), $S(\Lambda_B)$ is the action of the bounce of size $R = \Lambda_B^{-1}$, given by

$$S(\Lambda_B) = \frac{8\pi^2}{3|\lambda(\Lambda_B)|}. \tag{2.23}$$

At the classical level, the Higgs theory with only quartic coupling is scale-invariant and the size of the bounce Λ_B^{-1} is arbitrary. The RG flow breaks scale invariance and the tree level action gets replaced by the one-loop action, as calculated in ref. [49]. Then, Λ_B is determined as the scale at which $\Lambda_B^4 e^{-S(\Lambda_B)}$ is maximised. In practice this roughly amounts to minimising $\lambda(\Lambda_B)$, which corresponds to the condition $\beta_\lambda(\Lambda_B) = 0$. As long as $\Lambda_B \ll M_{\rm Pl}$, gravitational effects are irrelevant, since corrections

[1] In this analysis, we can safely neglect the non-logarithmic corrections to the effective potential and so we do not distinguish between λ and $\lambda_{\rm eff}$.

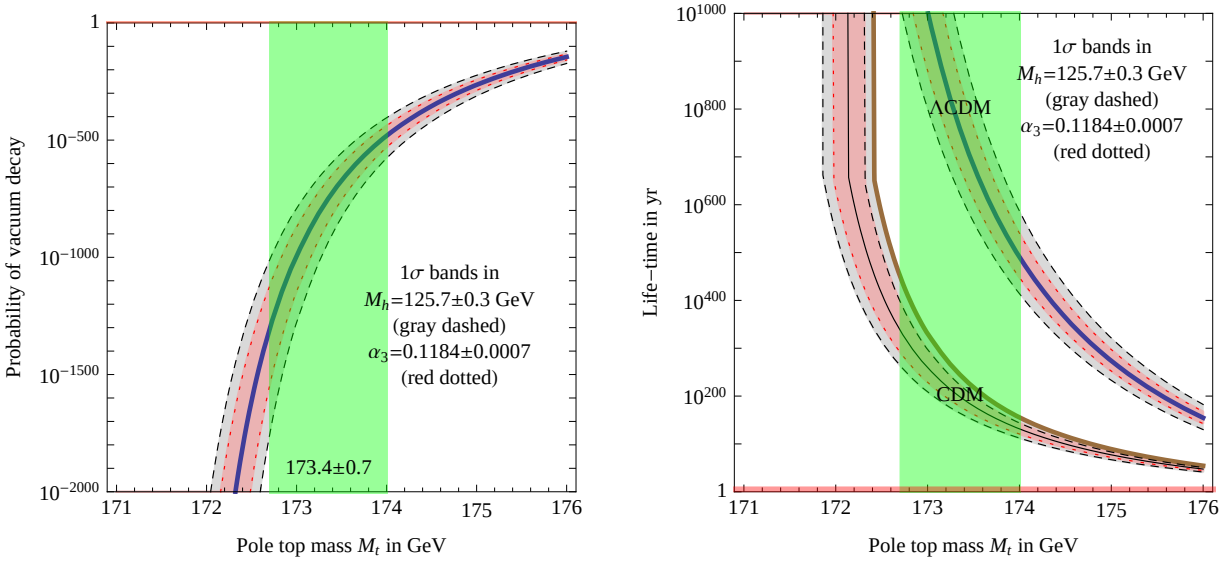

Figure 2.7: **Left:** *The probability that electroweak vacuum decay happened in our past light-cone, taking into account the expansion of the universe.* **Right***: The life-time of the electroweak vacuum, with two different assumptions for future cosmology: universes dominated by the cosmological constant (*Λ*CDM) or by dark matter (CDM).*

to the action in minimal Einstein gravity are given by $\delta S_G = 256\pi^3\Lambda_B^2/45|\lambda|M_{\rm Pl}^2$ [45]. The effect of gravitational corrections is to slow down the tunnelling rate [76]. Whenever $\Lambda_B > M_{\rm Pl}$, one can only obtain a lower bound on the tunnelling probability by setting $\lambda(\Lambda_B) = \lambda(M_{\rm Pl})$. For the physical values of M_h and M_t, our results are fairly insensitive to Planckian dynamics.

The total probability $\wp$ for vacuum decay to have occurred during the history of the universe can be computed by integrating equation (2.22) over the space-time volume of our past light-cone,

$$\int dt\, dV = \int_0^{t_0} dt \int_{|x|<a(\eta_0-\eta)} d^3x = \frac{4\pi}{3}\int_0^{\eta_0} d\eta\, a^4(\eta_0-\eta)^3 \approx \frac{0.15}{H_0^4}. \tag{2.24}$$

Here a is the scale factor, η is conformal time ($d\eta/dt = 1/a$), $\eta_0 \approx 3.4/H_0$ is the present conformal time and $H_0 \approx 67.4\,$km/sec Mpc is the present Hubble rate. Equation (2.24) roughly amounts to saying that the 'radius' of the universe is given by cT_U, where $T_U \approx 0.96/H_0$ is the present age. The present value of the vacuum-decay probability $\wp$ is

$$\wp_0 = 0.15\,\frac{\Lambda_B^4}{H_0^4}\,e^{-S(\Lambda_B)}\,, \tag{2.25}$$

and is dominated by late times and this makes our result more robust, since it is independent of the early cosmological history. In fig. 2.7a we plot, as a function of the top mass, the probability $\wp_0$ that the EW vacuum had decayed during the past history of the universe. We find that the probability is spectacularly small, as a consequence of the proximity of the SM parameters to the boundary with the region of absolute stability.

The lifetime of the present EW vacuum $\tau_{\rm EW}$ depends on the future cosmological history. If dark energy shuts off and the future universe is matter dominated, the space-time volume of the past

light-cone at time t_0 is given by

$$\int dt\, dV = \frac{4\pi}{3}\int_0^{\eta_0} d\eta\, a^4(\eta_0-\eta)^3 = \frac{16\,\pi}{1485\,H_0^4}. \tag{2.26}$$

Here H_0 is the Hubble parameter at time t_0, and we have performed the integral using the relations $a^{1/2} = H_0\eta/2 = (3H_0t/2)^{1/3}$ and $t_0 = 2/(3H_0)$, valid in a matter-dominated flat universe. The lifetime $\tau_{\rm EW}$ is given by the time at which $\wp = 1$:

$$\tau_{\rm EW} = \left(\frac{55}{3\pi}\right)^{1/4}\frac{e^{S(\Lambda_B)/4}}{\Lambda_B} \approx \frac{T_U}{\wp_0^{1/4}} \qquad \text{(Matter Domination)}, \tag{2.27}$$

where $\wp_0$ is given in equation (2.25) and shown in fig. 2.7a.

If instead the universe keeps being accelerated by the cosmological constant, entering into a de Sitter phase with Hubble constant $H = H_0\sqrt{\Omega_\Lambda}$, at a time t_0 in the far future the volume of the past light-cone will be

$$\int dt\; dV = \frac{4\pi}{3}\int_0^{\eta_0} d\eta\, a^4(\eta_0-\eta)^3 = \frac{4\pi}{3H^4}\left[Ht_0 - \frac{11}{6} + \mathcal{O}(e^{-Ht_0})\right]. \tag{2.28}$$

Here we have used the relations $a = (1-H\eta)^{-1} = e^{Ht}$, valid in a vacuum-energy dominated universe. The lifetime $\tau_{\rm EW}$ is now equal to

$$\tau_{\rm EW} = \frac{3H^3e^{S(\Lambda_B)}}{4\pi\Lambda_B^4} \approx \frac{0.02\;T_U}{\wp_0} \qquad \text{(Vacuum Energy Domination)}. \tag{2.29}$$

The lifetime of the present EW vacuum is plotted in fig. 2.7b in both cases of matter or vacuum-energy domination. As shown, the SM vacuum is likely to survive for times that are enormously longer than any significant astrophysical age (*e.g.* the sun will exhaust its fuel in about five billion years).

2.4 Interpretations of the high-energy SM couplings

We conclude this chapter with some possible interpretations of the measured values of the SM parameters. As we said before, if the SM remains valid at high energies, the SM parameters, in particular λ and y_t, put the EW vacuum in a near-critical meta-stable condition. It is natural to ask if this is the result of some kind of unknown dynamics. In particular one can speculate that the special value of the Higgs quartic coupling is due to a matching condition with some high-energy theory in the vicinity of $M_{\rm Pl}$. On the other hand more "exotic" explanations can not be excluded, such as that of "multiverse" dynamics. Here we will report a couple of possible interpretations, presented in [1] (we refer to that paper for further details).

2.4.1 Matching conditions

It is not difficult to imagine theories able to drive $\lambda(M_{\rm Pl})$ to zero: high-scale supersymmetry with $\tan\beta = 1$ [77–82]; partial $N = 2$ supersymmetry insuring D-flatness [83,84]; an approximate Goldstone or shift symmetry [85, 86]; an infrared fixed-point of some transplanckian physics [47]; a power-law running in a quasi-conformal theory.

Present data suggest that an exact zero of λ is reached at scales of about 10^{10}–10^{12} GeV, see eq (2.15), well below the Planck mass. It is not difficult to imagine theories that give $\lambda(M_{\rm Pl})$ in

agreement with equation (2.7e) as a result of a vanishing matching condition modified by threshold corrections.

Supersymmetry is probably one of the best candidates able to explain the vanishing of λ as a high-energy boundary condition, because of the natural appearance of radiatively-stable flat directions. Such flat directions give a well-grounded justification for scalar particles with vanishing potentials, and yet interacting at zero momentum (contrary to the case of Goldstone bosons).

Note also that the smallness of the Higgs quartic β-function at high energy is the key ingredient that allows for the possibility of extending the SM up to a matching scale much larger than Λ_I. If λ ran fast above Λ_I, it would rapidly trigger vacuum instability and the region of metastability would be limited to SM cut-off scales only slightly larger than Λ_I. This is another peculiarity of the measured values of M_h and M_t.

2.4.2 Criticality as an attractor

Statistical properties of the multiverse offer alternatives to dynamical determinations of $\lambda(M_{\rm Pl})$ from matching conditions with new theories. This possibility is motivated by the observation that the measured value of M_h looks special, in the sense that it corresponds to a near-critical parameter separating two phases. As remarked in ref. [87], also Higgs naturalness can be viewed as a problem of near-criticality between two phases (*i.e.* why is the Higgs bilinear carefully selected just to place our universe at the edge between the broken and unbroken EW phases?). This leads to the speculation that, within the multiverse, critical points are attractors. If this vision is correct, the probability density in the multiverse is peaked around the boundaries between different phases, and generic universes are likely to live near critical lines. Then, near-criticality would be the result of probability distributions in the multiverse, and would not necessarily follow from anthropic considerations. In this picture, the Higgs parameters found in our universe are not at all special. On the contrary, they correspond to the most likely occurrence in the multiverse.

Suppose that the probability distribution of the Higgs quartic coupling in the multiverse is not uniform, but is a monotonically decreasing function of λ. In other words, there is a pressure in the multiverse towards the smallest (possibly negative) λ. However, in universes where λ is sufficiently negative, the Higgs field is destabilised, forming a bubble of AdS space with a negative cosmological constant of order $-M_{\rm Pl}^4$ in its interior. Such regions of space would rapidly contract and finally disappear. Therefore, the cosmological evolution removes regions that correspond to unstable EW vacua, leaving the vast majority of universes crowded around the critical boundary.

We can also imagine alternative scenarios. Suppose that the Higgs quartic coupling is a function of some new fields Φ participating in Planckian dynamics and that their vacuum structure prefers low values of λ, as before. Once λ becomes smaller than the critical value, the Higgs potential develops an instability at large field values. If tunnelling is sufficiently fast, the Higgs field slides towards Planckian scales. Such large Higgs configurations will in general affect the scalar potential of the fields Φ, which will readjust into a different vacuum structure. The new vacua will give a different probability distribution for the Higgs quartic coupling λ and it is imaginable that now larger values of λ are preferred. In summary: universes in the stable or metastable phases will experience pressure towards small λ; universes in the unstable phase will experience pressure towards large λ. As a result, the most probable universes lie around the critical line separating the two phases.

We stress that these examples do not use anthropic arguments: near-criticality is achieved by cosmological selection and/or by probability distributions in the multiverse.

2.A Appendix

2.A.1 Weak scale thresholds at one loop

We summarise here the one-loop corrections $\theta^{(1)}$ to the various SM parameters

$$\theta = \{\lambda, m, y_t, g_2, g_Y\} = \theta^{(0)} + \theta^{(1)} + \theta^{(2)} + \cdots . \tag{2.30}$$

We perform one-loop computations in a generic ξ gauge, confirming that $\theta^{(1)}$ is gauge-independent, as it should. Our expressions for $\theta^{(1)}$ are equivalent to the well known expressions in the literature. We write $\theta^{(1)}$ in terms of finite parts of the the Passarino-Veltman functions

$$A_0(M) = M^2(1 - \ln\frac{M^2}{\bar{\mu}^2}), \qquad B_0(p; M_1, M_2) = -\int_0^1 \ln\frac{xM_1^2 + (1-x)M_2^2 - x(1-x)p^2}{\bar{\mu}^2}dx. \tag{2.31}$$

The dependence of $\theta^{(1)}$ on the renormalisation scale $\bar{\mu}$ reproduces the well known one-loop RGE equations for θ. Below we report the expressions valid in the limit $M_b = M_\tau = 0$; the negligible effect of light fermions masses is included in our full code.

The Higgs mass term

The correction is obtained from equation (3.69):

$$\begin{aligned}\delta^{(1)}m^2(\bar{\mu}) &= \frac{1}{(4\pi)^2V^2}\mathrm{Re}\Big[6M_t^2(M_h^2 - 4M_t^2)B_0(M_h; M_t, M_t) + 24M_t^2A_0(M_t) + \\ &+(M_h^4 - 4M_h^2M_W^2 + 12M_W^4)B_0(M_h; M_W, M_W) - 2(M_h^2 + 6M_W^2)A_0(M_W) + \\ &+\frac{1}{2}\left(M_h^4 - 4M_h^2M_Z^2 + 12M_Z^4\right)B_0(M_h; M_Z, M_Z) - (M_h^2 + 6M_Z^2)A_0(M_Z) + \\ &+\frac{9}{2}M_h^4B_0(M_h; M_h, M_h) - 3M_h^2A_0(M_h)\Big].\end{aligned} \tag{2.32}$$

The quartic Higgs coupling

The one-loop result is obtained from equation (3.67):

$$\begin{aligned}\lambda^{(1)}(\bar{\mu}) &= \frac{1}{(4\pi)^2V^4}\mathrm{Re}\Big[3M_t^2(M_h^2 - 4M_t^2)B_0(M_h; M_t, M_t) + 3M_h^2A_0(M_t) + \\ &+\frac{1}{4}\left(M_h^4 - 4M_h^2M_Z^2 + 12M_Z^4\right)B_0(M_h; M_Z, M_Z) + \frac{M_h^2(7M_W^2 - 4M_Z^2)}{2(M_Z^2 - M_W^2)}A_0(M_Z) + \\ &+\frac{1}{2}(M_h^4 - 4M_h^2M_W^2 + 12M_W^4)B_0(M_h; M_W, M_W) - \frac{3M_h^2M_W^2}{2(M_h^2 - M_W^2)}A_0(M_h) + \\ &+\frac{M_h^2}{2}\left(-11 + \frac{3M_h^2}{M_h^2 - M_W^2} - \frac{3M_W^2}{M_Z^2 - M_W^2}\right)A_0(M_W) + \\ &+\frac{9}{4}M_h^4B_0(M_h; M_h, M_h) + \frac{1}{4}(M_h^4 + M_h^2(M_Z^2 + 2M_W^2 - 6M_t^2) - 8(M_Z^4 + 2M_W^4))\Big].\end{aligned} \tag{2.33}$$

Each one of the terms in equation (3.67) is gauge dependent, e.g. the one-loop correction to muon decay is

$$\begin{aligned}\Delta r_0^{(1)}\Big|_{\text{fin}} &= \frac{1}{(4\pi V)^2}\Big[3M_t^2 - M_W^2 - \frac{M_Z^2}{2} - \frac{M_h^2}{2} + \frac{3M_W^2 A_0(M_h)}{M_h^2 - M_W^2} + \frac{6M_W^2 - 3M_Z^2}{M_W^2 - M_Z^2}A_0(M_Z) + \\ &\quad -6A_0(M_t) + \left(9 - \frac{3M_h^2}{M_h^2 - M_W^2} - \frac{3M_W^2}{M_W^2 - M_Z^2}\right)A_0(M_W) + 2A_0(\sqrt{\xi}M_W) + A_0(\sqrt{\xi}M_Z)\Big].\end{aligned} \tag{2.34}$$

and the gauge dependence cancels out in the sum $\lambda^{(1)}(\bar{\mu})$.

The top Yukawa coupling

The gauge-invariant one-loop correction to the top Yukawa coupling is obtained from equation (3.73)

$$\begin{aligned}y_t^{(1)}(\bar{\mu}) &= \frac{M_t}{\sqrt{2}V^3(4\pi)^2}\text{Re}\Big[-\left(M_h^2 - 4M_t^2\right)B_0\left(M_t; M_h, M_t\right) + \\ &\quad + \frac{M_t^2\left(80M_W^2M_Z^2 - 64M_W^4 - 7M_Z^4\right) + 40M_W^2M_Z^4 - 32M_W^4M_Z^2 - 17M_Z^6}{9M_t^2M_Z^2}B_0\left(M_t; M_t, M_Z\right) + \\ &\quad + \frac{\left(M_t^2M_W^2 + M_t^4 - 2M_W^4\right)}{M_t^2}B_0\left(M_t; 0, M_W\right) + \\ &\quad + \left(\frac{3M_h^2}{M_h^2 - M_W^2} + \frac{2M_W^2}{M_t^2} + \frac{3M_W^2}{M_W^2 - M_Z^2} - 10\right)A_0\left(M_W\right) + \left(\frac{3M_W^2}{M_W^2 - M_h^2} + 1\right)A_0\left(M_h\right) + \\ &\quad + \frac{\left(36M_t^2M_Z^2 - 56M_W^2M_Z^2 + 64M_W^4 - 17M_Z^4\right)}{9M_t^2M_Z^2}A_0\left(M_t\right) + \\ &\quad + \left(\frac{3M_W^2}{M_Z^2 - M_W^2} + \frac{32M_W^4 - 40M_W^2M_Z^2 + 17M_Z^4}{9M_t^2M_Z^2} - 3\right)A_0\left(M_Z\right) + \\ &\quad + \frac{M_h^2}{2} - 3M_t^2 - 9M_W^2 + \frac{7M_Z^2}{18} + \frac{64M_W^2}{9M_Z^2}\Big] + \frac{M_t}{\sqrt{2}V(4\pi)^2}g_3^2\left(-\frac{8A_0\left(M_t\right)}{M_t^2} - \frac{8}{3}\right).\end{aligned} \tag{2.35}$$

The weak gauge couplings

The one-loop correction to the $\text{SU}(2)_L$ gauge coupling is obtained from equation (3.75):

$$\begin{aligned}g_2^{(1)}(\bar{\mu}) &= \frac{2M_W}{(4\pi)^2V^3}\text{Re}\Big[\left(\frac{M_h^4}{6M_W^2} - \frac{2M_h^2}{3} + 2M_W^2\right)B_0\left(M_W, M_h, M_W\right) + \\ &\quad + \left(-\frac{M_t^4}{M_W^2} - M_t^2 + 2M_W^2\right)B_0\left(M_W, 0, M_t\right) + \\ &\quad + \frac{1}{6}\left(-\frac{48M_W^4}{M_Z^2} + \frac{M_Z^4}{M_W^2} - 68M_W^2 + 16M_Z^2\right)B_0\left(M_W, M_W, M_Z\right) + \\ &\quad + \frac{1}{6}\left(M_h^2\left(\frac{9}{M_h^2 - M_W^2} + \frac{1}{M_W^2}\right) + \frac{M_Z^2}{M_W^2} + M_W^2\left(\frac{9}{M_W^2 - M_Z^2} + \frac{48}{M_Z^2}\right) - 27\right)A_0\left(M_W\right) + \\ &\quad + \left(2 - \frac{M_h^2\left(M_h^2 + 8M_W^2\right)}{6M_W^2\left(M_h^2 - M_W^2\right)}\right)A_0\left(M_h\right) + \left(\frac{M_t^2}{M_W^2} + 1\right)A_0\left(M_t\right) + \\ &\quad + \frac{1}{6}\left(\frac{24M_W^2}{M_Z^2} - \frac{M_Z^2}{M_W^2} + \frac{9M_W^2}{M_Z^2 - M_W^2} - 17\right)A_0\left(M_Z\right) + \\ &\quad + \frac{1}{36}\left(-3M_h^2 + 18M_t^2 + \frac{288M_W^4}{M_Z^2} - 374M_W^2 - 3M_Z^2\right)\Big].\end{aligned} \tag{2.36}$$

The one-loop correction to the $\mathrm{U}(1)_\mathrm{Y}$ gauge coupling is obtained from equation (3.77):

$$
\begin{aligned}
g_Y^{(1)}(\bar{\mu}) \;=\; & \frac{2\sqrt{M_Z^2-M_W^2}}{(4\pi)^2 V^3}\mathrm{Re}\left[\left(\frac{88}{9}-\frac{124M_W^2}{9M_Z^2}+\frac{M_h^2+34M_W^2}{6(M_Z^2-M_W^2)}\right)A_0\left(M_Z\right)+\right.\\
& +\frac{M_h^2-4M_W^2}{2(M_h^2-M_W^2)}A_0\left(M_h\right)+\left(-\frac{7}{9}-\frac{M_t^2}{M_Z^2-M_W^2}+\frac{64M_W^2}{9M_Z^2}\right)A_0\left(M_t\right)+\\
& +\frac{M_h^4+2M_W^2(M_W^2-15M_Z^2)+3M_H^2(2M_W^2+7M_Z^2)}{6\left(M_h^2-M_W^2\right)\left(M_W^2-M_Z^2\right)}A_0\left(M_W\right)+\\
& -\frac{M_t^4+M_W^2M_t^2-2M_W^4}{M_W^2-M_Z^2}B_0\left(M_W,0,M_t\right)-\frac{M_h^4-4M_Z^2M_h^2+12M_Z^4}{6(M_W^2-M_Z^2)}B_0\left(M_Z,M_h,M_Z\right)+\\
& +\frac{M_h^4-4M_W^2M_h^2+12M_W^4}{6(M_W^2-M_Z^2)}B_0\left(M_W,M_h,M_W\right)+\\
& +\frac{M_Z^6-48M_W^6-68M_Z^2M_W^4+16M_Z^4M_W^2}{6M_Z^2\left(M_W^2-M_Z^2\right)}B_0\left(M_W,M_W,M_Z\right)+\\
& +\frac{1}{9}\left(-23M_W^2+7M_t^2+17M_Z^2-\frac{64M_t^2M_W^2}{M_Z^2}-\frac{9M_W^2(M_t^2-M_W^2)}{M_Z^2-M_W^2}\right)B_0\left(M_Z,M_t,M_t\right)+\\
& +\frac{M_Z^6-48M_W^6-68M_Z^2M_W^4+16M_Z^4M_W^2}{6M_Z^2\left(M_Z^2-M_W^2\right)}B_0\left(M_Z,M_W,M_W\right)+\\
& \left.+\frac{1}{36}\left(\frac{576M_W^4}{M_Z^2}-242M_W^2-3M_h^2+257M_Z^2+\frac{36M_W^2}{M_Z^2-M_W^2}+M_t^2\left(82-\frac{256M_W^2}{M_Z^2}\right)\right)\right].
\end{aligned}
\tag{2.37}
$$

2.A.2 SM RGE equations up to three loops

We list here the known results for the renormalisation group equations up to 3 loop order for the sizeable SM couplings, g_1, g_2, g_3, y_t and λ in the $\overline{\mathrm{MS}}$ scheme. We write numerically those 3-loop coefficients that involve the ζ_3 constant. Stopping for simplicity at two loops, we also write RGE equations for the smaller bottom and tau Yukawa coupling and their contributions to the RGE of the large couplings. Our numerical code includes full RGE at 3 loops.

Gauge couplings

RGE for the hypercharge gauge coupling in GUT normalisation ($g_1^2 = 5g_Y^2/3$):

$$
\begin{aligned}
\frac{dg_1^2}{d\ln\bar{\mu}^2} \;=\; & \frac{g_1^4}{(4\pi)^2}\left[\frac{41}{10}\right]+\frac{g_1^4}{(4\pi)^4}\left[\frac{44g_3^2}{5}+\frac{27g_2^2}{10}+\frac{199g_1^2}{50}-\frac{17y_t^2}{10}-\frac{y_b^2}{2}-\frac{3y_\tau^2}{2}\right]+\\
& +\frac{g_1^4}{(4\pi)^6}\left[y_t^2\left(\frac{189y_t^2}{16}-\frac{29g_3^2}{5}-\frac{471g_2^2}{32}-\frac{2827g_1^2}{800}\right)+\lambda\left(-\frac{36\lambda}{5}+\frac{9g_2^2}{5}+\frac{27g_1^2}{25}\right)+\right.\\
& \left.+\frac{297g_3^4}{5}+\frac{789g_2^4}{64}-\frac{388613g_1^4}{24000}-\frac{3g_3^2g_2^2}{5}-\frac{137g_3^2g_1^2}{75}+\frac{123g_2^2g_1^2}{160}\right].
\end{aligned}
$$

RGE for the $\mathrm{SU}(2)_L$ gauge coupling:

$$\begin{aligned}\frac{dg_2^2}{d\ln\bar{\mu}^2} &= \frac{g_2^4}{(4\pi)^2}\left[-\frac{19}{6}\right]+\frac{g_2^4}{(4\pi)^4}\left[12g_3^2+\frac{35g_2^2}{6}+\frac{9g_1^2}{10}-\frac{3y_t^2}{2}-\frac{3y_b^2}{2}-\frac{y_\tau^2}{2}\right]+\\ &+\frac{g_2^4}{(4\pi)^6}\left[y_t^2\left(\frac{147y_t^2}{16}-7g_3^2-\frac{729g_2^2}{32}-\frac{593g_1^2}{160}\right)+\lambda\left(-3\lambda+\frac{3g_2^2}{2}+\frac{3g_1^2}{10}\right)+\right.\\ &\left.+81g_3^4+\frac{324953g_2^4}{1728}-\frac{5597g_1^4}{1600}+39g_3^2g_2^2-\frac{g_3^2g_1^2}{5}+\frac{873g_2^2g_1^2}{160}\right].\end{aligned}$$

RGE for the strong gauge coupling, including also pure QCD terms at 4 loops:

$$\begin{aligned}\frac{dg_3^2}{d\ln\bar{\mu}^2} &= \frac{g_3^4}{(4\pi)^2}\left[-7\right]+\frac{g_3^4}{(4\pi)^4}\left[-26g_3^2+\frac{9g_2^2}{2}+\frac{11g_1^2}{10}-2y_t^2-2y_b^2\right]+\\ &+\frac{g_3^4}{(4\pi)^6}\left[y_t^2\left(15y_t^2-40g_3^2-\frac{93g_2^2}{8}-\frac{101g_1^2}{40}\right)+\right.\\ &\left.+\frac{65g_3^4}{2}+\frac{109g_2^4}{8}-\frac{523g_1^4}{120}+21g_3^2g_2^2+\frac{77g_3^2g_1^2}{15}-\frac{3g_2^2g_1^2}{40}\right]+\frac{g_3^{10}}{(4\pi)^8}\left[-2472.28\right].\end{aligned}$$

Higgs quartic coupling

RGE for the Higgs quartic coupling:

$$\begin{aligned}\frac{d\lambda}{d\ln\bar{\mu}^2} &= \frac{1}{(4\pi)^2}\left[\lambda\left(12\lambda+6y_t^2+6y_b^2+2y_\tau^2-\frac{9g_2^2}{2}-\frac{9g_1^2}{10}\right)-3y_t^4-3y_b^4-y_\tau^4+\frac{9g_2^4}{16}+\frac{27g_1^4}{400}+\frac{9g_2^2g_1^2}{40}\right]+\\ &+\frac{1}{(4\pi)^4}\left[\lambda^2\left(-156\lambda-72y_t^2-72y_b^2-24y_\tau^2+54g_2^2+\frac{54g_1^2}{5}\right)+\lambda y_t^2\left(-\frac{3y_t^2}{2}-21y_b^2+40g_3^2+\right.\right.\\ &\left.+\frac{45g_2^2}{4}+\frac{17g_1^2}{4}\right)+\lambda y_b^2\left(-\frac{3y_b^2}{2}+40g_3^2+\frac{45g_2^2}{4}+\frac{5g_1^2}{4}\right)+\lambda y_\tau^2\left(\frac{15g_2^2}{4}+\frac{15g_1^2}{4}\right)+\lambda\left(-\frac{73g_2^4}{16}+\right.\\ &\left.+\frac{1887g_1^4}{400}+\frac{117g_2^2g_1^2}{40}\right)+y_t^4\left(15y_t^2-3y_b^2-16g_3^2-\frac{4g_1^2}{5}\right)+y_t^2\left(-\frac{9g_2^2}{8}-\frac{171g_1^4}{200}+\frac{63g_2^2g_1^2}{20}\right)+\\ &+y_b^4\left(-3y_t^2+15y_b^2-16g_3^2+\frac{2g_1^2}{5}\right)+y_b^2\left(-\frac{9g_2^2}{8}+\frac{9g_1^4}{40}+\frac{27g_2^2g_1^2}{20}\right)+y_\tau^4\left(5y_\tau^2-\frac{6g_1^2}{5}\right)+\\ &+y_\tau^2\left(-\frac{3g_2^2}{8}-\frac{9g_1^4}{8}+\frac{33g_2^2g_1^2}{20}\right)+\frac{305g_2^6}{32}-\frac{3411g_1^6}{4000}-\frac{289g_2^4g_1^2}{160}-\frac{1677g_2^2g_1^4}{800}\Big]+\\ &+\frac{1}{(4\pi)^6}\Big[\lambda^3\left(6011.35\lambda+873y_t^2-387.452g_2^2-77.490g_1^2\right)+\lambda^2y_t^2\left(1768.26y_t^2+160.77g_3^2\right.\\ &\left.-359.539g_2^2-63.869g_1^2\right)+\lambda^2\left(-790.28g_2^4-185.532g_1^4-316.64g_2^2g_1^2\right)+\lambda y_t^4\left(-223.382y_t^2+\right.\\ &\left.-662.866g_3^2-5.470g_2^2-21.015g_1^2\right)+\lambda y_t^2\left(356.968g_3^4-319.664g_2^4-74.8599g_1^4+15.1443g_3^2g_2^2+\right.\\ &\left.+17.454g_3^2g_1^2+5.615g_2^2g_1^2\right)+\lambda g_2^4\left(-57.144g_3^2+865.483g_2^2+79.638g_1^2\right)+\lambda g_1^4\left(-8.381g_3^2+\right.\\ &\left.+61.753g_2^2+28.168g_1^2\right)+y_t^6\left(-243.149y_t^2+250.494g_3^2+74.138g_2^2+33.930g_1^2\right)+\\ &+y_t^4\left(-50.201g_3^4+15.884g_2^4+15.948g_1^4+13.349g_3^2g_2^2+17.570g_3^2g_1^2-70.356g_2^2g_1^2\right)+\\ &+y_t^2g_3^2\left(16.464g_2^4+1.016g_1^4+11.386g_2^2g_1^2\right)+y_t^2g_2^2\left(62.500g_2^2+13.041g_1^2\right)+\\ &+y_t^2g_1^4\left(10.627g_2^2+11.117g_1^2\right)+g_3^2\left(7.536g_2^6+0.663g_1^6+1.507g_2^4g_1^2+1.105g_2^2g_1^4\right)+\\ &-114.091g_2^8-1.508g_1^8-37.889g_2^6g_1^2+6.500g_2^4g_1^4-1.543g_2^2g_1^6\Big].\end{aligned}$$

Higgs mass term

RGE for the Higgs mass term:

$$\begin{aligned}
\frac{dm^2}{d\ln\bar{\mu}^2} &= \frac{m^2}{(4\pi)^2}\left[6\lambda+3y_t^2+3y_b^2+y_\tau^2-\frac{9g_2^2}{4}-\frac{9g_1^2}{20}\right]+\\
&+\frac{m^2}{(4\pi)^4}\left[\lambda\left(-30\lambda-36y_t^2-36y_b^2-12y_\tau^2+36g_2^2+\frac{36g_1^2}{5}\right)+\right.\\
&+y_t^2\left(-\frac{27y_t^2}{4}-\frac{21y_b^2}{2}+20g_3^2+\frac{45g_2^2}{8}+\frac{17g_1^2}{8}\right)+y_b^2\left(-\frac{27y_b^2}{4}+20g_3^2+\frac{45g_2^2}{8}+\frac{5g_1^2}{8}\right)+\\
&\left.+y_\tau^2\left(-\frac{9y_\tau^2}{4}+\frac{15g_2^2}{8}+\frac{15g_1^2}{8}\right)-\frac{145}{32}g_2^4+\frac{1671}{800}g_1^4+\frac{9g_2^2g_1^2}{16}\right]+\\
&+\frac{m^2}{(4\pi)^6}\left[\lambda^2\left(1026\lambda+\frac{297y_t^2}{2}-192.822g_2^2-38.564g_1^2\right)+\lambda y_t^2\left(347.394y_t^2+80.385g_3^2+\right.\right.\\
&-318.591g_2^2-59.699g_1^2\big)+\lambda\left(-64.5145g_2^4-65.8056g_1^4-37.8231g_2^2g_1^2\right)+y_t^4\left(154.405y_t^2+\right.\\
&-209.24g_3^2-3.82928g_2^2-7.50769g_1^2\big)+y_t^2\left(178.484g_3^4-102.627g_2^4-27.721g_1^4+\right.\\
&+7.572g_3^2g_2^2+8.727g_3^2g_1^2+11.470g_2^2g_1^2\big)+g_2^4\left(-28.572g_3^2+301.724g_2^2+9.931g_1^2\right)+\\
&\left.\left.+g_1^4\left(-4.191g_3^2+9.778g_2^2+8.378g_1^2\right)\right]\right.\,.
\end{aligned}$$

Yukawa couplings

RGE for the top Yukawa coupling:

$$\begin{aligned}
\frac{dy_t^2}{d\ln\bar{\mu}^2} &= \frac{y_t^2}{(4\pi)^2}\left[\frac{9y_t^2}{2}+\frac{3y_b^2}{2}+y_\tau^2-8g_3^2-\frac{9g_2^2}{4}-\frac{17g_1^2}{20}\right]+\\
&+\frac{y_t^2}{(4\pi)^4}\left[y_t^2\left(-12y_t^2-\frac{11y_b^2}{4}-\frac{9y_\tau^2}{4}-12\lambda+36g_3^2+\frac{225g_2^2}{16}+\frac{393g_1^2}{80}\right)+\right.\\
&+y_b^2\left(-\frac{y_b^2}{2}+\frac{5y_\tau^2}{4}+4g_3^2+\frac{99g_2^2}{16}+\frac{7g_1^2}{80}\right)+y_\tau^2\left(-\frac{9y_\tau^2}{4}+\frac{15}{8}g_2^2+\frac{15}{8}g_1^2\right)+\\
&\left.+6\lambda^2-108g_3^4-\frac{23g_2^4}{4}+\frac{1187g_1^4}{600}+9g_3^2g_2^2+\frac{19}{15}g_3^2g_1^2-\frac{9}{20}g_2^2g_1^2\right]+\\
&+\frac{y_t^2}{(4\pi)^6}\left[y_t^4\left(58.6028y_t^2+198\lambda-157g_3^2-\frac{1593g_2^2}{16}-\frac{2437g_1^2}{80}\right)+\lambda y_t^2\left(\frac{15\lambda}{4}+16g_3^2+\right.\right.\\
&\left.-\frac{135g_2^2}{2}-\frac{127g_1^2}{10}\right)+y_t^2\left(363.764g_3^4+16.990g_2^4-24.422g_1^4+48.370g_3^2g_2^2+18.074g_3^2g_1^2+\right.\\
&\left.+34.829g_2^2g_1^2\right)+\lambda^2\left(-36\lambda+45g_2^2+9g_1^2\right)+\lambda\left(-\frac{171g_2^4}{16}-\frac{1089g_1^4}{400}+\frac{117g_2^2g_1^2}{40}\right)+\\
&-619.35g_3^6+169.829g_2^6+16.099g_1^6+73.654g_3^4g_2^2-15.096g_3^4g_1^2-21.072g_3^2g_2^4+\\
&\left.-22.319g_3^2g_1^4-\frac{321}{20}g_3^2g_2^2g_1^2-4.743g_2^4g_1^2-4.442g_2^2g_1^4\right]\,.
\end{aligned}$$

RGE for the bottom Yukawa coupling (up to two loops):

$$\begin{aligned}\frac{dy_b^2}{d\ln\bar{\mu}^2} &= \frac{y_b^2}{(4\pi)^2}\left[\frac{3y_t^2}{2}+\frac{9y_b^2}{2}+y_\tau^2-8g_3^2-\frac{9g_2^2}{4}-\frac{g_1^2}{4}\right]+\\ &+\frac{y_b^2}{(4\pi)^4}\left[y_t^2\left(-\frac{y_t^2}{4}-\frac{11y_b^2}{4}+\frac{5y_\tau^2}{4}+4g_3^2+\frac{99g_2^2}{16}+\frac{91g_1^2}{80}\right)+\right.\\ &+y_b^2\left(-12y_b^2-\frac{9y_\tau^2}{4}-12\lambda+36g_3^2+\frac{225g_2^2}{16}+\frac{237g_1^2}{80}\right)+y_\tau^2\left(-\frac{9y_\tau^2}{4}+\frac{15}{8}g_2^2+\frac{15}{8}g_1^2\right)+\\ &\left.+6\lambda^2-108g_3^4-\frac{23g_2^4}{4}-\frac{127g_1^4}{600}+9g_3^2g_2^2+\frac{31}{15}g_3^2g_1^2-\frac{27}{20}g_2^2g_1^2\right].\end{aligned}$$

RGE for the tau Yukawa coupling (up to two loops):

$$\begin{aligned}\frac{dy_\tau^2}{d\ln\bar{\mu}^2} &= \frac{y_\tau^2}{(4\pi)^2}\left[3y_t^2+3y_b^2+\frac{5y_\tau^2}{2}-\frac{9g_2^2}{4}-\frac{9g_1^2}{4}\right]+\frac{y_\tau^2}{(4\pi)^4}\left[+6\lambda^2-\frac{23g_2^4}{4}+\frac{1371g_1^4}{200}+\frac{27}{20}g_2^2g_1^2+\right.\\ &y_t^2\left(-\frac{27y_t^2}{4}+\frac{3y_b^2}{2}-\frac{27y_\tau^2}{4}+20g_3^2+\frac{45g_2^2}{8}+\frac{17g_1^2}{8}\right)+\\ &\left.+y_b^2\left(-\frac{27y_b^2}{4}-\frac{27y_\tau^2}{4}+20g_3^2+\frac{45g_2^2}{8}+\frac{5g_1^2}{8}\right)+y_\tau^2\left(-3y_\tau^2-12\lambda+\frac{165}{16}g_2^2+\frac{537}{80}g_1^2\right)\right].\end{aligned}$$

2.A.3 Effective potential at two loops

The effective potential including one-loop and two-loop corrections in Landau gauge for $h \gg v$ is given by equation (2.11), where [33, 95]

$$\lambda_{\rm eff}(h) = e^{4\Gamma(h)}\left[\lambda(\bar{\mu}=h)+\lambda^{(1)}_{\rm eff}(\bar{\mu}=h)+\lambda^{(2)}_{\rm eff}(\bar{\mu}=h)\right]. \tag{2.38}$$

All running couplings are evaluated at $\bar{\mu} = h$. Here, $\Gamma(h) \equiv \int_{M_t}^{h}\gamma(\bar{\mu})d\ln\bar{\mu}$, with γ the Higgs field anomalous dimension,

$$\gamma = \frac{1}{(4\pi)^2}\left[\frac{9}{4}g_2^2+\frac{9}{20}g_1^2-3y_t^2-3y_b^2-y_\tau^2\right]+ \tag{2.39}$$

$$\begin{aligned}&+\frac{1}{(4\pi)^4}\left[y_t^2\left(-\frac{3y_b^2}{2}-\frac{17g_1^2}{8}-\frac{45g_2^2}{8}-20g_3^2+\frac{27y_t^2}{4}\right)-y_\tau^2\left(\frac{15g_1^2}{8}+\frac{15g_2^2}{8}-\frac{9y_\tau^2}{4}\right)+\right.\\ &\left.+y_b^2\left(-\frac{5g_1^2}{8}-\frac{45g_2^2}{8}-20g_3^2+\frac{27y_b^2}{4}\right)-\frac{1293g_1^4}{800}-\frac{27}{80}g_2^2g_1^2+\frac{271g_2^4}{32}-6\lambda^2\right]+\end{aligned} \tag{2.40}$$

$$\begin{aligned}&+\frac{1}{(4\pi)^6}\left[-9g_1^2\lambda^2-45g_2^2\lambda^2+1.07g_1^4\lambda+3.57g_2^2g_1^2\lambda+8.92g_2^4\lambda+\right.\\ &+14.99g_1^4y_t^2+14.13g_1^2y_t^4-13.21g_2^2g_1^2y_t^2-8.73g_3^2g_1^2y_t^2+40.11g_2^2y_t^4+79.05g_3^2y_t^4+\\ &+23.40g_2^4y_t^2-178.48g_3^4y_t^2-7.57g_2^2g_3^2y_t^2-5.26g_1^6+1.93g_2^2g_1^4+4.19g_3^2g_1^4+\\ &\left.+1.81g_2^4g_1^2-158.51g_2^6+28.57g_2^4g_3^2+36\lambda^3+\frac{135}{2}\lambda^2y_t^2-45.00\lambda y_t^4-60.13y_t^6\right].\end{aligned}$$

The one-loop correction is

$$\lambda_{\rm eff}^{(1)} = \frac{1}{(4\pi)^2}\Big[\frac{3g_2^4}{8}(\ln\frac{g_2^2}{4}-\frac{5}{6}+2\Gamma)+\frac{3}{16}(g_2^2+g_Y^2)^2(\ln\frac{g_2^2+g_Y^2}{4}-\frac{5}{6}+2\Gamma)+ \\ -3y_t^4(\ln\frac{y_t^2}{2}-\frac{3}{2}+2\Gamma)+3\lambda^2(4\ln\lambda-6+3\ln 3+8\Gamma)\Big]. \tag{2.41}$$

The two-loop correction is

$$\begin{aligned}\lambda_{\rm eff}^{(2)} = \frac{1}{(4\pi)^4}\Big[&8g_3^2y_t^4\left(3r_t^2-8r_t+9\right)+\frac{1}{2}y_t^6\left(-6r_tr_W-3r_t^2+48r_t-6r_{tW}-69-\pi^2\right)+\\
&+\frac{3y_t^2g_2^4}{16}\left(8r_W+4r_Z-3r_t^2-6r_tr_Z-12r_t+12r_{tW}+15+2\pi^2\right)+\\
&+\frac{y_t^2g_Y^4}{48}\left(27r_t^2-54r_tr_Z-68r_t-28r_Z+189\right)+\frac{y_t^2g_2^2g_Y^2}{8}(9r_t^2-18r_tr_Z+4r_t+44r_Z-57)+\\
&+\frac{g_2^6}{192}(36r_tr_Z+54r_t^2-414r_Wr_Z+69r_W^2+1264r_W+156r_Z^2+632r_Z-144r_{tW}-2067+90\pi^2)+\\
&+\frac{g_2^4g_Y^2}{192}(12r_tr_Z-6r_t^2-6r_W(53r_Z+50)+213r_W^2+4r_Z(57r_Z-91)+817+46\pi^2)+\\
&+\frac{g_2^2g_Y^4}{576}(132r_tr_Z-66r_t^2+306r_Wr_Z-153r_W^2-36r_W+924r_Z^2-4080r_Z+4359+218\pi^2)+\\
&+\frac{g_Y^6}{576}(6r_Z(34r_t+3r_W-470)-102r_t^2-9r_W^2+708r_Z^2+2883+206\pi^2)+\\
&+\frac{y_t^4}{6}\left(4g_Y^2(3r_t^2-8r_t+9)-9g_2^2\left(r_t-r_W+1\right)\right)+\frac{3}{4}\left(g_2^6-3g_2^4y_t^2+4y_t^6\right)\mathrm{Li}_2\frac{g_2^2}{2y_t^2}+\\
&+\frac{y_t^2}{48}\xi(\frac{g_2^2+g_Y^2}{2y_t^2})\left(9g_2^4-6g_2^2g_Y^2+17g_Y^4+2y_t^2\big(7g_Y^2-73g_2^2+\frac{64g_2^4}{g_Y^2+g_2^2}\big)\right)+\\
&+\frac{g_2^2}{64}\xi(\frac{g_2^2+g_Y^2}{g_2^2})\left(18g_2^2g_Y^2+g_Y^4-51g_2^4-\frac{48g_2^6}{g_Y^2+g_2^2}\right)\Big].\end{aligned} \tag{2.42}$$

Here we have given $\lambda_{\rm eff}^{(2)}$ in the approximation $\lambda = 0$, which is well justified around the instability region. The full expression of $\lambda_{\rm eff}^{(2)}$ can be found in ref. [33]. Moreover, we have defined

$$\xi(z) \equiv \sqrt{z^2-4z}\left[2\ln^2\left(\frac{z-\sqrt{z^2-4z}}{2z}\right)-\ln^2 z-4\mathrm{Li}_2\left(\frac{z-\sqrt{z^2-4z}}{2z}\right)+\frac{\pi^2}{3}\right], \tag{2.43}$$

where Li_2 is the dilogarithm function, and

$$r_W = \ln\frac{g_2^2}{4}+2\Gamma, \qquad r_Z = \ln\frac{g_2^2+g_Y^2}{4}+2\Gamma, \qquad r_t = \ln\frac{y_t^2}{2}+2\Gamma \tag{2.44}$$

and

$$r_{tW} = (r_t-r_W)\left[\ln\left(\frac{y_t^2}{2}-\frac{g_2^2}{4}\right)+2\Gamma\right]. \tag{2.45}$$

Bibliography

[1] D. Buttazzo, G. Degrassi, P. P. Giardino, G. F. Giudice, F. Sala, A. Salvio and A. Strumia, arXiv:1307.3536 [hep-ph].

[2] D. J. Gross and F. Wilczek, Phys. Rev. Lett. 30 (1973) 1343.

[3] H. D. Politzer, Phys. Rev. Lett. 30 (1973) 1346.

[4] W. E. Caswell, Phys. Rev. Lett. 33 (1974) 244.

[5] D. R. T. Jones, Nucl. Phys. B 75 (1974) 531.

[6] D. R. T. Jones, Phys. Rev. D 25 (1982) 581.

[7] O. V. Tarasov, A. A. Vladimirov and A. Y. Zharkov, Phys. Lett. B 93 (1980) 429.

[8] S. A. Larin and J. A. M. Vermaseren, Phys. Lett. B 303 (1993) 334 [arXiv:hep-ph/9302208].

[9] M. Steinhauser, Phys. Rev. D 59 (1999) 054005 [arXiv:hep-ph/9809507].

[10] T. van Ritbergen, J. A. M. Vermaseren and S. A. Larin, Phys. Lett. B 400 (1997) 379 [arXiv:hep-ph/9701390].

[11] M. Czakon, Nucl. Phys. B 710 (2005) 485 [arXiv:hep-ph/0411261].

[12] M. E. Machacek and M. T. Vaughn, Nucl. Phys. B 222 (1983) 83.

[13] L. N. Mihaila, J. Salomon and M. Steinhauser, Phys. Rev. Lett. 108 (2012) 151602 [arXiv:1201.5868].

[14] L. N. Mihaila, J. Salomon and M. Steinhauser, Phys. Rev. D 86 (2012) 096008 [arXiv:1208.3357].

[15] T. P. Cheng, E. Eichten and L. -F. Li, Phys. Rev. D 9 (1974) 2259.

[16] M. Fischler and J. Oliensis, Phys. Lett. B 119 (1982) 385.

[17] M. E. Machacek and M. T. Vaughn, Nucl. Phys. B 236 (1984) 221.

[18] K. G. Chetyrkin and M. F. Zoller, JHEP 1206 (2012) 033 [arXiv:1205.2892].

[19] A. V. Bednyakov, A. F. Pikelner and V. N. Velizhanin, Phys. Lett. B 722 (2013) 336 [arXiv:1212.6829].

[20] M. E. Machacek and M. T. Vaughn, Nucl. Phys. B 249 (1985) 70.

[21] M. -X. Luo and Y. Xiao, Phys. Rev. Lett. 90 (2003) 011601 [arXiv:hep-ph/0207271].

[22] K. G. Chetyrkin and M. F. Zoller, JHEP 1304 (2013) 091 [arXiv:1303.2890].

[23] A. V. Bednyakov, A. F. Pikelner and V. N. Velizhanin, [arXiv:1303.4364].

[24] A. Sirlin, Phys. Rev. D 22 (1980) 971.

[25] W. J. Marciano and A. Sirlin, Phys. Rev. D 22 (1980) 2695 [Erratum-ibid. D 31 (1985) 213.

[26] R. Tarrach, Nucl. Phys. B 183 (1981) 384.

[27] R. Hempfling and B. A. Kniehl, Phys. Rev. D 51 (1995) 1386 [arXiv:hep-ph/9408313].

[28] F. Bezrukov, M. Y. Kalmykov, B. A. Kniehl and M. Shaposhnikov, JHEP 1210 (2012) 140 [arXiv:1205.2893].

[29] K. G. Chetyrkin and M. Steinhauser, Phys. Rev. Lett. 83 (1999) 4001 [arXiv:hep-ph/9907509].

[30] K. G. Chetyrkin and M. Steinhauser, Nucl. Phys. B 573 (2000) 617 [arXiv:hep-ph/9911434].

[31] K. Melnikov and T. v. Ritbergen, Phys. Lett. B 482 (2000) 99 [arXiv:hep-ph/9912391].

[32] A. Sirlin and R. Zucchini, Nucl. Phys. B 266 (1986) 389.

[33] G. Degrassi, S. Di Vita, J. Elias-Miro, J. R. Espinosa, G. F. Giudice, G. Isidori and A. Strumia, JHEP 1208 (2012) 098 [arXiv:1205.6497].

[34] Particle Data Group, J. Phys. G 37 (2010) 075021. The LEP Electroweak Working Group, `http://lepewwg.web.cern.ch`. We thank Jens Erler and Paul Langacker for the latest fit we quote, and Martin Grünewald for useful discussions.

[35] TeVatron average: FERMILAB-TM-2532-E. LEP average: CERN-PH-EP/2006-042.

[36] 2012 Particle Data Group average, pdg.lbl.gov.

[37] M_h from $h \to \gamma\gamma$: CMS Collaboration, CMS-PAS-HIG-13-001. ATLAS Collaboration, ATLAS-CONF-2013-012. M_h from $h \to ZZ$: CMS Collaboration, CMS-PAS-HIG-13-002. ATLAS Collaboration, ATLAS-CONF-2013-013. Naive average: P. P. Giardino, K. Kannike, I. Masina, M. Raidal and A. Strumia, arXiv:1303.3570.

[38] Tevatron Electroweak Working Group, arXiv:1107.5255. CMS collaboration, CMS top physics web site and talks at the Moriond 2013 conference. ATLAS collaboration, ATLAS top physics web site.

[39] MuLan Collaboration. arXiv:1211.0960.

[40] S. Bethke, arXiv:1210.0325.

[41] W. E. Caswell and F. Wilczek, Phys. Lett. B 49 (1974) 291. See also T. Muta, "Foundations of quantum chromodynamics", p. 192.

[42] C. D. Froggatt and H. B. Nielsen, Phys. Lett. B 368 (1996) 96 [arXiv:hep-ph/9511371].

[43] C. D. Froggatt, H. B. Nielsen and Y. Takanishi, Phys. Rev. D 64 (2001) 113014 [arXiv:hep-ph/0104161].

[44] C. P. Burgess, V. Di Clemente and J. R. Espinosa, JHEP 0201 (2002) 041 [arXiv:hep-ph/0201160].

[45] G. Isidori, V. S. Rychkov, A. Strumia and N. Tetradis, Phys. Rev. D 77 (2008) 025034 [arXiv:0712.0242].

[46] F. Bezrukov and M. Shaposhnikov, JHEP 0907 (2009) 089 [arXiv:0904.1537].

[47] M. Shaposhnikov and C. Wetterich, Phys. Lett. B 683 (2010) 196 [arXiv:0912.0208].

[48] C. Ford, I. Jack and D. R. T. Jones, Nucl. Phys. B 387 (1992) 373 [Erratum-ibid. B 504 (1997) 551] [arXiv:hep-ph/0111190].

[49] G. Isidori, G. Ridolfi and A. Strumia, Nucl. Phys. B 609 (2001) 387 [arXiv:hep-ph/0104016].

[50] M. Holthausen, K. S. Lim and M. Lindner, JHEP 1202 (2012) 037 [arXiv:1112.2415].

[51] J. Elias-Miro, J. R. Espinosa, G. F. Giudice, G. Isidori, A. Riotto and A. Strumia, Phys. Lett. B 709 (2012) 222 [arXiv:1112.3022].

[52] C. -S. Chen and Y. Tang, JHEP 1204 (2012) 019 [arXiv:1202.5717].

[53] O. Lebedev, Eur. Phys. J. C 72 (2012) 2058 [arXiv:1203.0156].

[54] J. Elias-Miro, J. R. Espinosa, G. F. Giudice, H. M. Lee and A. Strumia, JHEP 1206 (2012) 031 [arXiv:1203.0237].

[55] W. Rodejohann and H. Zhang, JHEP 1206 (2012) 022 [arXiv:1203.3825].

[56] A. Datta and S. Raychaudhuri, Phys. Rev. D 87 (2013) 035018 [arXiv:1207.0476].

[57] S. Alekhin, A. Djouadi and S. Moch, Phys. Lett. B 716 (2012) 214 [arXiv:1207.0980].

[58] J. Chakrabortty, M. Das and S. Mohanty, arXiv:1207.2027].

[59] L. A. Anchordoqui, I. Antoniadis, H. Goldberg, X. Huang, D. Lust, T. R. Taylor and B. Vlcek, JHEP 1302 (2013) 074 [arXiv:1208.2821].

[60] I. Masina, Phys. Rev. D 87 (2013) 053001 [arXiv:1209.0393].

[61] E. J. Chun, H. M. Lee and P. Sharma, JHEP 1211 (2012) 106 [arXiv:1209.1303].

[62] D. J. H. Chung, A. J. Long and L. -T. Wang, Phys. Rev. D 87 (2013) 023509 [arXiv:1209.1819].

[63] W. Chao, M. Gonderinger and M. J. Ramsey-Musolf, Phys. Rev. D 86 (2012) 113017 [arXiv:1210.0491].

[64] O. Lebedev and A. Westphal, Phys. Lett. B 719 (2013) 415 [arXiv:1210.6987].

[65] H. B. Nielsen, arXiv:1212.5716.

[66] A. Kobakhidze and A. Spencer-Smith, Phys. Lett. B 722 (2013) 130 [arXiv:1301.2846].

[67] Y. Tang, Mod. Phys. Lett. A 28 (2013) 1330002 [arXiv:1301.5812].

[68] F. R. Klinkhamer, JETP Letters 97, 297 (2013) [arXiv:1302.1496].

[69] X. -G. He, H. Phoon, Y. Tang and G. Valencia, JHEP 1305 (2013) 026 [arXiv:1303.4848].

[70] E. J. Chun, S. Jung and H. M. Lee, arXiv:1304.5815.

[71] F. Jegerlehner, arXiv:1304.7813.

[72] V. Agrawal, S. M. Barr, J. F. Donoghue and D. Seckel, Phys. Rev. D 57 (1998) 5480 [arXiv:hep-ph/9707380].

[73] I. Y. .Kobzarev, L. B. Okun and M. B. Voloshin, Sov. J. Nucl. Phys. 20 (1975) 644 [Yad. Fiz. 20 (1974) 1229].

[74] S. R. Coleman, Phys. Rev. D 15 (1977) 2929 [Erratum-ibid. D 16 (1977) 1248].

[75] C. G. Callan, Jr. and S. R. Coleman, Phys. Rev. D 16 (1977) 1762.

[76] S. R. Coleman and F. De Luccia, Phys. Rev. D 21 (1980) 3305.

[77] L. J. Hall and Y. Nomura, JHEP 1003 (2010) 076 [arXiv:0910.2235].

[78] G. F. Giudice and A. Strumia, Nucl. Phys. B 858 (2012) 63 [arXiv:1108.6077].

[79] M. E. Cabrera, J. A. Casas and A. Delgado, Phys. Rev. Lett. 108 (2012) 021802 [arXiv:1108.3867].

[80] A. Arbey, M. Battaglia, A. Djouadi, F. Mahmoudi and J. Quevillon, Phys. Lett. B 708 (2012) 162 [arXiv:1112.3028].

[81] L. E. Ibanez and I. Valenzuela, JHEP 1305 (2013) 064 [arXiv:1301.5167].

[82] A. Hebecker, A. K. Knochel and T. Weigand, Nucl. Phys. B 874 (2013) 1 [arXiv:1304.2767].

[83] P. J. Fox, A. E. Nelson and N. Weiner, JHEP 0208 (2002) 035 [arXiv:hep-ph/0206096].

[84] K. Benakli, M. D. Goodsell and F. Staub, JHEP 1306 (2013) 073 [arXiv:1211.0552].

[85] A. Hebecker, A. K. Knochel and T. Weigand, JHEP 1206 (2012) 093 [arXiv:1204.2551].

[86] M. Redi and A. Strumia, JHEP 1211 (2012) 103 [arXiv:1208.6013].

[87] G. F. Giudice and R. Rattazzi, Nucl. Phys. B 757 (2006) 19 [arXiv:hep-ph/0606105].

[88] P. Bak, C. Tang and K. Wiesenfeld, Phys. Rev. Lett. 59 (1987) 381.

[89] S. Weinberg, Phys. Rev. Lett. 59 (1987) 2607.

[90] J. F. Donoghue, K. Dutta and A. Ross, Phys. Rev. D 73 (2006) 113002 [arXiv:hep-ph/0511219].

[91] L. J. Hall, M. P. Salem and T. Watari, Phys. Rev. Lett. 100 (2008) 141801 [arXiv:0707.3444].

[92] G. W. Gibbons, S. Gielen, C. N. Pope and N. Turok, Phys. Rev. D 79 (2009) 013009 [arXiv:0810.4813].

[93] G. F. Giudice, G. Perez, Y. Soreq, arXiv:1207.4861.

[94] N. Arkani-Hamed, S. Dimopoulos and S. Kachru, arXiv:hep-th/0501082.

[95] J. A. Casas, J. R. Espinosa and M. Quiros, Phys. Lett. B 342 (1995) 171 [arXiv:hep-ph/9409458].

Chapter 3

Calculation of λ and y_t at NNLO

In the previous chapter we saw that a precise calculation of the quartic coupling of the Higgs is needed in order to study the stability of the E.W. vacuum and that we computed the missing NNLO threshold corrections for λ and y_t. In this chapter we will review the methods we used in the calculation of the relevant two-loops integrals.

The number of diagrams involved in a two-loops calculation easily exceeds the thousands. It is rather difficult to calculate so many diagrams by hand with standard techniques, therefore we used a method to reduce the diagrams in terms of a combination of some basis integrals. Specifically we used the algorithm developed by O.V. Tarasov [1, 2]. This algorithm has been implemented in the Mathematica code TARCER [3] that is part of the FEYNCALC [4] package. We also used the Mathematica package FEYNART [5] in order to write all the amplitudes. Once we reduced every relevant two-loop integral in terms of some basis integrals, we evaluated them using the C Program TSIL [6] based on the paper [7].

In section (3.1) we will review the main techniques on which our calculations are based. In particular we will see with more details Tarasov's algorithm and how we applied it to our problem. At the end of the section we will briefly examine the master integrals analyzing some possible methods to evaluate them. Section (3.2) will be dedicated to the renormalization of λ and y_t. We will also give some more details on the calculations of these quantities.

3.1 Master Integrals

Here we address the problem of calculating a generic two-loops two-points integral with arbitrary masses using the methods described in Tarasov's papers [1, 2]. Throughout the computation we will consider only dimensional regularized integrals with $d = 4 - 2\epsilon$, thus in general we will deal with integrals of the form

$$I^d(p^2, m_j^2) = \int\int d^d q_1 d^d q_2 \frac{N(q_1^2, q_2^2, q_1 p, q_2 p, q_1 q_2)}{P_1^{\nu_1} P_2^{\nu_2} P_3^{\nu_3} P_4^{\nu_4} P_5^{\nu_5}}, \tag{3.1}$$

where the numerator $N(q_1^2, q_2^2, q_1 p, q_2 p, q_1 q_2)$ is polynomial and

$$\begin{aligned} P_1 &= q_1^2 - m_1^2 + i\eta, \quad P_3 = (q_1 - p)^2 - m_3^2 + i\eta, \quad P_5 = (q_1 - q_2)^2 - m_5^2 + i\eta, \\ P_2 &= q_2^2 - m_2^2 + i\eta, \quad P_4 = (q_2 - p)^2 - m_4^2 + i\eta. \end{aligned}$$

We have considered numerators in scalar form, while in general a Feynman integral permits also a tensorial structure. However it is always possible to contract the diagram with a suitable projector operator and obtain a scalar numerator. Indeed this is a simple procedure and we used it in our

computations. In any case the techniques described here can be applied also to the general case. For brevity, from here on, we will call "scalar integral" an integral obtained by a Feynman diagram with only scalar fields, i. e. with $N(q_1^2, q_2^2, q_1p, q_2p, q_1q_2) = 1$. We will call "non-scalar integral" an integral with $N(q_1^2, q_2^2, q_1p, q_2p, q_1q_2) \neq 1$ and "tensor integral" an integral with a tensorial numerator.

The algorithm we used decomposes the computation of equation (3.1) in three parts: the simplification of the numerator $N(q_1^2, q_2^2, q_1p, q_2p, q_1q_2)$ such that the integral is expressed only in terms of scalar integrals, the reduction of these scalar integrals in terms of a set of "Master Integrals", *i.e.* irreducible integrals, and the evaluation of the basis integrals. The interesting question at this point is if it is possible to find a complete set of Master Integrals, that is if it is possible to reduce any given integrals, with generic numerators and integer powers of the propagators. The answer in general for a n-loops m-points integral is unknown, however the solution for one-loop m-points integrals was found by G. Passarino and M. J. G. Veltman [8], while Tarasov found the complete basis for two-points two-loops integrals. Obviously what we are going to see is valid also for integrals with n = 1 *and* m $\leq$ 2 and n = 2 *and* m $\leq$ 1 as special cases. In particular any two-loops m-points integrals with zero external momentum can be studied as a vacuum (that is zero-point) diagram. In any case we want to underline the fact that the techniques described here are valid for any Feynman integrals, although we do not know the complete basis for n $\geq$ 2 *and* m $>$ 2.

We will start addressing the problem of the reduction of scalar integrals and the ways to eliminate the numerators. At the end of the section we will see some techniques used in the evaluation of the basis integrals.

3.1.1 Integration by Parts

We are interested in rewriting a generic scalar integral in terms of simpler integrals. One of the possible ways is to use a set of recurrence relations. A standard method to find such relations is the well-known integration by parts (IBP) technique (see for example [9]), in which we impose that the relation

$$\int \prod_i d^d q_i \frac{\partial f}{\partial q_j^\mu} = 0 \tag{3.2}$$

is true. Here f stand for an integrand of a Feynman integral and it will depend in general by internal as well as external momenta and masses. Note that in order to relation (3.2) to be true we are assuming that the integral vanishes on the surface. To illustrate how this method works we will give an example.

Let us consider a massless one-loop two-points integral $I(a_1, a_2)$ in which we raise the propagators respectively to a_1 and a_2 powers. That is we consider

$$I(a_1, a_2) = \int d^d q \frac{1}{(q^2)^{a_1}((q-p)^2)^{a_2}} \tag{3.3}$$

where q is the loop momentum and p is the external momentum. In order to find a valid recursion relation for this integral we impose the IBP relation (3.2):

$$\int d^d q \frac{\partial}{\partial q^\mu} \frac{q^\mu}{(q^2)^{a_1}((q-p)^2)^{a_2}} = 0, \tag{3.4}$$

that gives us the recurrence relation

$$\left(d - 2a_1 - a_2 - a_2 \mathbf{2}^+(\mathbf{1}^- - q^2)\right) I(a_1, a_2) = 0. \tag{3.5}$$

Here we used the standard notation for "raising" or "lowering" the a_j indices: $\mathbf{1}^-\mathbf{2}^+ I(a_1, a_2) =$

$I(a_1-1,a_2+1)$. After sending $a_2 \to a_2-1$, from equation (3.5) we find,

$$I(a_1,a_2) = -\frac{(d-2a_1-a_2+1)I(a_1,a_2-1)-(a_2-1)I(a_1-1,a_2)}{(a_2-1)q^2}. \tag{3.6}$$

Taking in account the symmetry properties of the integral $I(a_1,a_2) = I(a_2,a_1)$, it is simple to use equation (3.6) to find a complete solution for the reduction problem of $I(a_1,a_2)$. Indeed we are now able to write any integral of the form $I(a_1,a_2)$ as $g(a_1,a_2,d)I(1,1)$ where $g(a_1,a_2,d)$ is a rational function. The demonstration is quite simple in this case and is based on the fact that for $a_2 = 1$ one can use the symmetry property of $I(a_1,a_2)$ to get rid of the divergence. Furthermore it should be noted that the integral $I(1,1)$ cannot be further reduced: if either a_1 or a_2 are non-positive $I(a_1,a_2)$ is zero since it becomes a massless tadpole, hence $I(1,1)$ is a master integral.

For a purely scalar theory the recurrence relations found via the IBP technique are enough, however if other kind of fields are present in our theory we have to deal also with numerators. If the numerator is "reducible" the technique described is still valid. For example the integral

$$\int d^dq \frac{2pq}{(q^2)^{a_1}((q-p)^2)^{a_2}} \tag{3.7}$$

can be easily solved using the relation $I(a_1,a_2) = g(a_1,a_2)I(1,1)$ since

$$\begin{aligned}&\int d^dq \frac{2pq}{(q^2)^{a_1}((q-p)^2)^{a_2}} = \\ &\int d^dq \frac{1}{(q^2)^{a_1}((q-p)^2)^{a_2-1}} - \frac{1}{(q^2)^{a_1-1}((q-p)^2)^{a_2}} - \frac{p^2}{(q^2)^{a_1}((q-p)^2)^{a_2}}.\end{aligned} \tag{3.8}$$

On the other hand for an integral of the form

$$I^{(d)}_{rs}(p^2,m_j^2) = \iint \frac{d^dq_1 d^dq_2}{P_1^{\nu_1}P_2^{\nu_2}P_3^{\nu_3}P_4^{\nu_4}P_5^{\nu_5}}(q_1p)^r(q_2p)^s, \tag{3.9}$$

we can not use the same method and we need to rely on other kind of relations.

3.1.2 Dealing with Numerators I: recurrence relation between different number of space-time dimensions

Here we introduce the recurrence relations between Feynman integrals computed in different numbers of space-time dimensions. These relations are complementary to the IBP ones and are necessary to reduce generic non-scalar integrals. They are quite simple to deduce once we have written the Feynman integrals in terms of the α-parametrization.

The so-called α-parametrization is based on the possibility of rewriting a given propagator in terms of a parameter:

$$\frac{1}{(q^2-m^2+i\eta)^\nu} = \frac{i^{-\nu}}{\Gamma(\nu)}\int_0^\infty d\alpha\ \alpha^{\nu-1}\exp[i\alpha(q^2-m^2+i\eta)]. \tag{3.10}$$

The equation (3.10) allows us to use the Gaussian integration in d dimension

$$\int d^dq \exp[i(Aq^2+2(pq))] = i(\frac{\pi}{iA})^{\frac{d}{2}}\exp[-\frac{ip^2}{A}] \tag{3.11}$$

to get rid of the integration over the internal momentum and obtain

$$\int \frac{d^d q}{(q^2 - m^2 + i\eta)^\nu} = \frac{i^{1-\nu-\frac{d}{2}}\pi^{\frac{d}{2}}}{\Gamma(\nu)} \int_0^\infty d\alpha\ \alpha^{\nu-1-\frac{d}{2}} e^{-i\alpha(m^2-i\eta)}. \tag{3.12}$$

If we carry out the integration over α in the right hand side of equation (3.12), we obtain an analytical solution for the Feynman integral.

We can generalize the equality (3.12) to an arbitrary dimensionally regularized L-loop scalar Feynman integral

$$I^{(d)}(s_i, m_s^2) = \prod_{i=1}^{L} \int d^d q_i \prod_{j=1}^{N} P_j^{\nu_j}(\overline{q}_j, m_j), \tag{3.13}$$

where

$$P_j^\nu(q_j, m_j) = \frac{1}{(q_j^2 - m_j^2 + i\eta)^\nu}, \qquad \overline{q}_j^\mu = \sum_{n=1}^{L} \omega_{jn} q_n^\mu + \sum_{m=1}^{E} \sigma_{jm} p_m^\mu, \tag{3.14}$$

p_m are the external momenta, s_i is a set of scalar invariants formed from p_m, N is the number of internal propagator, E is the number of external legs, ω and σ are matrices of incidences of the diagram with the matrix elements being ± 1 or 0. Using the same procedure explained above we find:

$$I^{(d)}(s_i, m_s^2) = i^L \left(\frac{\pi}{i}\right)^{\frac{dL}{2}} \prod_{j=1}^{N} \frac{i^{-\nu_j}}{\Gamma(\nu_j)} \int_0^\infty \cdots \int_0^\infty \frac{d\alpha_j \alpha_j^{\nu_j - 1}}{[D(\alpha)]^{\frac{d}{2}}} e^{i[\frac{Q(s_i,\alpha)}{D(\alpha)} - \sum_{l=1}^{N} \alpha_l (m_l^2 - i\eta)]}, \tag{3.15}$$

where $D(\alpha)$ and $Q(s_i, \alpha)$ are homogeneous polynomials in α of degree L and $L+1$, respectively. These polynomials are characteristic functions of the topology of the diagram and of its subgraphs and they can be represented as sums over trees and two-trees of the graph:

$$D = \sum_{T \in T^1} \left(\prod_{l \notin T} \alpha_l\right) \tag{3.16}$$

$$Q = \sum_{T \in T^2} \left(\prod_{l \notin T} \alpha_l \Big(\sum_{comp.\ T^2} p\Big)^2\right), \tag{3.17}$$

where T^1 are the trees, T^2 the two-trees and l the chords of the diagram[1], and in the second line the last sum is done over the external momenta that flow in one of the connected components of the two-tree. As an example, in the case of the generic two-loops two-points integral in equation (3.1) the trees and two-trees are reported in figures (3.2) and (3.3).

The calculation of the two relevant polynomials in equations (3.16) and (3.17) at this point is trivial:

$$D(\alpha) = \alpha_5(\alpha_1 + \alpha_2 + \alpha_3 + \alpha_4) + (\alpha_1 + \alpha_3)(\alpha_2 + \alpha_4), \tag{3.18}$$

$$Q(p^2, \alpha) = p^2[(\alpha_1 + \alpha_2)(\alpha_3 + \alpha_4)\alpha_5 + \alpha_1\alpha_2(\alpha_3 + \alpha_4) + \alpha_3\alpha_4(\alpha_1 + \alpha_2)]. \tag{3.19}$$

Note that the third and fourth diagrams of figure (3.3) do not contribute to $Q(p^2, \alpha)$ since the total momentum that flows in those diagrams is zero.

Equation (3.15) tells us that the only dependence of the integral on the dimension d enters in the integral only as an exponent of $(\frac{\pi}{i})^L \frac{1}{D(\alpha)}$. In order to proceed we assume that in equation (3.13)

[1] In graph theory a tree of a diagram G is any sub-diagram of G that contains all the vertices of G but is free of cycles (loops). A two-tree is a sub-diagram of G that contains all the vertices of G, is free of cycles and consist of 2 connected components. A chord of a tree (two-tree) is any line that does not belong to this tree (two-tree).

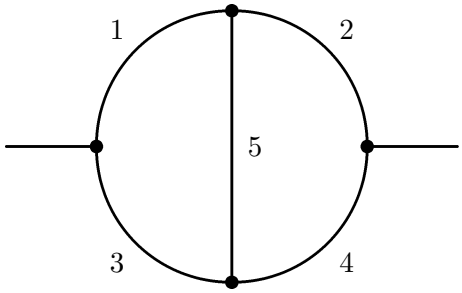

Figure 3.1: Topology for a generic two-loops two-points integrals with five internal lines. Specific topology can be obtained "shrinking" the internal lines.

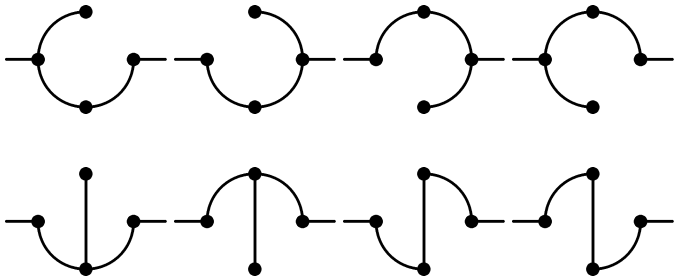

Figure 3.2: The trees of diagram 3.1

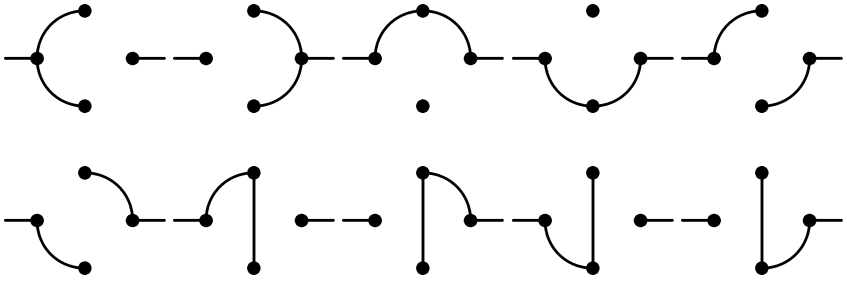

Figure 3.3: All the two-trees of diagram 3.1

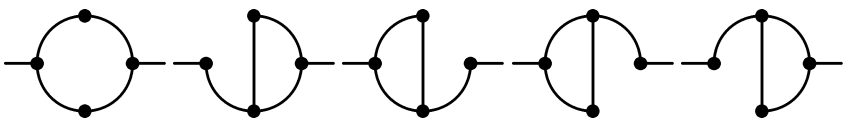

Figure 3.4: The pseudo-trees of diagram 3.1

$m_j \neq m_i$ for $j \neq i$. Next, we make the substitution $\alpha_j \to \partial_j \equiv \partial/\partial m_j^2$ in $D(\alpha)$ so as to obtain the polynomial differential operator

$$D\left(\frac{\partial}{\partial m_j^2}\right). \tag{3.20}$$

The application of the operator $D(\partial)$ to the integral (3.15) gives $D(\alpha)$ in the numerator of the integrand:

$$D(\partial)e^{-i\sum \alpha_l m_l^2} \to D(\alpha)(-i)^L e^{-i\sum \alpha_l m_l^2}. \tag{3.21}$$

The resulting integral is proportional to the same integral with d changed to $d-2$:

$$I^{(d-2)}(s_j, m_s^2) = \left(-\frac{1}{\pi}\right)^L D(\partial) I^{(d)}(s_j, m_s^2). \tag{3.22}$$

Once performed the differentiation, we identify the masses with those of the original integral. The differential operator in the right side of equation (3.22) increases the powers of the propagators in the denominator of I^d. The integrals obtained in this way can be reduced using IBP recurrence relations.

3.1.3 Dealing with Numerators II: scalar numerators

A tensorial numerator can be rewritten as

$$\prod_{r=1}^{n_1} q_{1\mu_r} \cdots \prod_{s=1}^{n_L} q_{L\lambda_s} = \prod_{r=1}^{n_1} \frac{\partial}{\partial a_{1\mu_r}} \cdots \prod_{s=1}^{n_L} \frac{\partial}{\partial a_{L\lambda_s}} e^{i\sum_j^L a_j q_j}. \tag{3.23}$$

That permits us to write the Feynman integral with a tensorial structure as

$$\prod_{i=1}^{L} \int d^d q_i \prod_{j=1}^{N} P_{\bar{q}_j, m_j}^{\nu_j} \prod_{r=1}^{n_1} q_{1\mu_r} \cdots \prod_{s=1}^{n_L} q_{L\lambda_s} = i^L \left(\frac{\pi}{i}\right)^{\frac{dL}{2}} \prod_{j=1}^{N} \frac{i^{-\nu_j - n_j}}{\Gamma(\nu_j)}$$
$$\times \prod_{r=1}^{n_1} \frac{\partial}{\partial a_{1\mu_r}} \cdots \prod_{s=1}^{n_L} \frac{\partial}{\partial a_{L\lambda_s}} \int_0^\infty \cdots \int_0^\infty \frac{d\alpha_j \alpha_j^{\nu_j - 1}}{[D(\alpha)]^{\frac{d}{2}}} e^{i[\frac{Q+B-\frac{1}{4}K}{D(\alpha)} - \sum_{l=1}^N \alpha_l (m_l^2 - i\eta)]} \Big|_{a_j=0}. \tag{3.24}$$

For convenience we have introduced other two polynomials:

$$B = \sum_l a_l \sum_{T \in T_l^1} p_T \prod_{l' \notin T} \alpha_{l'} \tag{3.25}$$

$$K = \sum_{T \in T^0} \prod_{l \notin T} \alpha_l \Big(\sum_{l' \in T loop} \pm a_{l'} \Big)^2, \tag{3.26}$$

where in the first line the sum is done over trees that include a given line l and p_T is the total external momentum that flows in that line. In the second line the sum is done over all the pseudo-trees, that is trees with an added line. For a generic tensorial two-points two-loops integrals we have only two a_i parameters. The pseudo-trees are represented in figure (3.4). Applying the definition, it is simple to find the polynomials:

$$\begin{aligned} B &= p a_1(\alpha_3\alpha_5 + \alpha_4\alpha_5 + \alpha_2\alpha_3 + \alpha_3\alpha_4) \\ &+ p a_2(\alpha_3\alpha_5 + \alpha_4\alpha_5 + \alpha_1\alpha_4 + \alpha_3\alpha_4) \end{aligned} \tag{3.27}$$

$$K = a_1^2(\alpha_2 + \alpha_4) + a_2^2(\alpha_1 + \alpha_3) + (a_1 + a_2)^2\alpha_5. \tag{3.28}$$

Differentiating with respect to a_j in equation (4.12) will produce external momenta and metric tensors multiplied by a polynomial $R(\alpha)$ and $D(\alpha)$ to some powers in the integrand. We can make the changes $\alpha_j \to \partial_j \equiv \partial/\partial m_j^2$, as we did before, in $R(\alpha) \to R(\partial)$ and $D(\alpha) \to D(\partial)$. In this way we obtain a methods for expressing a tensorial integral in terms of scalar integrals with a shifted dimension, since, as we saw, the operator $D(\partial)$ is connected with a change of the space-time dimension. This procedure corresponds to apply the equality

$$\prod_{i=1}^{L} \int d^d q_i \prod_{j=1}^{N} P_{\overline{q}_j,m_j}^{\nu_j} \prod_{r=1}^{n_1} q_{1\mu_r} \dots \prod_{s=1}^{n_L} q_{L\lambda_s} = T(p,\partial,\mathbf{d}^+) \prod_{i=1}^{L} \int d^d q_i \prod_{j=1}^{N} P_{\overline{q}_j,m_j}^{\nu_j}, \tag{3.29}$$

where the T is a proper tensor, function of the external momentum ed of the "shifting dimensions" operator $\mathbf{d}^+$. Anyway it could be cumbersome to utilize this method for tensorial integrals, while it simplifies enough for a scalar integral.

We said at the very beginning of this chapter that we can always contract a tensorial numerator with a proper projector in order to produce a scalar numerator. We also saw that it is often possible to simplify an integral provided with a scalar numerator in terms of a sum of scalar integrals. The techniques used to reduce these numerators are quite well known and we will not give them here. We will address the case in which a numerator can not be reduced. The form of the most general irreducible numerator depends on the number of loops and external legs. For this reason here we specialize ourselves in the case of two-loops two-points integrals. At two-loops order, irreducible numerators have the scalar products $(q_1 p)^\alpha$ and/or $(q_2 p)^\beta$. So we restrict our discussion to the integral

$$I_{rs}^{(d)}(p^2, m_j) = \iint \frac{d^d q_1 d^d q_2}{P_1^{\nu_1} P_2^{\nu_2} P_3^{\nu_3} P_4^{\nu_4} P_5^{\nu_5}} (q_1 p)^r (q_2 p)^s. \tag{3.30}$$

Equation (3.23) in this case takes the form

$$(q_1 p)^r (q_2 p)^s = \frac{\partial^r}{(i\partial a_1)^r} \frac{\partial^s}{(i\partial a_2)^s} \exp\left\{ i[a_1(q_1 p) + a_2(q_2 p)] \right\} |_{a_i=0} \,, \tag{3.31}$$

and it allows us to rewrite (3.30) in α-parametrization:

$$\begin{aligned} I_{r,s}^{(d)}(p^2, m_j) = {} & i^2 \left(\frac{\pi}{i}\right)^d \prod_{j=1}^{5} \frac{i^{-\nu_j}}{\Gamma(\nu_j)} \int_0^\infty \dots \int_0^\infty \frac{d\alpha_j \alpha_j^{\nu_j - 1}}{[D(\alpha)]^{\frac{d}{2}}} \\ & \exp\left[i \left(\frac{Q(\alpha) + B(\alpha, a_1, a_2) - \frac{1}{4} K(\alpha, a_1, a_2)}{D(\alpha)} - \sum_{l=1}^{5} \alpha_l (m_l^2 - i\eta) \right) \right], \end{aligned} \tag{3.32}$$

where Q and D are given in equations (3.18) and (3.19), while B and K are obtained by equations (3.27) and (3.28) with the replacements $a_1 \to p a_1$ and $a_2 \to p a_2$:

$$\begin{aligned} B &= p^2 a_1 (\alpha_3\alpha_5 + \alpha_4\alpha_5 + \alpha_2\alpha_3 + \alpha_3\alpha_4) && (3.33) \\ &+ p^2 a_2 (\alpha_3\alpha_5 + \alpha_4\alpha_5 + \alpha_1\alpha_4 + \alpha_3\alpha_4) \\ K &= p^2 (a_1^2(\alpha_2 + \alpha_4) + a_2^2(\alpha_1 + \alpha_3) + (a_1 + a_2)^2 \alpha_5). && (3.34) \end{aligned}$$

The relation between the non-scalar and the scalar integral is given by

$$I_{rs}^{(d)}(p^2, m_j) = T_{rs}(p^2, \partial, \mathbf{d}^+) I_{00}^{(d)}(p^2, m_j), \tag{3.35}$$

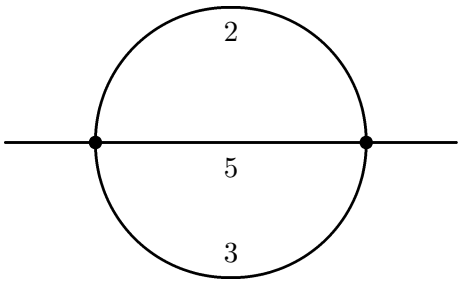

Figure 3.5: Topology of the London Transport diagram (3.37).

where

$$T_{rs}(p^2,\partial,\mathbf{d}^+) = \frac{1}{i^{r+s}}\frac{\partial^r}{\partial a_1^r}\frac{\partial^s}{\partial a_2^s}$$
$$\times \exp\left\{i[B(\alpha,a_1,a_2) - \frac{1}{4}K(\alpha,a_1,a_2)]\rho\right\}\Bigg|_{\substack{a_i=0\\ \alpha_j=i\partial_j\\ \rho=-\frac{1}{\pi^2}\mathbf{d}^+}}, \tag{3.36}$$

As an example of the techniques described here we consider the integral:

$$I_{11} = \int\!\!\int \frac{d^dq_1 d^dq_2}{P_2P_3P_5}(q_1p)(q_2p), \tag{3.37}$$

that is given by the topology in figure (3.5) (London Transport), and is obtained from figure (3.1) by shrinking the first and fourth lines. The tensor T can be calculated from the general formula (3.36) taking in account that since we have eliminated P_1 and P_4 we have to put to zero α_1 and α_2:

$$T_{11} = \frac{p^2}{2\pi^2}\mathbf{d}^+\partial_5 + \frac{p^4}{\pi^4}(\mathbf{d}^+)^2\partial_3^2\partial_5(\partial_2+\partial_5). \tag{3.38}$$

With this operator (3.35) leads to the desired relation:

$$\int\!\!\int d^dq_1 d^dq_2 \frac{(q_1p)(q_2p)}{P_2P_3P_5} =$$
$$\frac{p^2}{2\pi^2}\int\!\!\int \frac{d^{d+2}q_1 d^{d+2}q_2}{P_2P_3P_5^2} + \frac{p^4}{\pi^4}\int\!\!\int d^{d+4}q_1 d^{d+4}q_2\left[\frac{2}{P_2^2P_3^3P_5^2} + \frac{4}{P_2P_3^3P_5^3}\right]. \tag{3.39}$$

Integrals on the right-hand side of (3.39) can be reduced to basic ones in the generic dimension d by using the recurrence relations given above.

3.1.4 Two-loops Two-points Master Integrals

We saw that it is possible to reduce any given integral with a generic numerator in terms of scalar integrals (in general with a different number of space-time dimensions), and that these scalar integrals can be reduced again. In the case of two-points two-loops integrals, the first problem of the reduction

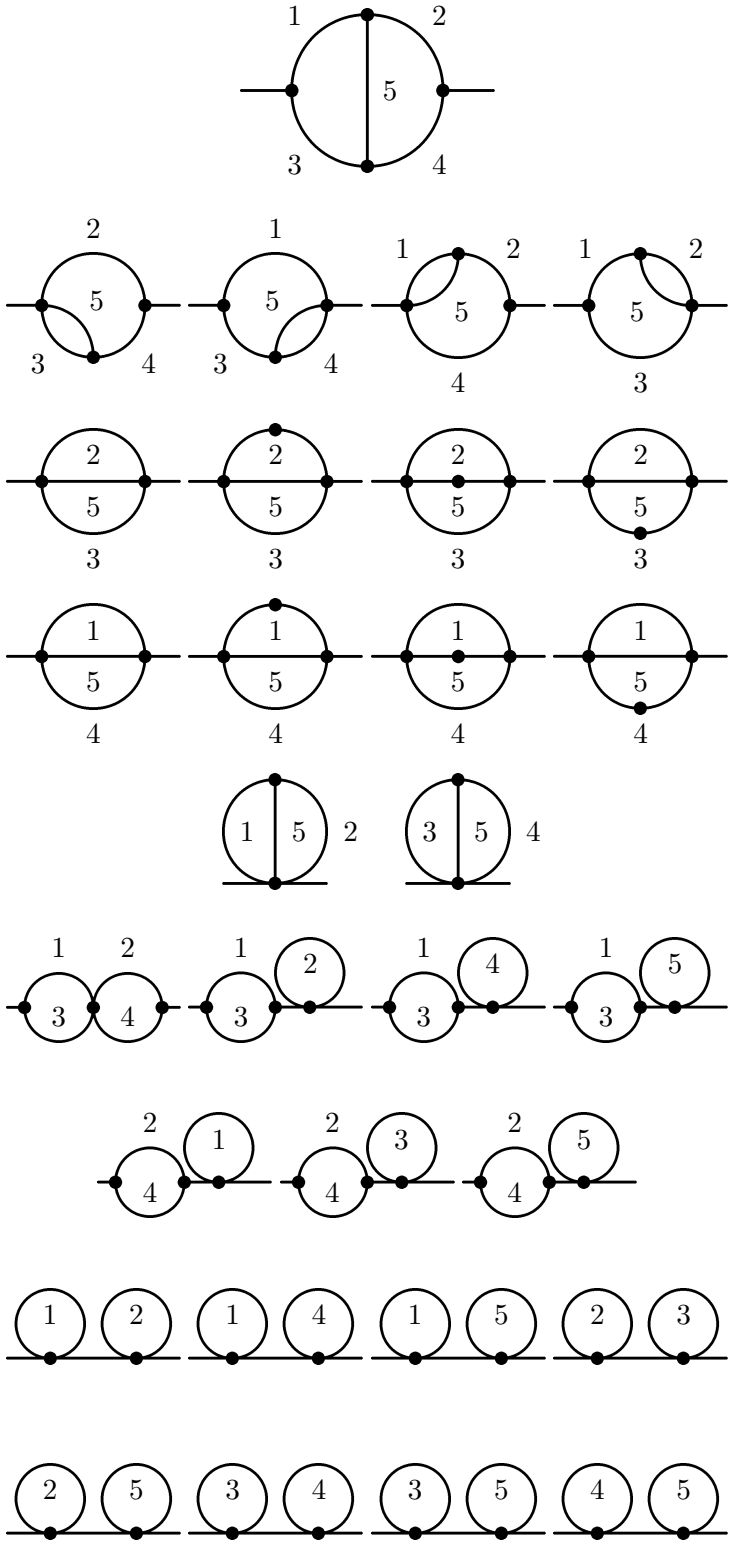

Figure 3.6: A set of Master Integrals for two-loops two-points integrals. The dots in the internal lines of the integrals of the third and fourth lines represent a derivative with respect to the mass of the dotted propagator.

has been solved and any Feynman diagrams can be represented as a combination of Master Integrals. That is we know a compete basis of irreducible integrals. Tarasov found that a possible basis is composed by the 30 integrals listed in figure (3.6). Before proceeding we should notice that the integrals that we have to compute are actually only six: two one-loop integrals and four two-loops integrals. The one-loops integrals are the well-known Passarino-Veltman integrals [8]:

$$\begin{aligned} A_0(m^2) &= \mathcal{C}\int d^dq \frac{1}{(q^2-m^2+i\eta)}, \\ B_0(p^2,m_1^2,m_2^2) &= \mathcal{C}\int d^dq \frac{1}{(q^2-m_1^2+i\eta)((q-p)^2-m_2^2+i\eta)} \end{aligned} \tag{3.40}$$

where $\mathcal{C} = \frac{(2\pi\mu)^{2\epsilon}}{i\pi^2}$ and $\epsilon = 2-\frac{d}{2}$. The Laurent expansion of these functions around $d=4$ is

$$\begin{aligned} \frac{A_0(m^2)}{m^2} &= \frac{1}{\epsilon} + \frac{A_{0f}(m^2)}{m^2} \\ &= \frac{1}{\epsilon} + (1-\ln(\frac{m^2}{\bar{\mu}^2})) + \epsilon(1+\frac{\pi^2}{12} - \ln(\frac{m^2}{\bar{\mu}^2}) + \frac{1}{2}\ln(\frac{m^2}{\bar{\mu}^2})^2) + O(\epsilon^2), \\ B_0(p^2,m_1^2,m_2^2) &= \frac{1}{\epsilon} + B_{0f}(p^2,m_1^2,m_2^2) \\ &= \frac{1}{\epsilon} - \int_0^1 dt \ln(\frac{tm_1^2+(1-t)m_2^2+(1-t)tp^2}{\bar{\mu}^2}) \\ &\quad +\epsilon(\frac{\pi^2}{12} + \frac{1}{2}\int_0^1 dt \ln^2(\frac{tm_1^2+(1-t)m_2^2+(1-t)tp^2}{\bar{\mu}^2})) + O(\epsilon^2), \end{aligned} \tag{3.41}$$

where we defined $\bar{\mu}^2 = 4\pi e^{-\gamma_E}\mu^2$. With this definition the $\overline{\text{MS}}$ renormalization scheme is obtained by subtracting only the poles, since the $\ln(4\pi)-\gamma_E$ is absorbed in the definition of the scale. The integrals in the definition of B_0 can be computed analytically [10]. The expansion (3.41) does not include only the divergent and the finite parts, but comprehends also the first evanescent term: since we are dealing with two-loops calculations, products of two one-loop integrals are present (as shown in figure (3.6)) and so we could have products of evanescent and divergent parts that contribute to the finite part. However, these products do not contribute to the renormalized object if we are in the MS and $\overline{\text{MS}}$ schemes. This is due to the fact that for these schemes the logarithms of a squared mass[2] can not be present in the subtracted poles (for a demonstration see for example [11]). This implies that all the terms $\frac{1}{\epsilon}A_{0f}$ and $\frac{1}{\epsilon}B_{0f}$ must cancel out. The other four integrals that we need to calculate are

$$\begin{aligned} M_0(p^2,m_j^2) &= \mathcal{C}^2\int d^dq_1 d^dq_2 \frac{1}{P_1P_2P_3P_4P_5}, \\ U_0(p^2,m_j^2) &= \mathcal{C}^2\int d^dq_1 d^dq_2 \frac{1}{P_2P_3P_4P_5}, \\ S_0(p^2,m_j^2) &= \mathcal{C}^2\int d^dq_1 d^dq_2 \frac{1}{P_2P_3P_5}, \\ T_0(p^2,m_j^2) &= \frac{\partial}{\partial m_2^2}S_0(p^2,m_j^2) = \mathcal{C}^2\int d^dq_1 d^dq_2 \frac{1}{P_2^2P_3P_5}. \end{aligned} \tag{3.42}$$

(3.43)

[2]Locality prevents the logarithms of the external momenta from appearing in the poles of normalized quantity for any renormalization scheme, but it does not impose conditions on the logarithms of the masses.

M_0 is the first integral represented in figure (3.6), U_0 is the first of the second line, while S_0 and T_0 are respectively the first and second of the third line. The other integrals can be obtained from these by opportunely changing the masses or as a product of two one-loop integrals. Notice that the integrals on the fifth line are actually S_0 with zero external momentum.

For generic external momentum and masses, we know analytically only the divergent part of the master integrals:

$$\begin{aligned} M_{0,\mathrm{div}}(p^2, m_j^2) &= 0, \\ U_{0,\mathrm{div}}(p^2, m_j^2) &= \frac{B_0(p^2, m_1^2, m_2^2)}{\epsilon} - \frac{1}{2\epsilon^2} + \frac{1}{2\epsilon}, \end{aligned} \tag{3.44}$$

$$\begin{aligned} S_{0,\mathrm{div}}(p^2, m_j^2) &= \frac{A_0(m_1^2) + A_0(m_2^2) + A_0(m_3^2)}{\epsilon} - \frac{m_1^2 + m_2^2 + m_3^2}{2\epsilon^2} - \frac{\frac{p^2}{2} - m_1^2 - m_2^2 - m_3^2}{2\epsilon} \\ T_{0,\mathrm{div}}(p^2, m_j^2) &= \frac{\partial_{m_1^2} A_0(m_1^2)}{\epsilon} - \frac{1}{2\epsilon^2} + \frac{1}{2\epsilon}. \end{aligned} \tag{3.45}$$

As we said before, since A_0 and B_0 have an evanescent part for $\epsilon \to 0$ the terms $\frac{A_0}{\epsilon}$ or $\frac{B_0}{\epsilon}$ have also a finite part, thus the subscript "div" in equation (3.44) is an abuse of notation. However this definition of "divergent" part made more evident the cancellation of the products $\frac{1}{\epsilon} A_{0f}$ and $\frac{1}{\epsilon} B_{0f}$ in the poles.

The finite parts of equation (3.42) are analytical only for particular values of the parameters, in particular for a vanishing momentum the basis integrals can be rewritten in terms of only two basis integrals:

$$\begin{aligned} I_0(m_j^2) &= \mathcal{C}^2 \int d^d q_1 d^d q_2 \frac{1}{(q_1^2 - m_1^2 + i\eta)(q_2^2 - m_2^2 + i\eta)((q_1 - q_2)^2 - m_3^2 + i\eta)}, \\ A_0(m^2) &= \mathcal{C} \int d^d q \frac{1}{(q^2 - m^2 + i\eta)}, \end{aligned} \tag{3.46}$$

that are well known in literature (see for example [12, 13]).

In any case it is quite simple to approach the finite parts of these integrals with standard methods, and we can write them in terms of numerical integrals over the Feynman parameters. Another possible technique to evaluate numerically these integrals is the utilization of IBP methods in order to find a system of differential equations [7]. In Appendix (3.A.1) we give more details on the integral representation of the master integrals.

Unfortunately, the knowledge of a valid numerical representation for the integrals is not sufficient. It can happen that for some particular choice of the parameters the integrals cancel out and a very high precision in the numerical evaluation is required. Thus we used the TSIL program [6] that was created with the sole purpose of calculating these integrals at high precisions.

The problem of the cancellations has actually a theoretical explanation. It is true that the basis found by Tarasov is complete, but this is a good basis only when all the masses are different: for particular values of the masses and momenta some of the basis integrals become linear-dependent. In the case of zero-external momentum we already know that the basis reduce to only the two integrals in equation (3.46), and in this case it is simple to find the relations between the old and the new basis:

$$U_0(0, m_1^2, m_2^2, m_3^2, m_4^2) = \frac{1}{m_1^2 - m_2^2}(I_0(m_1^2, m_3^2, m_4^2) - I_0(m_2^2, m_3^2, m_4^2)). \tag{3.47}$$

There are however other relations, more difficult to spot:

$$\begin{aligned}&(m_1^2 - m_2^2)T_0(p^2 = m_1^2, m_2^2, m_1^2, m_2^2) = \\ &-\frac{13m_1^2}{8} + 2m_2^2 - \frac{A_0(m_1^2)}{2} + 2A_0(m_2^2) + \frac{m_1^2 A_0(m_2^2)}{m_2^2} + \\ &\frac{A_0(m_1^2)A_0(m_2^2)}{m_2^2} + \frac{A_0(m_2^2)^2}{2m_2^2} - S_0(p^2 = m_1^2, m_2^2, m_1^2, m_2^2).\end{aligned} \tag{3.48}$$

3.2 Two-loop correction to the Higgs pole mass

In this section we discuss the two-loop renormalization of the Higgs sector of the SM and then derive the two-loop relation between $\lambda(\mu)$ and the physical parameters G_μ, M_t, M_W, M_Z and M_h, following references [14–16]. To determine the $\overline{\rm MS}$ parameters in terms of physical observables two strategies can be envisaged.

i) Perform an $\overline{\rm MS}$ renormalisation to obtain directly the $\overline{\rm MS}$ quantity of interest in terms of $\overline{\rm MS}$ parameters. Then express the $\overline{\rm MS}$ parameters in terms of the physical ones via appropriately derived two-loop relations.

ii) Use a renormalisation scheme in which the renormalised parameters are directly expressed in terms of physical observables (we call this scheme generically on-shell (OS) and label quantities in this scheme with an OS). Then relate the parameters as expressed in the OS scheme to their $\overline{\rm MS}$ counterparts we are looking for.

This last step can be easily done using the relation

$$\theta_0 = \theta_{\rm OS} - \delta\theta_{\rm OS} = \theta(\bar\mu) - \delta\theta_{\overline{\rm MS}} \tag{3.49}$$

or

$$\theta(\bar\mu) = \theta_{\rm OS} - \delta\theta_{\rm OS} + \delta\theta_{\overline{\rm MS}}\,, \tag{3.50}$$

where θ_0 is the bare parameter, $\theta(\bar\mu)$ ($\theta_{\rm OS}$) is the renormalised $\overline{\rm MS}$ (OS) version and $\delta\theta_{\overline{\rm MS}}$ ($\delta\theta_{\rm OS}$) the corresponding counterterm. By definition $\delta\theta_{\overline{\rm MS}}$ subtracts only the terms proportional to powers of $1/\epsilon$ and $\gamma - \ln(4\pi)$ in dimensional regularisation, with $d = 4 - 2\,\epsilon$ being the space-time dimension. Concerning the structure of the $1/\epsilon$ poles in the OS and $\overline{\rm MS}$ counterterms, one notices that it should be identical once the poles in the OS counterterms are expressed in terms of $\overline{\rm MS}$ quantities. Then, after this operation is performed, the desired $\theta(\bar\mu)$ is obtained from

$$\theta(\bar\mu) = \theta_{\rm OS} - \delta\theta_{\rm OS}|_{\rm fin} + \Delta_\theta \tag{3.51}$$

where the subscript 'fin' denotes the finite part of the quantity involved and Δ is the two-loop finite contribution that is obtained when the OS parameters entering the $1/\epsilon$ pole in the OS counterterm are expressed in terms of $\overline{\rm MS}$ quantities, the finite contribution coming from the $\mathcal{O}(\epsilon)$ part of the shifts. Here we will adopt the second strategy.

The quantities of interests are $\theta = (m^2, \lambda, v, y_t, g_2, g_1)$, i.e. the quadratic and quartic couplings in the Higgs potential, the vacuum expectation value (vev), the top Yukawa coupling, the $\mathrm{SU}(2)_L$ and $\mathrm{U}(1)_Y$ gauge couplings g_2 and g_Y (with $g_1 = \sqrt{5/3}g_Y$ being the hypercharge coupling rewritten in SU(5) normalisation), are directly determined in terms of the pole masses of the Higgs (M_h), of the top (M_t), of the Z (M_Z), of the W (M_W), the Fermi constant G_μ and the $\overline{\rm MS}$ strong coupling $\alpha_3(M_Z)$.

Their input values are listed in Table 2.2 in chapter 2. Then, using equation (3.51), the $\overline{\rm MS}$ quantities are obtained.

3.2.1 Renormalization of the Higgs potential

We start from the classical Higgs potential

$$V_0 = -m_0^2|H|^2 + \lambda_0|H|^4 \ , \tag{3.52}$$

where the classical Higgs doublet H is defined by

$$H = \begin{pmatrix} \chi \\ (v_0 + h + i\,\sigma)/\sqrt{2} \end{pmatrix} \tag{3.53}$$

in terms of the physical higgs field h, and of the neutral and charged Goldstones σ and χ, and m_0^2, λ_0 and v_0 are bare quantities. We then introduce the renormalized quantities $m_{\rm OS}$, $\lambda_{\rm OS}$ and $v_{\rm OS}$ through the conditions

$$m_{\rm OS}^2 = \lambda_{\rm OS} v_{\rm OS}^2 \ , \qquad M_h^2 = 2\lambda_{\rm OS} v_{\rm OS}^2 \ , \qquad v_{\rm OS}^2 = \frac{1}{\sqrt{2}G_\mu} \ , \tag{3.54}$$

where M_h is the Higgs pole mass and G_μ is the muon decay constant. Equations (3.54) tell us

$$\lambda_{\rm OS} = \frac{G_\mu}{\sqrt{2}} M_h^2 \ . \tag{3.55}$$

The quantum correction to the potential is

$$\delta V = V_{\rm OS} - V_0 \ , \tag{3.56}$$

where $V_{\rm OS}$ is the classical Higgs potential in which we simply substitute m_0^2, λ_0 and v_0 with $m_{\rm OS}$, $\lambda_{\rm OS}$ and $v_{\rm OS}$ respectively; it is explicitly given by

$$\begin{aligned} V_{\rm OS} \ &= \ \lambda_{\rm OS}\left[\chi^*\chi\left(\chi^*\chi + h^2 + \sigma^2\right) + \frac{1}{4}\left(h^2+\sigma^2\right)^2\right] + \\ &\quad + \lambda_{\rm OS} v_{\rm OS} h\left(2\,\chi^*\chi + h^2 + \sigma^2\right) + \frac{1}{2}M_h^2 h^2 . \end{aligned} \tag{3.57}$$

Up to second order in the variations,

$$\delta m^2 = m_{\rm OS}^2 - m_0^2 \ , \qquad \delta\lambda = \lambda_{\rm OS} - \lambda_0 \ , \qquad \delta v = v_{\rm OS} - v_0 \tag{3.58}$$

we have

$$\begin{aligned} \delta V \ &= \ \delta\lambda\left[\chi^*\chi\left(\chi^*\chi + h^2 + \sigma^2\right) + \frac{1}{4}\left(h^2+\sigma^2\right)^2\right] + \\ &\quad + \left[\lambda_{\rm OS}\left(\frac{\delta v^2}{2\,v_{\rm OS}} + \frac{(\delta v^2)^2}{8\,v_{\rm OS}^3}\right) + v_{\rm OS}\delta\lambda\left(1 - \frac{\delta v^2}{2\,v_{\rm OS}^2}\right)\right] h\left(2\,\chi^*\chi + h^2 + \sigma^2\right) + \\ &\quad + \delta\tau\left(\frac{1}{2}\sigma^2 + \chi^*\chi\right) + \frac{\delta M_h^2}{2}h^2 + v_{\rm OS}\delta\tau\left(1 - \frac{\delta v^2}{2\,v_{\rm OS}^2}\right) h \, . \end{aligned} \tag{3.59}$$

Here δv^2 is defined implicitly by $\sqrt{v_{\rm OS}^2 - \delta v^2} = v_{\rm OS} - \delta v$, and we introduced

$$\delta M_h^2 \equiv 3\left[\lambda_{\rm OS}\delta v^2 + v_{\rm OS}^2\delta\lambda\left(1 - \frac{\delta v^2}{v_{\rm OS}^2}\right)\right] - \delta m^2\,, \tag{3.60}$$

$$\delta\tau \equiv \lambda_{\rm OS}\delta v^2 + v_{\rm OS}^2\delta\lambda\left(1 - \frac{\delta v^2}{v_{\rm OS}^2}\right) - \delta m^2\,. \tag{3.61}$$

Subtracting equations (3.60) and (3.61),

$$\delta M_h^2 - \delta\tau = 2v_{\rm OS}^2\delta\lambda\left(1 - \frac{\delta v^2}{v_{\rm OS}^2}\right) + 2\lambda_{\rm OS}\delta v^2\,, \tag{3.62}$$

one can see that $\delta\lambda$ can be determined once we know δM_h^2, $\delta\tau$ and δv^2.

- The first of these variations is fixed by the condition that M_h is the pole Higgs mass, which implies
$$\delta M_h^2 = \mathrm{Re}\,\Pi_{hh}(M_h^2)\,, \tag{3.63}$$
where $\Pi_{hh}(p^2)$ is the Higgs self-energy function.

- To determine $\delta\tau$ we impose that the Higgs tadpole diagrams cancel, which leads to (see the last term of eq. (3.59))
$$\delta\tau = -\frac{T}{v_{\rm OS}(1 - \delta v^2/2v_{\rm OS}^2)}\,, \tag{3.64}$$
where $i\,T$ is the sum of the Higgs tadpole diagrams.

- Finally, δv^2 is fixed by computing G_μ in terms of the SM parameters. This computation will be discussed in the next sections; here we parametrise the result as
$$\frac{G_\mu}{\sqrt{2}} = \frac{1}{2v_0^2}(1 + \Delta r_0)\,, \tag{3.65}$$
which simply states that G_μ is given by its tree-level value plus radiative corrections, $\Delta r_0/(2v_0^2)$.

By inserting the last definitions of (3.54) and (3.58) into equation (3.65) we have

$$\delta v^2 = -\frac{\Delta r_0}{\sqrt{2}G_\mu} = -v_{\rm OS}^2\Delta r_0\,. \tag{3.66}$$

Equations (3.54), (3.62), (3.63), (3.64) and (3.66) allow us to compute $\delta\lambda$: at one-loop we have

$$\delta\lambda^{(1)} = \frac{G_\mu}{\sqrt{2}}M_h^2\left\{\Delta r_0^{(1)} + \frac{1}{M_h^2}\left[\frac{T^{(1)}}{v_{\rm OS}} + \mathrm{Re}\,\Pi_{hh}^{(1)}(M_h^2)\right]\right\}\,, \tag{3.67}$$

and the two-loop correction is

$$\begin{aligned}\delta\lambda^{(2)} = \frac{G_\mu}{\sqrt{2}}M_h^2\Bigg\{&\Delta r_0^{(2)} + \frac{1}{M_h^2}\left[\frac{T^{(2)}}{v_{\rm OS}} + \mathrm{Re}\,\Pi_{hh}^{(2)}(M_h^2)\right]\\ &-\frac{\Delta r_0^{(1)}}{M_h^2}\left[M_h^2\Delta r_0^{(1)} + \frac{3\,T^{(1)}}{2\,v_{\rm OS}} + \mathrm{Re}\,\Pi_{hh}^{(1)}(M_h^2)\right]\Bigg\}\,,\end{aligned} \tag{3.68}$$

where the labels (1) and (2) denote the one-loop and two-loop terms respectively. Similarly, one finds for the counterterm of the quadratic Higgs coupling in the potential

$$\delta^{(1)} m^2_{\rm OS} = 3\frac{T^{(1)}}{v_{\rm OS}} + \delta^{(1)} M_h^2 \,, \tag{3.69}$$

$$\delta^{(2)} m^2_{\rm OS} = 3\frac{T^{(2)}}{v_{\rm OS}} + \delta^{(2)} M_h^2 - \frac{3\,T^{(1)}}{2\,v_{\rm OS}} \Delta r_0^{(1)} \,. \tag{3.70}$$

The top Yukawa and gauge couplings are fixed using M_t, M_W and M_Z via

$$M_t = \frac{y_{t_{\rm OS}}}{\sqrt{2}} v_{\rm OS}, \qquad M_W^2 = \frac{g_{2_{\rm OS}}^2}{4} v_{\rm OS}^2, \qquad M_Z^2 = \frac{g_{2_{\rm OS}}^2 + g_{Y_{\rm OS}}^2}{4} v_{\rm OS}^2 \tag{3.71}$$

or

$$y_{t_{\rm OS}} = 2\left(\frac{G_\mu}{\sqrt{2}} M_t^2\right)^{1/2}, \quad g_{2_{\rm OS}} = 2\left(\sqrt{2}\,G_\mu\right)^{1/2} M_W, \quad g_{Y_{\rm OS}} = 2\left(\sqrt{2}\,G_\mu\right)^{1/2} \sqrt{M_Z^2 - M_W^2} \,. \tag{3.72}$$

The corresponding counterterms are found to be

$$\delta^{(1)} y_{t_{\rm OS}} = 2\left(\frac{G_\mu}{\sqrt{2}} M_t^2\right)^{1/2} \left(\frac{\delta^{(1)} M_t}{M_t} + \frac{\Delta r_0^{(1)}}{2}\right), \tag{3.73}$$

$$\delta^{(2)} y_{t_{\rm OS}} = 2\left(\frac{G_\mu}{\sqrt{2}} M_t^2\right)^{1/2} \left(\frac{\delta^{(2)} M_t}{M_t} + \frac{\Delta r_0^{(2)}}{2} - \frac{\Delta r_0^{(1)}}{2}\left[\frac{\delta^{(1)} M_t}{M_t} + \frac{3\,\Delta r_0^{(1)}}{4}\right]\right), \tag{3.74}$$

for the top Yukawa coupling,

$$\delta^{(1)} g_{2_{\rm OS}} = \left(\sqrt{2}\,G_\mu\right)^{1/2} M_W \left(\frac{\delta^{(1)} M_W^2}{M_W^2} + \Delta r_0^{(1)}\right), \tag{3.75}$$

$$\delta^{(2)} g_{2_{\rm OS}} = \left(\sqrt{2}\,G_\mu\right)^{1/2} M_W \left(\frac{\delta^{(2)} M_W^2}{M_W^2} + \Delta r_0^{(2)} + \right.$$
$$\left. - \frac{\Delta r_0^{(1)}}{2}\left[\frac{\delta^{(1)} M_W^2}{M_W^2} + \frac{3\Delta r_0^{(1)}}{2}\right] + \frac{1}{4}\left(\frac{\delta^{(1)} M_W^2}{M_W^2}\right)^2\right), \tag{3.76}$$

for the $\mathrm{SU}(2)_L$ gauge coupling and for the hypercharge gauge coupling

$$\delta^{(1)} g_{Y_{\rm OS}} = \left(\sqrt{2}\,G_\mu\right)^{1/2} \sqrt{M_Z^2 - M_W^2}\ \left(\frac{\delta^{(1)} M_Z^2 - \delta^{(1)} M_W^2}{M_Z^2 - M_W^2} + \Delta r_0^{(1)}\right) \tag{3.77}$$

$$\delta^{(2)} g_{Y_{\rm OS}} = \left(\sqrt{2}\,G_\mu\right)^{1/2} \sqrt{M_Z^2 - M_W^2}\ \left(\frac{\delta^{(2)} M_Z^2 - \delta^{(2)} M_W^2}{M_Z^2 - M_W^2} + \Delta r_0^{(2)} + \right.$$
$$\left. - \frac{\Delta r_0^{(1)}}{2}\left[\frac{\delta^{(1)} M_Z^2 - \delta^{(1)} M_W^2}{M_Z^2 - M_W^2} + \frac{3\Delta r_0^{(1)}}{2}\right] + \frac{1}{4}\left(\frac{\delta^{(1)} M_Z^2 - \delta^{(1)} M_W^2}{M_Z^2 - M_W^2}\right)^2\right) \,. \tag{3.78}$$

The $\overline{\rm MS}$ Higgs quartic coupling is given by

$$\lambda(\bar\mu) = \frac{G_\mu}{\sqrt{2}} M_h^2 + \lambda^{(1)}(\bar\mu) + \lambda^{(2)}(\bar\mu) \tag{3.79}$$

with

$$\begin{aligned}\lambda^{(1)}(\bar{\mu}) &= -\,\delta^{(1)}\lambda_{\rm OS}\Big|_{\rm fin} \\ \lambda^{(2)}(\bar{\mu}) &= -\,\delta^{(2)}\lambda_{\rm OS}\Big|_{\rm fin} + \Delta_\lambda\ .\end{aligned} \tag{3.80}$$

The one-loop contribution in eq. (3.79), $\lambda^{(1)}$, is given by the finite part of eq. (3.67). Concerning the two-loop part, $\lambda^{(2)}(\bar{\mu})$, the QCD corrections were presented in refs. [15, 19], and the two-loop electroweak (EW) part, $\lambda^{(2)}_{\rm EW}(\bar{\mu})$, was computed in ref. [15] in the so-called gauge-less limit of the SM, in which the electroweak gauge interactions are switched off. The main advantage of this limit results in a simplified evaluation of $\Delta r_0^{(2)}$. The computation of the two-loop EW part in the full SM requires instead the complete evaluation of this quantity and was presented in [16]. In the next section we outline the computation of the Fermi constant.

3.2.2 Two-loop correction to the Fermi constant

The experimental measurement of G_μ is presented within the Fermi theory of muon decay, supplemented by QED

$$\mathcal{L}_{\rm Fermi} = \mathcal{L}_{\rm QED} + \frac{G_\mu}{\sqrt{2}}\left[\bar{e}\gamma_\alpha(1-\gamma_5)\nu_e\right]\left[\bar{\nu}_\mu\gamma^\alpha(1-\gamma_5)\mu\right]\ , \tag{3.81}$$

which is the correct low-energy theory at leading order in $(E/M_W)^2$. As usual, $\mathcal{L}_{\rm QED}$ contains the kinetic terms of all the light SM fermions, their interactions with the photon, and the photon kinetic term. Working at first order in G_μ (as we will do and as appropriate for this approximation), $\mathcal{L}_{\rm Fermi}$ defines a renormalizable theory.

The Fermi constant G_μ is defined in terms of the muon lifetime τ_μ as

$$\frac{1}{\tau_\mu} = \frac{G_\mu^2 m_\mu^5}{192\pi^3} F\!\left(\frac{m_e^2}{m_\mu^2}\right)(1+\Delta q)\left(1+\frac{3m_\mu^2}{5M_W^2}\right)\ , \tag{3.82}$$

where $F(\rho) = 1 - 8\rho + 8\rho^3 - \rho^4 - 12\rho^2\ln\rho = 0.9981295$ is the phase space factor and $\Delta q = \Delta q^{(1)} + \Delta q^{(2)} = (-4.234 + 0.036)\ 10^{-3}$ are the QED corrections computed at one and two loops [18]. From the measurement $\tau_\mu = (2196980.3 \pm 2.2)$ ps [17] we extract $G_\mu = 1.1663781(6)\ 10^{-5}/\,\mathrm{GeV}^2$. This is 1σ lower than the value quoted in [17] because we do not follow the convention of including in the definition of G_μ itself the latter term of(3.82), which is the contribution from dimension-8 SM operators.

The computation of Δr_0 requires the subtraction of the QED corrections by matching the result in the SM with that in the Fermi theory. However, it is well known that the Fermi theory is renormalisable to all order in the electromagnetic interaction but to lowest order in G_μ due to a Ward identity that becomes manifest if the 4-fermion interaction is rewritten via a Fierz transformation in the "charge retention order". As a consequence, in the limit of neglecting the fermion masses, Δr_0 as computed in the Fermi theory vanishes and we are just left with the calculation in the SM[3].

Starting from equation (3.65) we write Δr_0 as a sum of different terms:

$$\Delta r_0 = V_W - \frac{A_{WW}}{M_{W0}^2} + 2\,v_0^2\mathcal{B}_W + \mathcal{E} + \mathcal{M}\ , \tag{3.83}$$

where M_{W0} is the bare W mass; A_{WW} is the W self-energy at zero momentum, $A_{WW} = A_{WW}(0)$; V_W

[3] We explicitly verified that Δr_0 vanishes when computed in the Fermi theory.

is the vertex contribution; $\mathcal{B}_W$ is the box contribution; $\mathcal{E}$ is the term due to the renormalisation of the external legs; $\mathcal{M}$ is the mixed contribution due to product of different objects among V_W, A_{WW}, $\mathcal{B}_W$ and $\mathcal{E}$ (see below for an explicit expression at two-loops). All quantities in equation (3.83) are computed at zero external momenta. We point out that in the right-hand side of equation (3.83) no tadpole contribution is included because of our choice of identifying the renormalised vacuum with the minimum of the radiatively corrected potential. As a consequence Δr_0 is a gauge-dependent quantity.

From equation (3.83) the one-loop term is given by:

$$\Delta r_0^{(1)} = V_W^{(1)} - \frac{A_{WW}^{(1)}}{M_W^2} + \frac{\sqrt{2}}{G_\mu}\mathcal{B}_W^{(1)} + \mathcal{E}^{(1)} \ , \tag{3.84}$$

where we have used that $\mathcal{M}^{(1)} = 0$, while at two-loops

$$\begin{aligned}\Delta r_0^{(2)} \ &= \ V_W^{(2)} - \frac{A_{WW}^{(2)}}{M_W^2} + \sqrt{2}\,\frac{\mathcal{B}_W^{(2)}}{G_\mu} + \mathcal{E}^{(2)} + \mathcal{M}^{(2)} + \\ &\quad -\delta^{(1)}M_W^2\,\frac{A_{WW}^{(1)}}{M_W^4} + \frac{\sqrt{2}}{G_\mu}\mathcal{B}_W^{(1)}\left(V_W^{(1)} - \frac{A_{WW}^{(1)}}{M_W^2} + \sqrt{2}\,\frac{\mathcal{B}_W^{(1)}}{G_\mu} + \mathcal{E}^{(1)}\right) \ .\end{aligned} \tag{3.85}$$

Here

$$\delta^{(1)}M_W^2 = \mathrm{Re}\,\Pi_{WW}(M_W^2) \tag{3.86}$$

with $\Pi_{WW}(M_W^2)$ the W boson self-energy evaluated at external momentum equal to M_W, and

$$\mathcal{M}^{(2)} = \frac{\sqrt{2}}{G_\mu}\mathcal{E}^{(1)}\,\mathcal{B}_W^{(1)} + \sum_{i<j}\mathcal{E}_i^{(1)}\mathcal{E}_j^{(1)} + \mathcal{E}^{(1)}V^{(1)} - \left(\mathcal{E}^{(1)} + V^{(1)}\right)\frac{A_{WW}^{(1)}}{M_W^2} \ . \tag{3.87}$$

The indices i, j in equation (3.87) label the different species in the muon decay: μ, e, ν_μ and ν_e with the sum that runs over $i < j$ because the terms with $i = j$ are included in $\mathcal{E}^{(2)}$.

We recall that Δr_0 is an infrared (IR) safe quantity but not ultraviolet (UV) finite. However, the $\mathcal{E}$ and $\mathcal{B}_W$ terms in eq. (3.84) and (3.85) contain IR-divergent contributions from photon diagrams. To separate the UV-divergent terms from the IR ones we regulated the latter giving a small mass to the photon. We then explicitly verified the cancellation of all IR divergent contributions.

The calculation of this quantity followed the methods outlined in section (3.1). We want to note the fact that, although we have contributions from three- and four-points integrals, we calculated them at zero external momentum and so we could use as basis the integrals in equation (3.46). Also, in order to reduce the V_W and $\mathcal{B}_W$ terms in terms of scalar numerators we used the projector presented in ref. [20].

3.2.3 Two-loop correction to the Higgs quartic coupling

The other proper two-loop contributions to $\lambda^{(2)}(\bar{\mu})$ are the two-loop tadpole diagrams and the two-loop Higgs boson mass counterterm. The Higgs mass counterterm, not taking into account negligible width effects, is given by

$$\delta M_h^2 = \mathrm{Re}\,\Pi_{hh}(M_h^2) \tag{3.88}$$

with $\Pi_{hh}(M_h^2)$ the Higgs self-energy evaluated at external momentum equal to M_h. It should be noted that the Higgs mass counterterm as defined in eq. (3.88) and $\Delta r_0^{(2)}$ in equation (3.85) are gauge-dependent quantities. Yet $\lambda(\bar{\mu})$ is a gauge-invariant object, as shown in appendix (3.A.2).

The two loop correction to λ is the sum of a QCD term and of an electroweak (EW) term. The QCD correction $\lambda^{(2)}_{\rm QCD}(\bar\mu)$ is reported as an approximated formula in eq. (47) of [15]. For simplicity here we present it also in a numerical form:

$$\lambda^{(2)}_{\rm QCD}(\bar\mu = M_t) = \frac{g_3^2}{(4\pi)^4}\left[-23.89 + 0.12\left(\frac{M_h}{\rm GeV} - 125\right) - 0.64\left(\frac{M_t}{\rm GeV} - 173\right)\right]. \tag{3.89}$$

The result for $\lambda^{(2)}_{\rm EW}(\bar\mu)$ is too long to be displayed explicitly. Here we present it in a numerical form valid around the measured values of M_h and M_t. Using the inputs in Table 2.2 we find

$$\lambda^{(2)}_{\rm EW}(\bar\mu = M_t) = \frac{1}{(4\pi)^4}\left[-9.45 - 0.11\left(\frac{M_h}{\rm GeV} - 125\right) - 0.21\left(\frac{M_t}{\rm GeV} - 173\right)\right]. \tag{3.90}$$

The numerical expression in eq. (3.90) is accidentally very close to the gaugeless limit of the SM presented in eq. (2.45) of [15]. Furthermore, as a check of our result, we verified that in the (physically irrelevant) limit $M_h = 0$, it agrees with an independent computation of $\lambda^{(2)}$ performed using the known results for the two-loop effective potential in the Landau gauge.

3.2.4 Two-loop correction to the Higgs mass term

The result for the mass term in the Higgs potential can be easily obtained from that on $\lambda(\bar\mu)$. We write

$$m^2(\bar\mu) = M_h^2 + \delta^{(1)}m^2(\bar\mu) + \delta^{(2)}m^2(\bar\mu) \tag{3.91}$$

with

$$\begin{aligned} \delta^{(1)}m^2(\bar\mu) &= -\,\delta^{(1)}m^2_{\rm OS}\Big|_{\rm fin} \\ \delta^{(2)}m^2(\bar\mu) &= -\,\delta^{(2)}m^2_{\rm OS}\Big|_{\rm fin} + \Delta_{m^2}\ . \end{aligned} \tag{3.92}$$

The one-loop contribution in equation (3.91), $\delta^{(1)}m^2(\bar\mu)$, is given by the finite part of equation (3.69). The two-loop corrections in equation (3.91), $\delta^{(2)}m^2(\bar\mu)$, can be divided into a QCD contribution plus an EW contribution.

The QCD contribution, $\delta^{(2)}_{\rm QCD}m^2(\bar\mu)$, can be obtained evaluating the relevant diagrams via a Taylor series in $x_{ht} \equiv M_h^2/M_t^2$ up to fourth order

$$\begin{aligned} \delta^{(2)}_{\rm QCD}m^2(\bar\mu) &= \frac{G_\mu M_t^4}{\sqrt{2}(4\pi)^4} N_c\, C_F g_3^2\Big[-96 + (41 - 12\ln^2\frac{M_t^2}{\bar\mu^2} + 12\ln^2\frac{M_t^2}{\bar\mu^2})x_{ht} + \\ &\qquad + \frac{122}{135}x_{ht}^2 + \frac{1223}{3150}x_{ht}^3 + \frac{43123}{661500}x_{ht}^4\Big] \end{aligned} \tag{3.93}$$

where N_c and C_F are colour factors ($N_c = 3$, $C_F = 4/3$), such that it is numerically approximated as

$$\delta^{(2)}_{\rm QCD}m^2(\bar\mu = M_t) = \frac{g_3^2 M_h^2}{(4\pi)^4}\left[-140.50 + 2.89\left(\frac{M_h}{\rm GeV} - 125\right) - 3.71\left(\frac{M_t}{\rm GeV} - 173\right)\right]. \tag{3.94}$$

The two-loop EW part, $\delta^{(2)}_{\rm EW}m^2(\bar\mu)$, can be obtained as a byproduct of the calculation of $\lambda^{(2)}_{\rm EW}(\bar\mu)$. Also in this case the result is too long to be displayed and we present an interpolating formula. Using the

inputs in table 2.2 we find

$$\delta^{(2)}_{\rm EW} m^2(\bar\mu = M_t) = \frac{M_h^2}{(4\pi)^4}\left[-149.47 + 2.53\left(\frac{M_h}{\rm GeV} - 125\right) - 4.69\left(\frac{M_t}{\rm GeV} - 173\right)\right]. \tag{3.95}$$

3.2.5 Two loop correction to the top Yukawa coupling

The $\overline{\rm MS}$ top Yukawa coupling is given by

$$y_t(\bar\mu) = 2\left(\frac{G_\mu}{\sqrt{2}} M_t^2\right)^{1/2} + y_t^{(1)}(\bar\mu) + y_t^{(2)}(\bar\mu) \tag{3.96}$$

with

$$\begin{aligned} y_t^{(1)}(\bar\mu) &= -\,\delta^{(1)} y_{t_{\rm OS}}\Big|_{\rm fin} \\ y_t^{(2)}(\bar\mu) &= -\,\delta^{(2)} y_{t_{\rm OS}}\Big|_{\rm fin} + \Delta_{y_t}\ . \end{aligned} \tag{3.97}$$

According to equations (3.73)–(3.74) the corrections to the tree-level value of y_t are given in terms of Δr_0 and the top mass counterterm. Regarding the latter, a general discussion on the mass counterterm for unstable fermions in parity-nonconserving theories is presented in ref. [21]. Writing the fermion self-energy as

$$\begin{aligned} \Sigma(p) &= \Sigma_1(p) + \Sigma_2(p)\gamma_5\ , \\ \Sigma_{1,2}(p) &= \not{p} B_{1,2}(p^2) + m_0 A_{1,2}(p^2) \end{aligned} \tag{3.98}$$

the fermion propagator is given by

$$iS(p) = \frac{i}{\not{p} - m_0 - \Sigma(p)} = \frac{i}{\not{p} - m_0 - \Sigma_{\rm eff}(p)}\left[1 - \frac{\Sigma_2(p)}{\not{p} - \Sigma_1(p) + m_0[1 + 2A_1(p^2)]}\gamma_5\right]\ , \tag{3.99}$$

where m_0 is the bare fermion mass and

$$\Sigma_{\rm eff}(p) = \Sigma_1(p) + \frac{\Sigma_2(p)\left[\Sigma_2(p) - 2m_0 A_2(p^2)\right]}{\not{p} - \Sigma_1(p) + m_0[1 + 2A_1(p^2)]}\ . \tag{3.100}$$

Identifying the position $\not{p} = \tilde M$ of the complex pole in eq. (3.99) by

$$\tilde M = m_0 + \Sigma_{\rm eff}(\tilde M) \tag{3.101}$$

and parametrizing $\tilde M = M - i\Gamma/2$ with M the pole mass of the unstable fermion and Γ its width, the mass counterterm for the unstable fermion is found to be

$$\delta M = {\rm Re}\,\Sigma_{\rm eff}(\tilde M)\ . \tag{3.102}$$

Specialising the above discussion to the top, we find, including up to two-loop contributions,

$$\delta M_t = {\rm Re}\left[\Sigma_1(\widetilde{M}_t) + \frac{\Sigma_2(M_t)\left[\Sigma_2(M_t) - 2M_t A_2(M_t^2)\right]}{2M_t}\right] \tag{3.103}$$

with $\widetilde{M_t} = M_t - i\Gamma_t/2$. The mass counterterm defined in equation (3.103) is expressed in terms of the self-energy diagrams only, without including the tadpole contribution. While this definition follows from our choice of identifying the renormalised vacuum with the minimum of the radiatively corrected potential, it gives rise to a δM_t that is gauge-dependent and, as a consequence, in this framework, the $\overline{\text{MS}}$ top mass, $M_t(\bar{\mu})$, is a gauge-dependent quantity. However, a $\overline{\text{MS}}$ mass is not a physical quantity nor a Lagrangian parameter and therefore the requirement of gauge-invariance is not mandatory. A gauge-invariant definition of $M_t(\bar{\mu})$ can be obtained by including the tadpole contribution in the mass counterterm [22]. However, with this choice the relation between the pole and $\overline{\text{MS}}$ masses of top quark acquires a very large electroweak correction [23]. The top Yukawa coupling computed in this paper is a parameter of the Lagrangian, and thereby does not suffer of these problems.

Concerning the two-loop contributions in equation (3.96), we have computed the QCD corrections to the one-loop term and the two-loop EW contribution.

These contributions are too long to be displayed explicitly, and we report them as interpolating formulæ. Using the inputs in table 2.2 we find

$$\begin{aligned} y_t^{(2)}(\bar{\mu} = M_t) \;=\; & \frac{1}{(4\pi)^4}\left[5.22 - 0.01\left(\frac{M_h}{\text{GeV}} - 125\right) + 0.15\left(\frac{M_t}{\text{GeV}} - 173\right)\right] + \\ & + \frac{g_3^2}{(4\pi)^4}\left[-7.53 + 0.09\left(\frac{M_h}{\text{GeV}} - 125\right) - 0.23\left(\frac{M_t}{\text{GeV}} - 173\right)\right] + \\ & + \frac{g_3^4}{(4\pi)^4}\left[-145.08 - 0.84\left(\frac{M_t}{\text{GeV}} - 173\right)\right]. \end{aligned} \tag{3.104}$$

where the latter term is the well known pure QCD contribution; the second term is the mixed QCD/EW contribution that agrees with [19]; the first term is the pure EW contribution computed for the first time in [16].

3.A Appendix

3.A.1 Integral form

The master integrals can be written in terms of Feynman parameters in a quite easy way. There are no particular point that we should address, the only difficulty arises from a naive calculation of S_0, since part of the UV divergence of the integral can be "transferred" to the Feynman parameter. The complete calculation of S_0 and T_0 is reported in [24]. The one-loop master integrals and the divergent parts of the two-loops master integrals are reported in section (3.1.4), here we report their finite parts.

$$
\begin{aligned}
M_{0,\text{fin}}(p^2,m_j^2) = \quad & \iiint_0^1 dt\ dr\ dl\ \partial_\zeta g(\xi(p^2,m_1^2,m_3^2;r),\zeta,m_5^2,(l+r)p^2;t)|_{\zeta\to\xi(p^2,m_2^2,m_4^2;r)},\\
U_{0,\text{fin}}(p^2,m_j^2) = \quad & -\frac{1}{2}+\iint_0^1 dt\ dl\ (-\ln(\frac{\xi(p^2,m_1^2,m_2^2;t)}{\mu^2})+\frac{1}{2}\ln^2(\frac{\xi(p^2,m_1^2,m_2^2;t)}{\mu^2})\\
& +g(\xi(p^2,m_1^2,m_2^2;l),m_3^2,m_4^2,(1-l)p^2)),\\
S_{0,\text{fin}}(p^2,m_j^2) = \quad & -\frac{13}{8}p^2+\frac{1}{2}p^2\ln(\frac{m_1^2}{\mu^2})+\sum_{j=1}^{3}(\frac{3}{2}m_j^2-2m_j^2\ln(\frac{m_j^2}{\mu^2})+\frac{1}{2}m_j^2\ln^2(\frac{m_j^2}{\mu^2}) =\\
& +\int_0^1 dt\ (-p^2 f(p^2,m_1^2,m_2^2,m_3^2;t)+m_1^2\ g(p^2,m_1^2,m_2^2,m_3^2;t)\\
& +m_2^2\ g(p^2,m_2^2,m_1^2,m_3^2;t)+m_3^2\ g(p^2,m_3^2,m_1^2,m_2^2;t)),\\
T_{0,\text{fin}}(p^2,m_j^2) = \quad & -\frac{1}{2}-\ln(\frac{m_1^2}{\mu^2})+\frac{1}{2}\ln^2(\frac{m_1^2}{\mu^2})+\int_0^1 dt\ g(p^2,m_1^2,m_2^2,m_3^2;t),
\end{aligned}
\tag{3.105}
\tag{3.106}
$$

where $t,\ l,\ r$ are Feynman parameters ($t,\ l,\ r\in[0,1]$), and we defined the following functions:

$$
\begin{aligned}
g(s,x,y,z;t) = \quad & Li_2(\frac{1}{1-y_1(s,x,y,z;t)})+y_1(s,x,y,z;t)\ln(\frac{y_1(s,x,y,z;t)}{y_1(s,x,y,z;t)-1})\\
& +Li_2(\frac{1}{1-y_2(s,x,y,z;t)})+y_2(s,x,y,z;t)\ln(\frac{y_2(s,x,y,z;t)}{y_2(s,x,y,z;t)-1}),\\
f(s,x,y,z;t) = \quad & x\frac{1-\delta(x,y,z;t)}{-2s}-\frac{1}{2}y_1^2(s,x,y,z;t)\ln(\frac{y_1(s,x,y,z;t)}{y_1(s,x,y,z;t)-1})\\
& -\frac{1}{2}y_2^2(s,x,y,z;t)\ln(\frac{y_2(s,x,y,z;t)}{y_2(s,x,y,z;t)-1}),\\
\xi(s,x,y;t) = \quad & xt+y(1-t)-s(1-t)t,\\
\delta(x,y,z;t) = \quad & \frac{yt+z(1-t)}{xt(1-t)},\\
y_{1,2}(s,x,y,z;t) = \quad & \frac{x-s-x\delta(x,y,z;t)}{-2s}\pm x\frac{\sqrt{(1-\frac{s}{x}-\delta(x,y,z;t))^2-4\frac{s}{x}\delta(x,y,z;t)+i4\frac{s}{x}\eta}}{-2s}.
\end{aligned}
\tag{3.107}
$$

3.A.2 Gauge Invariance

All $\overline{\text{MS}}$ parameters have gauge-invariant renormalisation group equations [28] and are gauge invariant, as we now prove.[4] Let us consider a generic $\overline{\text{MS}}$ coupling θ measuring the strength of a gauge invariant term in the Lagrangian and a generic gauge fixing parametrized by ξ (for example the R_ξ gauges).

[4] Gauge invariance of fermion pole masses has been proved in [25–27], here we generalise their proof.

Let us first recall the definition of θ in terms of the bare coupling θ_0,

$$\bar{\mu}^{d-4}\theta_0 = \sum_{k=0}^{\infty} \frac{c_k(\theta,\xi)}{(d-4)^k}, \tag{3.108}$$

where the c_k are defined to be the residues at the divergence $d = 4$. The important point is that $c_0 = \theta$, with no dependence on ξ. Since θ_0 is gauge independent, we have

$$0 = \bar{\mu}^{d-4}\frac{d\theta_0}{d\xi} = \frac{d\theta}{d\xi} + \sum_{k=1}^{\infty} \frac{1}{(d-4)^k}\frac{dc_k(\theta,\xi)}{d\xi}. \tag{3.109}$$

Since this equation is valid for any d, and θ has no poles at $d = 4$ by definition, we obtain $d\theta/d\xi = 0$, that is θ is gauge invariant (as well as all the residues c_k).[5]

[5]Notice that this proof does not apply to the Higgs vev v, because it is not the coefficient of a gauge-invariant term in the Lagrangian.

Bibliography

[1] O. V. Tarasov, Phys. Rev. D **54** (1996) 6479 [hep-th/9606018].

[2] O. V. Tarasov, Nucl. Phys. B 502 (1197) 455 [hep-ph/9703319].

[3] R. Mertig and R. Scharf, Comput. Phys. Commun. 111 (1998) 265 [hep-ph/9801383].

[4] R. Mertig, M. Bohm and A. Denner, Comput. Phys. Commun. 64 (1991) 345.

[5] T. Hahn, Comput. Phys. Commun. 140 (2001) 418 [hep-ph/0012260].

[6] S. P. Martin and D. G. Robertson [hep-ph/0501132].

[7] S. P. Martin, Phys. Rev. D 68 (2003) 075002 [hep-ph/0307101].

[8] G. Passarino and M. J. G. Veltman, Nucl. Phys. B **160** (1979) 151.

[9] V. A. Smirnov, Springer Tracts Mod. Phys. **211** (2004) 1.

[10] U. Nierste, D. Muller and M. Bohm, Z. Phys. C **57** (1993) 605.

[11] H. Kleinert and V. Schulte-Frohlinde "Critical Properties of phi^4-Theories," World Scientific, Singapore (2001).

[12] C. Ford, I. Jack and D. R. T. Jones, Nucl. Phys. B 387 (1992) 373 [Erratum-ibid. B 504 (1997) 551] [arXiv:hep-ph/0111190].

[13] S. P. Martin, Phys. Rev. D **65** (2002) 116003 [hep-ph/0111209].

[14] A. Sirlin and R. Zucchini, Nucl. Phys. B 266 (1986) 389.

[15] G. Degrassi, S. Di Vita, J. Elias-Miro, J. R. Espinosa, G. F. Giudice, G. Isidori and A. Strumia, JHEP 1208 (2012) 098 [arXiv:1205.6497].

[16] D. Buttazzo, G. Degrassi, P. P. Giardino, G. F. Giudice, F. Sala, A. Salvio and A. Strumia, arXiv:1307.3536 [hep-ph].

[17] MuLan1 Collaboration. arXiv:1211.0960.

[18] T. van Ritbergen and R. G. Stuart, Nucl. Phys. B 564 (2000) 343 [arXiv:hep-ph/9904240].

[19] F. Bezrukov, M. Y. Kalmykov, B. A. Kniehl and M. Shaposhnikov, JHEP 1210 (2012) 140 [arXiv:1205.2893].

[20] M. Awramik, M. Czakon, A. Onishchenko and O. Veretin, Phys. Rev. D 68 (2003) 053004 [hep-ph/0209084].

[21] B. A. Kniehl and A. Sirlin, Phys. Rev. D 77 (2008) 116012 [arXiv:0801.0669].

[22] R. Hempfling and B. A. Kniehl, Phys. Rev. D 51 (1995) 1386 [arXiv:hep-ph/9408313].

[23] F. Jegerlehner, M. Y. Kalmykov and B. A. Kniehl, Phys. Lett. B 722 (2013) 123 [arXiv:1212.4319].

[24] A. Ghinculov and J. J. van der Bij, Nucl. Phys. B **436** (1995) 30 [hep-ph/9405418].

[25] D. Atkinson and M. P. Fry, Nucl. Phys. B 156 (1979) 301.

[26] J. C. Breckenridge, M. J. Lavelle and T. G. Steele, Z. Phys. C 65 (1995) 155 [arXiv:hep-th/9407028].

[27] A. S. Kronfeld, Phys. Rev. D 58 (1998) 051501 [arXiv:hep-ph/9805215].

[28] W. E. Caswell and F. Wilczek, Phys. Lett. B 49 (1974) 291. See also T. Muta, "Foundations of quantum chromodynamics", p. 192.

Chapter 4

Large Extra Dimensions

Another interesting search that can be done at LHC is that of large extra dimensions, since large extra dimensions with quantum gravity at the electroweak scale can naturally explain the hierarchy problem. Although we do not know exactly the theory of quantum gravity, it is still possible to obtain predictions from collider experiments, using either effective theories or semi-classical approximations. Hereafter we will see how to build a feasible theory of gravity in extra dimensions and how the validity of the theory can be tested at LHC.

The first section is dedicated to the most important theoretical aspects of the problem. In the second section we will illustrate how we can use the LHC data for testing the Large Extra Dimensions. As example, we use early LHC data at $\sqrt{s} = 7\,\text{TeV}$ and 36 pb^{-1}, showing that even with a very-low statistics we are able to investigate the LED scenario.

4.1 Theory

4.1.1 Overview

Since the pioneering work of Kaluza and Klein, the possible existence of more than four space-time dimensions in our universe has attracted physicists. An important feature of this kind of models is the possibility to explain the hierarchy problem [1], that is the existence of two scale of energy, the electroweak and the Planck scale, that are widely separate, being $\frac{m_{ew}}{M_{Pl}} \sim 10^{-15}$. If the gravity is free to propagate in all the $D = 4 + \delta$ dimensions we can explain this separation simply compactifying the extra dimensions, setting their length conveniently and allowing for quantum gravity at the weak scale. Indeed from the Gauss theorem the potential between two masses m_1 and m_2 at distance r in a D dimensional space is

$$V(r) \sim \frac{m_1\ m_2}{M_D^{\delta+2}} \frac{1}{r^{\delta+1}} \tag{4.1}$$

for $r << R$, where R is the compactification radius of the extra-dimensions, while for $r >> R$ is

$$V(r) \sim \frac{m_1 m_2}{M_D^{\delta+2} R^{\delta}} \frac{1}{r}. \tag{4.2}$$

So our effective 4 dimensional Planck mass M_{Pl} is

$$M_{Pl}^2 = R^{\delta} M_D^{\delta+2} \tag{4.3}$$

and requiring $M_D \sim m_{ew}$, we find the compactification radius has to be

$$R \sim \frac{1}{m_{ew}}(\frac{M_{Pl}}{m_{ew}})^{\frac{2}{\delta}} \sim 10^{\frac{30}{\delta}-17}\left(\frac{\text{TeV}}{m_{ew}}\right)\text{cm}. \tag{4.4}$$

If both gravity and SM fields propagate in the extra dimensions, R must be at least less than 10^{-16} - 10^{-17} cm corresponding to the energy the electroweak theory has been probed, so in ordered to obtain the desired $\frac{m_{ew}}{M_{Pl}} \sim 1$ we need to add a "warping", that is we have to construct our theory in a curved background, as done, for $\delta = 1$, in the well-known Randall-Sundrum model [2].

On the other hand if only gravity can propagate in the extra dimensions, the conditions on the radius are looser[1], but we can still probe these large extra dimensions identifying processes involving gravitons in collider experiments, even without knowledge of the exact model for quantum gravity at the weak scale.

Here we will study the last kind of theory, where the Standard Model fields are bound to live on a four dimensional brane, while gravity is free to propagate in all the extra dimensions.

4.1.2 Kaluza-Klein expansion of the graviton

In this section we will study the equations for a graviton in extra dimensions. For more details see, for example, reference [4]. In a D dimensional space-time a point is described by a set of coordinates

$$z = (x, y), \qquad x = (x_0, \vec{x}), \qquad y = (y_1, \dots, y_\delta), \qquad \delta = D - 4. \tag{4.5}$$

where for convenience we made a distinction between the usual four dimensional space-time coordinates x and the coordinates of the extra dimensions y. We can compactify the extra dimensions through the identification[2]

$$y_j \to y_j + 2\pi R \qquad j = 1, \dots, \delta, \tag{4.6}$$

where R is the compactification radius and demanding for a generic field to be periodic under the (4.6):

$$\phi(x, y_i) = \phi(x, y_i + 2\pi R). \tag{4.7}$$

Now we want to study the Kaluza-Klein excitations of the Graviton. At low energy and small curvature the equations of motion of the effective theory reduce to the Einstein equation in $D = 4+\delta$ dimensions:

$$\mathcal{G}_{AB} \equiv \mathcal{R}_{AB} - \frac{1}{2}g_{AB}\mathcal{R} = -\frac{T_{AB}}{\bar{M}_D^{2+\delta}} \qquad A, B = 1, \dots, D, \tag{4.8}$$

where $\bar{M}_D$ is the reduced D-dimensional Planck mass defined as $\bar{M}_D = (2\pi)^{-\delta/(2+\delta)}M_D$.

Expanding the metric g_{AB} around its Minkowski value η_{AB} [3]

$$g_{AB} = \eta_{AB} + 2\bar{M}_D^{-1-\delta/2}h_{AB}. \tag{4.9}$$

[1] Although from astrophysical bounds also in the case of $\delta = 1, 2, 3$ we need a bit of warping [3]

[2] For simplicity the compactified space is assumed to be a torus

[3] In general the existence of the brane on which Standard Model fields are localized create a non trivial metric background, however is reasonable that if we are probing distances much bigger than $1/M_D$ we can consider the metric essentially flat.

Replacing in equation (4.8) the definition (4.9) and keeping only the first power of h, we found

$$\begin{aligned} \bar{M}_D^{1+\delta/2}\mathcal{G}_{AB} &= \Box h_{AB} - \partial_A\partial^C h_{CB} - \partial_B\partial^C h_{CA} + \partial_A\partial_B h^C_C \\ &- \eta_{AB}\Box h^C_C + \eta_{AB}\partial^C\partial^D h_{CD} = -\bar{M}_D^{-1-\delta/2}T_{AB}, \end{aligned} \tag{4.10}$$

where indices are raised or lowered using the flat-space metric and summation over repeated indices is understood.

If we demand periodicity for the graviton, as in equation (4.7), we found that the field h could be expressed as

$$h_{AB}(z) = \sum_{n_1=-\infty}^{+\infty} \cdots \sum_{n_\delta=-\infty}^{+\infty} \frac{{h^{(n)}}_{AB}(x)}{\sqrt{(2\pi R)^\delta}} e^{i\frac{n^j y_j}{R}}. \tag{4.11}$$

In this way, from a field that lives in a D dimensional world we obtain an infinite sum of Kaluza-Klein modes $h^{(n)}(x)$ that live in the four dimensional world.

Before continuing we have to clarify what happens to the Standard Model fields. As we said in the introduction, we assume the ordinary matter to be confined on the brane, and therefore, in the limit of weak gravitational field, their energy-momentum tensor is

$$T_{AB}(z) = \eta^\mu_A\eta^\nu_B T_{\mu\nu}(x)\delta(y) \qquad \mu,\nu = 0,\ldots,3. \tag{4.12}$$

Equation (4.12) means that the Kaluza-Klein modes of the energy-momentum tensor are independent of n, at least in the low-energy region. This is crucial for the analysis we are going to do, since it implies that all the $h^{(n)}(x)$ fields are coupled to ordinary matter by means of a universal coupling, allowing us to make definite predictions on their cross-sections.

We replace the expressions (4.11) and (4.12) into the equations of motion. After multiplying both sides of eq. (4.10) by $e^{-i\frac{n'}{R}\cdot y}$ and integrating over the extra-dimensional coordinates, we obtain the following set of equations:

$$\begin{aligned} {\mathcal{G}^{(n)}}_{\mu\nu}(x) \equiv\ & (\Box + \hat{n}^2){h^{(n)}}_{\mu\nu} - \left[\partial_\mu\partial_\lambda {h^{(n)}}^\lambda_\nu + i\hat{n}_j\partial_\mu {h^{(n)}}^j_\nu + (\mu\leftrightarrow\nu)\right] + \\ & \left[\partial_\mu\partial_\nu - \eta_{\mu\nu}(\Box+\hat{n}^2)\right]\left[{h^{(n)}}^\lambda_\lambda + {h^{(n)}}^j_j\right] + \\ & \eta_{\mu\nu}\left[\partial^\lambda\partial^\sigma {h^{(n)}}_{\lambda\sigma} + 2i\hat{n}_j\partial^\lambda {h^{(n)}}^j_\lambda - \hat{n}^j\hat{n}^k {h^{(n)}}_{jk}\right] = -\frac{T_{\mu\nu}}{\bar{M}_P}, \end{aligned} \tag{4.13}$$

$$\begin{aligned} {\mathcal{G}^{(n)}}_{\mu j}(x) \equiv\ & (\Box + \hat{n}^2){h^{(n)}}_{\mu j} - \partial_\mu\partial_\nu {h^{(n)}}^\nu_j - i\hat{n}_k\partial_\mu {h^{(n)}}^k_j - i\hat{n}_j\partial_\nu {h^{(n)}}^\nu_\mu \\ & + \hat{n}_j\hat{n}_k {h^{(n)}}^k_\mu + i\hat{n}_j\partial_\mu\left[{h^{(n)}}^\nu_\nu + {h^{(n)}}^k_k\right] = 0, \end{aligned} \tag{4.14}$$

$$\begin{aligned} {\mathcal{G}^{(n)}}_{jk}(x) \equiv\ & (\Box + \hat{n}^2){h^{(n)}}_{jk} - \left[i\hat{n}_j\partial_\mu {h^{(n)}}^\mu_k - \hat{n}_j\hat{n}_\ell {h^{(n)}}^\ell_k + (j\leftrightarrow k)\right] \\ & - \left[\hat{n}_j\hat{n}_k + \eta_{jk}(\Box+\hat{n}^2)\right]\left[{h^{(n)}}^\mu_\mu + {h^{(n)}}^\ell_\ell\right] + \\ & \eta_{jk}\left[\partial^\mu\partial^\nu {h^{(n)}}_{\mu\nu} + 2i\hat{n}_\ell\partial^\mu {h^{(n)}}^\ell_\mu - \hat{n}^\ell\hat{n}^m {h^{(n)}}_{\ell m}\right] = 0. \end{aligned} \tag{4.15}$$

Where the D'Alambertian operator acts on the four-dimensional space $\Box = \partial^\mu\partial_\mu$, $\hat{n} \equiv n/R$, $\hat{n}^2 \equiv$

$-\hat{n}^j\hat{n}_j = \sum_{j=1}^{\delta} |\hat{n}_j|^2$ and we have defined

$$\bar{M}_P \equiv \sqrt{V_\delta}\bar{M}_D^{1+\delta/2} = (2\pi R)^{\delta/2}\bar{M}_D^{1+\delta/2} \tag{4.16}$$

as the ordinary reduced Planck mass, $\bar{M}_P = \mp/\sqrt{8\pi} = 2.4 \times 10^{18}$ GeV.

If we define new dynamical variables, we can rewrite the equations of motion as

$$\left(\Box + \hat{n}^2\right) \quad G^{(n)}{}_{\mu\nu} = \frac{1}{\bar{M}_P}\left[-T_{\mu\nu} + \left(\frac{\partial_\mu\partial_\nu}{\hat{n}^2} + \eta_{\mu\nu}\right)\frac{T^\lambda_\lambda}{3}\right] \tag{4.17}$$

$$\left(\Box + \hat{n}^2\right) \quad V^{(n)}{}_{\mu j} = 0 \tag{4.18}$$

$$\left(\Box + \hat{n}^2\right) \quad S^{(n)}{}_{jk} = 0 \tag{4.19}$$

$$\left(\Box + \hat{n}^2\right) \quad H^{(\vec{n})} = \frac{\kappa}{3\bar{M}_P}T^\mu_\mu, \tag{4.20}$$

where κ is defined as

$$\kappa = \sqrt{\frac{3(\delta-1)}{\delta+2}}. \tag{4.21}$$

We also find the constraints

$$\partial^\mu G^{(n)}{}_{\mu\nu} = \frac{\partial_\nu T^\mu_\mu}{3\hat{n}^2\bar{M}_P} \tag{4.22}$$

$$G^{(n)\mu}{}_{\mu} = \frac{T^\mu_\mu}{3\hat{n}^2\bar{M}_P} \tag{4.23}$$

$$\partial^\mu V^{(n)}{}_{\mu j} = 0. \tag{4.24}$$

The free propagation of $G^{(n)}{}_{\mu\nu}$ is given by eqs. (4.22) and (4.17) in the limit $T_{\mu\nu} = 0$,

$$\left(\Box + \hat{n}^2\right) G^{(n)}{}_{\mu\nu} = 0 \tag{4.25}$$

$$\partial^\mu G^{(n)}{}_{\mu\nu} = 0 \tag{4.26}$$

$$G^{(n)\mu}{}_{\mu} = 0. \tag{4.27}$$

These equations describes the propagation of a massive spin-two particle, the n-th Kaluza-Klein excitation of the graviton. Indeed counting the degrees of freedom, we see that out of the 10 contained in the symmetric tensor $G^{(n)}{}_{\mu\nu}$, 5 are eliminated by the equations (4.26) and (4.27), thus leaving only 5 propagating modes.

The fields $V^{(n)}{}_{\mu j}$ and $S^{(n)}{}_{jk}$ describe $\delta - 1$ spin-one massive particles and $(\delta^2 - \delta - 2)/2$ massive real scalars respectively . Neither of them is coupled to the energy-momentum tensor, so they will not play any role in our collider experiments.

Finally, there is the scalar $H^{(\vec{n})}$ which is coupled only to the trace of the energy-momentum tensor, see eq. (4.20). The scalar $H^{(\vec{n})}$ can only couple to ordinary particles at tree level proportionally to their masses. These couplings give effective interactions at best of order M_Z^2/M_D^2.

We conclude this section writing down the graviton Lagrangian. We start from the D-dimensional graviton Lagrangian corresponding to the Einstein equation (4.10),

$$\mathcal{L} = -\frac{1}{2}h^{AB}\Box h_{AB} + \frac{1}{2}h^A_A\Box h^B_B - h^{AB}\partial_A\partial_B h^C_C + h^{AB}\partial_A\partial_C h^C_B - \frac{1}{\bar{M}_D^{1+\delta/2}}h^{AB}T_{AB}, \tag{4.28}$$

that is, it in terms of the fields $G^{(n)}$, $V^{(n)}$, $S^{(n)}$ and $H^{(\vec{n})}$,

$$\begin{aligned}\mathcal{L} \;=\; & \sum_{\text{all } \vec{n}} -\frac{1}{2}G^{(-\vec{n})\mu\nu}(\Box+m^2)G^{(\vec{n})}{}_{\mu\nu} + \frac{1}{2}G^{(-\vec{n})\mu}{}_{\mu}(\Box+m^2)G^{(\vec{n})\nu}{}_{\nu} - G^{(-\vec{n})\mu\nu}\partial_\mu\partial_\nu G^{(\vec{n})\lambda}{}_{\lambda} \\ & + G^{(-\vec{n})\mu\nu}\partial_\mu\partial_\lambda G^{(\vec{n})\lambda}{}_{\nu} - \frac{1}{4}\left|\partial_\mu V^{(\vec{n})}{}_{\nu j} - \partial_\nu V^{(\vec{n})}{}_{\mu j}\right|^2 + \frac{m^2}{2}V^{(-\vec{n})\mu j}V^{(\vec{n})}{}_{\mu j} \\ & - \frac{1}{2}S^{(-\vec{n})jk}(\Box+m^2)S^{(\vec{n})}{}_{jk} - \frac{1}{2}H^{(-\vec{n})}(\Box+m^2)H^{(\vec{n})} \\ & - \frac{1}{\bar{M}_P}\left[G^{(\vec{n})\mu\nu} - \frac{\kappa}{3}\eta^{\mu\nu}H^{(\vec{n})}\right]T_{\mu\nu}.\end{aligned} \tag{4.29}$$

Here $m^2 \equiv \hat{n}^2$ is the Kaluza-Klein graviton squared mass and κ is that defined in equation (4.21).

Feynman rules involving gravitons, and changes in the cross sections significant for collider physics, can be obtained from (4.29) and can be found for example in reference [5].

4.2 Analysis

In this section we will give some details on possible studies that can be done at LHC in order to test Large Extra Dimensions.

4.2.1 Experimental signatures

Let us see now what kind of LHC signal can be interpreted in terms of D-dimensional gravity.

1. *Missing p_T from emission of massive gravitons* constituting the Kaluza-Klein tower. This signal is within control of the low-energy effective theory as long as the graviton energy is less than an ultraviolet cutoff Λ_{eff}, which characterizes the onset of the new quantum-gravity theory. Validity of the perturbative expansion sets an upper bound on the cutoff

$$\Lambda_{\text{eff}} < [\Gamma(2+\delta/2)]^{\frac{1}{2+\delta}}(4\pi)^{\frac{4+\delta}{4+2\delta}}M_D. \tag{4.30}$$

   This upper bound is saturated only when gravitons become fully strongly-interacting before entering the new regime of the underlying theory, and thus Λ_{eff} could actually turn out to be much smaller. This does not mean that missing p_T signals above Λ_{eff} vanish, but simply that they are not calculable without knowledge of the full theory.

2. *Tree-level exchange of gravitons* (fig. 4.1a) generating the effective dimension-8 operator $\mathcal{T}$ [4–6]

$$L_{\text{int}} = c_{\mathcal{T}} \times \mathcal{T} = \frac{8}{M_T^4} \times \frac{1}{2}\left(T_{\mu\nu}T^{\mu\nu} - \frac{T^\mu_\mu T^\nu_\nu}{\delta+2}\right), \tag{4.31}$$

   where $T_{\mu\nu}$ is the SM energy-momentum tensor. In most cases the dominant contribution to this operator comes from the ultraviolet end of the graviton spectrum. Therefore the parameter M_T cannot be computed without knowledge of the underlying quantum-gravity theory.

3. *Virtual graviton exchanges at one-loop level* (fig. 4.1b) can become more important than tree-level effects because they induce dimension-6 effective operators, as opposed to the dimension-8 $\mathcal{T}$ operator [7]. For pure graviton virtual intermediate states, a unique dimension-6 operator is generated

$$L = c_\Upsilon \times \Upsilon, \qquad \Upsilon = \frac{1}{2}\left(\sum_f \bar{f}\gamma_\mu\gamma_5 f\right)\left(\sum_f \bar{f}\gamma^\mu\gamma_5 f\right), \tag{4.32}$$

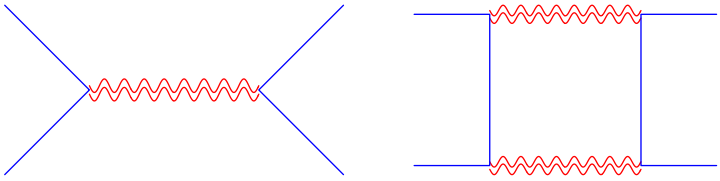

Figure 4.1: *Fig. 4.1*a*: Tree-level graviton exchange generating the dimension-8 operator* $\mathcal{T}$*. Fig. 4.1*b*: One-loop graviton exchange generating the dimension-6 operator* Υ*.*

where f is any SM quark or lepton. As in the case of tree-level graviton exchange, the coefficient c_Υ is fully sensitive to the ultraviolet completion of the theory and can be related to the fundamental parameters M_D and δ only by specifying a cutoff procedure.

4. *Dijet events at large invariant mass and large rapidity separation.* In this kinematic regime, gravitational scattering can be reliably computed in the eikonal approximation [8]. This is because scattering processes at center-of-mass energy larger than M_D (the so-called transplanckian region) are governed by classical dynamics and any quantum-gravity effect is subdominant.

5. *Black holes.* Black-hole formation and decay is expected to occur in the transplanckian region when the impact parameter becomes smaller than the corresponding Schwarzschild radius [9]. Therefore it supplants gravitational scattering, in the limit of small rapidity separation. While transplanckian gravitational scattering can be perturbatively calculated, black-hole formation occurs in the regime in which gravitational interactions are strong.

Furthermore brane fluctuations (massless 'branons') give rise to the same effect 1 (as in $\delta = 6$) and 2 (as in $\delta = 4$) [10]. Our main goal is to show how the operator in equation (4.31) can put stringent bounds on the extra dimensions. So we concentrate our studies on these signals.

In order to do that we study the effect of a single virtual-graviton exchange at tree-level in scattering processes[4]. The scattering amplitude in momentum space of the graviton-mediated process cam be found from the Feynman rules, derived from (4.29),

$$\mathcal{A} = \mathcal{S}(s)\ \mathcal{T} \tag{4.33}$$

$$\mathcal{S}(s) \equiv \frac{1}{\bar{M}_P^2} \sum_n \frac{1}{s - m^2} \tag{4.34}$$

$$\mathcal{T} \equiv T_{\mu\nu} T^{\mu\nu} - \frac{1}{\delta + 2} T^\mu_\mu T^\nu_\nu . \tag{4.35}$$

Here $T_{\mu\nu}$ is the energy-momentum tensor. The two terms in eq. (4.35) correspond to the exchange of the graviton ${G^{(n)}}_{\mu\nu}$ and the scalar $H^{(\vec{n})}$.

In eq. (4.34) $\sum_n$ represents the sum over all Kaluza-Klein modes, which has to be performed at the amplitude level. Since the operator $\mathcal{T}$ does not depend on the Kaluza-Klein index, we can perform the sum $\sum_n$ without specifying the particular physical scattering process under consideration.

As will be discussed below, if the typical energy resolution of the experiment is broader than the mass separation between two KK states, the sum can be approximated as an integral over the extra-dimensional momentum q of the graviton. Such integral is UV divergent for $\delta > 1$ extra dimensions.

[4]For simplicity we consider the case of pure s-channel exchange, but the discussion of the t- and u-channel exchange is completely analogous.

So we regularize the integral by including only KK excitations with mass $m = |q|$ below an arbitrary cut-off Λ, which parametrizes the onset of the unknown quantum-gravity physics. A small (large) ratio Λ/M_D effectively means that quantum gravity is weakly (strongly) coupled [7]. The use of the cutoff allows for a comparison of the experimental limits on the operator(4.31) with the searches for real graviton emission in missing p_T events. Cutting off the integral, we find

$$\mathcal{S}(s) = \frac{1}{M_D^{2+\delta}} \int_{|q|<\Lambda} \frac{d^\delta q}{s - q^2 + i\varepsilon} = \frac{\pi^{\delta/2}\,\Lambda^{\delta-2}}{\Gamma(\delta/2)\,M_D^{2+\delta}} F_\delta(\frac{s}{\Lambda^2}) \tag{4.36}$$

where Γ is the Euler function and F_δ is recursively defined as

$$F_{\delta+2}(x) = xF_\delta(x) - \frac{2}{\delta} \tag{4.37}$$

and

$$F_1(x) = \frac{2}{\sqrt{x}} \operatorname{arctanh}\frac{1}{\sqrt{x}}, \qquad F_2(x) = -\log\left(1 - \frac{1}{x}\right). \tag{4.38}$$

For $\delta > 2$ the integral is dominated by the heaviest graviton with mass $m \approx \Lambda$ and thus, for $s \ll \Lambda^2$, the function $\mathcal{S}$ can be treated as a constant with no momentum dependence and the scattering amplitude can be approximated by the effective operator $\mathcal{T}$ of eq.(4.31) with a coefficient which is usually defined as [6]

$$\mathcal{S}(s \ll \Lambda^2) = \begin{cases} \dfrac{\pi^{\delta/2}}{(1-\delta/2)\Gamma(\delta/2)}\,\dfrac{\Lambda^{\delta-2}}{M_D^{\delta+2}} \equiv \dfrac{8}{M_{\mathcal{T}}^4} & \text{for } \delta > 2 \\ \dfrac{\pi}{M_D^4} \ln\dfrac{s}{\Lambda^2} & \text{for } \delta = 2 \\ \dfrac{-i\pi}{M_D^3\sqrt{s}} & \text{for } \delta = 1 \end{cases} \tag{4.39}$$

However, in view of the high dimensionality of the operator, the dominant LHC bound comes from the highest energy events, and it is appropriate to retain the full amplitude, including the dependence on the cut-off Λ.

We would like now to comment on the validity of approximating the sum over virtual gravitons with an integral.

$\delta = 1$

As we said the gravity at macroscopic scales and astrophysical considerations constrain the cases $\delta =$ 1, 2, and 3. The corresponding fundamental mass M_D can lie around the weak scale only if the theory is modified in the infrared. This can be achieved by introducing a warping factor [2] with a small mass parameter μ (of a few MeV) which lifts the lightest KK mode of the graviton (and characterizes the KK graviton mass splitting, since $m_n \simeq \pi n\mu$ for $n \gg 1$), without modifying the UV behavior of the theory and its collider predictions [3].

Let us first consider the case $\delta = 1$, in which the KK summation can be explicitly performed with the result [11]

$$\mathcal{S}(s) = \frac{1}{\Lambda_\pi^2} \sum_n \frac{1}{s - m_n^2 + i m_n \Gamma_G(m_n)} = -\frac{\pi}{M_5^3\sqrt{s}} K \tag{4.40}$$

$$K = \frac{\sin 2A + i \sinh 2\epsilon}{2(\cos^2 A + \sinh^2 \epsilon)} \qquad A = \pi\left(\frac{\sqrt{s}}{\Delta m} + \frac{1}{4}\right) \qquad \epsilon = \left.\frac{\pi\Gamma_G}{2\Delta m}\right|_{m=\sqrt{s}}. \tag{4.41}$$

Here Λ_π is the interaction scale of individual gravitons, related to the fundamental mass of the 5-dimensional theory M_5 by [3]

$$\Lambda_\pi^2 = \frac{{M_5}^3}{2\pi\mu}. \tag{4.42}$$

The mass splitting between KK gravitons Δm and the decay width of the n-th KK graviton $\Gamma_G(m_n)$ are given by

$$\Delta m = \pi\mu \qquad \Gamma_G(m_n) = \frac{c\, m_n^3}{\pi\Lambda_\pi^2}, \tag{4.43}$$

where $c = 1/80,\ 1/320$, and $1/960$ for graviton decays into a massless vector, Weyl fermion, and conformally-coupled real scalar, respectively [5]. Consequently, we find $c = 283/960$ after summing over all SM particles. The parameter ϵ in eq.(4.41), which measures the relative separation of the individual graviton resonances ($\epsilon \ll 1$ means well separated resonances, $\epsilon \gtrsim 1$ means overlapping resonances), is given by

$$\epsilon = c\left(\frac{\sqrt{s}}{M_5}\right)^3. \tag{4.44}$$

Therefore ϵ remains finite in the limit $\mu \to 0$, which corresponds to sending the compactification volume to infinity ($M_{\rm Pl} \to \infty$).

The expression of $\mathcal{S}$ in eq.(4.40) is a rapidly oscillating function. However, we are interested in the case in which the energy spread of the initial and final states is broader than the mass separation μ. It is then convenient to average eq.(4.40) within one oscillation period, obtaining the smoothly varying function [3]

$$\langle\mathcal{S}\rangle = -\frac{i\pi}{M_5^3\sqrt{s}}. \tag{4.45}$$

We can now take an alternative approach and work directly in the continuum, by replacing the discrete KK summation with an integral

$$\mathcal{S}(s) = \frac{1}{\Lambda_\pi^2}\int\frac{dm}{\pi\mu}\,\frac{1}{s - m^2 + im\Gamma_G(m)} \overset{\Gamma_G\to 0}{\simeq} -\frac{i\pi}{M_5^3\sqrt{s}}. \tag{4.46}$$

Therefore, the procedure of integrating in the continuum, eq.(4.46), gives exactly the same result as the averaged summation in eq.(4.45). This shows that, as long as the energy resolution is broader than the mass separation, it is perfectly adequate to treat virtual gravitons as a continuum.

Let us now consider the modulus square of the expression in eq.(4.40), averaged over an oscillation period

$$\langle|\mathcal{S}|^2\rangle = \frac{\pi^2}{M_5^6 s}\left(1 + \frac{4}{e^{4\epsilon} - 1}\right) \overset{\epsilon\to 0}{\simeq} \frac{1}{\epsilon}\left(\frac{\pi}{M_5^3\sqrt{s}}\right)^2. \tag{4.47}$$

While for $\epsilon > 1$ we find $\langle|\mathcal{S}|^2\rangle \simeq |\langle\mathcal{S}\rangle|^2$, in the relevant case of small ϵ we obtain that eq.(4.47) leads to an enhancement of a factor $1/\epsilon$. Note that the enhanced term in eq.(4.47) has a lower order in powers of graviton coupling constants than expected for a scattering process, because it corresponds to the production of real gravitons.

The same result can be obtained also by calculating $|\mathcal{S}|^2$ in the continuum. If we are interested in the real production of well-separated narrow resonances, we can neglect interference effects. Then the calculation in the continuum, for $\epsilon < 1$, gives

$$|\mathcal{S}|^2 = \frac{1}{\Lambda_\pi^4}\int\frac{dm}{\pi\mu}\,\frac{1}{(s - m^2)^2 + m^2\Gamma_G^2} \overset{\Gamma_G\to 0}{\simeq} \frac{1}{\epsilon}\left(\frac{\pi}{M_5^3\sqrt{s}}\right)^2. \tag{4.48}$$

The result of the calculation in the continuum agrees with the discrete summation in eq.(4.47), when initial and final particle states are spread in energy more than the KK mass separation.

As mentioned above, the Feynman diagram in fig. 4.1a includes two effects: a) $2 \to 2$ scattering processes mediated by virtual gravitons, and b) $2 \to 1 \to 2$ production of one graviton KK resonance with mass equal to $\sqrt{s}$ that eventually decays into SM particles. The enhancement in eq.(4.47) is the contribution from process b). In the $\delta = 1$ scenario we are considering, the graviton decays well inside the detector, such that process b) must be included and there are no missing-energy signals (a point missed in previous works on the topic).

On the contrary, in the $\delta > 1$ scenarios considered in the next section, KK gravitons typically decay far away from the detectors, such that process b) does not contribute to $2 \to 2$ scatterings observed at LHC.

$\delta > 1$

The previous result can be generalized to $\delta > 1$. The amplitude smoothed over scattering wave packets broader than the mass splitting between KK gravitons is obtained by replacing the discrete summation with an integral

$$\mathcal{S}(s) = \frac{1}{M_{\rm Pl}^2} \sum_i \frac{1}{s - m_i^2 + i m_i \Gamma_G(m_i)} \to \frac{2\pi^{\delta/2}}{\Gamma(\delta/2) M_D^{2+\delta}} \int_0^\Lambda dm \, \frac{m^{\delta-1}}{s - m^2 + i m \Gamma_G(m)}, \tag{4.49}$$

where $M_{\rm Pl}$ is the reduced Planck mass. Writing the graviton propagator in the narrow-width approximation, we obtain an expression for $\langle \mathcal{S} \rangle$ that is identical to eq.(4.36).

For generic δ, the graviton width is $\Gamma_G(m) = c\, m^3/\pi M_{\rm Pl}^2$ and the mass difference is

$$\Delta m = \frac{\Gamma(\delta/2) M_D^{2+\delta}}{2\pi^{\delta/2} M_{\rm Pl}^2 m^{\delta-1}}. \tag{4.50}$$

Here we are considering the case in which the KK graviton spectrum is not distorted in the infrared ($\mu = 0$). Analogously to the $\delta = 1$ case, we can define

$$\epsilon \equiv \left. \frac{\pi \Gamma_G}{2\Delta m} \right|_{m=\sqrt{s}} = \frac{\pi^{\delta/2} c}{\Gamma(\delta/2)} \left(\frac{\sqrt{s}}{M_D} \right)^{2+\delta}. \tag{4.51}$$

Note that $\epsilon < 1$ as long as the low-energy effective theory can be trusted ($\sqrt{s} < M_D$), showing that the graviton resonances are narrow and well separated. Using the narrow-width approximation we find that the leading contribution is

$$\langle |\mathcal{S}(s)|^2 \rangle = \frac{(\mathrm{Im}\, \mathcal{S})^2}{\epsilon}. \tag{4.52}$$

As before, this term has to be interpreted as the production of a graviton with mass $\sqrt{s}$. Since the graviton decays well beyond the detector, this term contributes to "missing energy" and not to the signal we are considering and should be subtracted from the final result. Effectively, the rate of interest is obtained by taking the modulus square of eq.(4.36). The situation can be different in intermediate scenarios with $\mu > 0$ and shorter graviton life-time; a life-time comparable to the detector size would lead to $2 \to 2$ signals with displaced-vertex.

Experiment	Process	+	−
LEP [12]	$e^+e^- \to \gamma\gamma$	0.93 TeV	1.01 TeV
LEP [13]	$e^+e^- \to e^+e^-$	1.18 TeV	1.17 TeV
H1 [14]	e^+p and e^-p	0.74 TeV	0.71 TeV
ZEUS [15]	e^+p and e^-p	0.72 TeV	0.73 TeV
CDF [16]	$p\bar{p} \to e^+e^-, \gamma\gamma$	0.99 TeV	0.96 TeV
DØ [16]	$p\bar{p} \to e^+e^-, \gamma\gamma$	1.28 TeV	1.14 TeV
DØ [17]	$p\bar{p} \to jj$	1.48 TeV	1.48 TeV
CMS at 7 TeV with 40/pb [18]	$pp \to \mu^-\mu^+$	1.6 TeV	1.6 TeV
CMS at 7 TeV with 36/pb [27]	$pp \to \gamma\gamma$	1.74 TeV	1.71 TeV
ATLAS at 7 TeV with 3.1/pb	$pp \to jj$	2.2 TeV	2.1 TeV
ATLAS at 7 TeV with 36/pb	$pp \to jj$	4.2 TeV	3.2 TeV
CMS at 7 TeV with 36/pb	$pp \to jj$	4.2 TeV	3.4 TeV

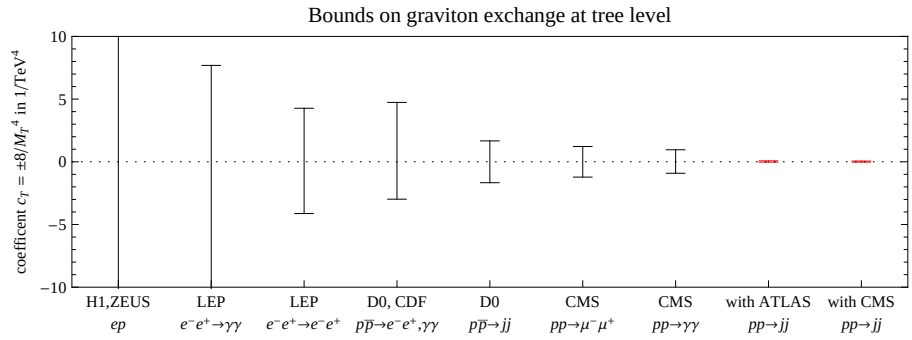

Table 4.1: **Tree-level graviton exchange**: *95% CL limits on the coefficient M_T (known as Hewett normalization [6]) of the dimension-8 operator $\mathcal{T}$ of eq.(4.31) for positive and negative interference. The last three limits are derived in [23]*

Experiment	Process	+	−
LEP combined [20]	$e^+e^- \to e^+e^-$	11.3	11.5
LEP combined [20]	$e^+e^- \to \mu^+\mu^-$	16.4	12.7
LEP combined [20]	$e^+e^- \to \ell^+\ell^-$	17.2	15.1
LEP combined [20]	$e^+e^- \to b\bar{b}$	15.3	11.5
H1 [14]	e^+p and e^-p	2.5	3.9
ZEUS [15]	e^+p and e^-p	4.6	5.3
DØ [21]	$p\bar{p} \to e^+e^-$	4.7	5.5
CDF [21]	$p\bar{p} \to \ell^+\ell^-$	4.5	5.6
CCFR [22]	νN scattering	3.7	5.9
DØ [21]	$p\bar{p} \to jj$	3.2	3.1
ATLAS at 7 TeV with 3.1/pb	$pp \to jj$	5.3	4.2
CMS at 7 TeV with 36/pb	$pp \to jj$	11	8.1
combined		22.4	15.7

Table 4.2: **Loop-level graviton exchange**: *95% CL limits on the coefficient $|c_\Upsilon/4\pi|^{-1/2}$ (in* TeV*) of the dimension-6 operator Υ of eq.(4.32) for positive and negative values of c_Υ.*

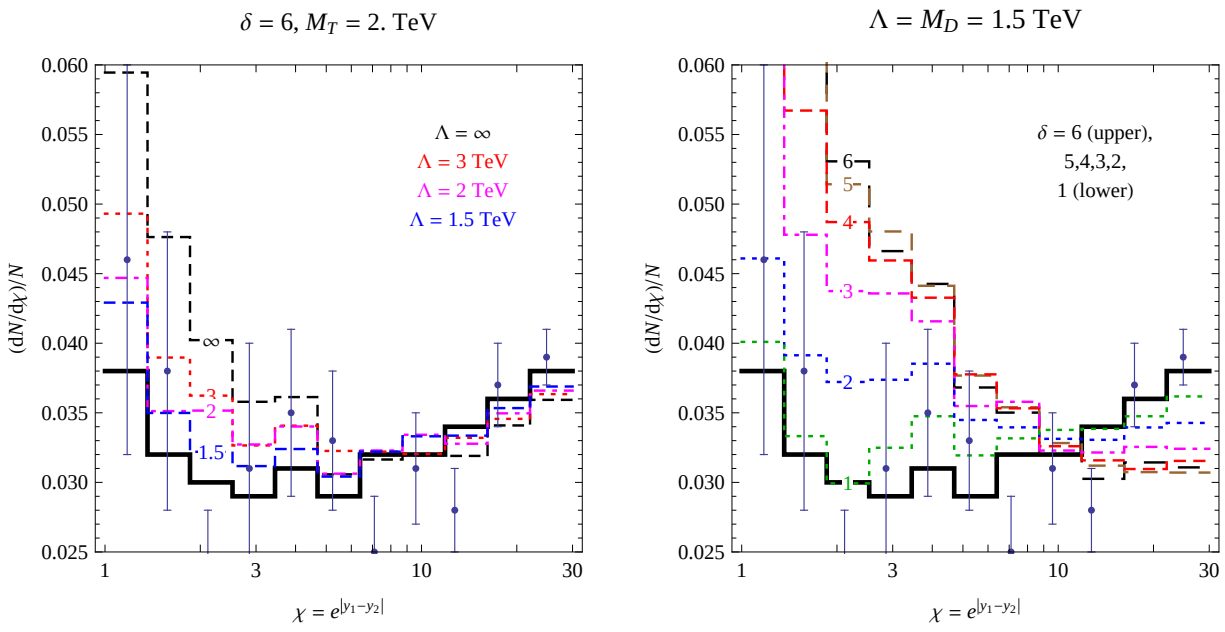

Figure 4.2: *Left: $pp \to jj$ angular distribution for fixed $\delta = 6$, $M_T = 2\,\text{TeV}$, $M_{jj} > 1.2\,\text{TeV}$ and different values of Λ (as indicated) and consequently of M_D. The effective-operator $\mathcal{T}$ is formally reproduced in the limit $\Lambda \to \infty$. Right: dependence on the number δ of extra dimensions at fixed $M_D = \Lambda = 1.5\,\text{TeV}$. The data are from ATLAS [24].*

4.2.2 Fit to the graviton-exchange effective operator

As an example of application of our studies, we compare the first LHC data at $\sqrt{s} = 7\,\text{TeV}$ and 36 pb^{-1} to the new physics described by eq.s(4.31) and(4.32). Since the δ-dependent double trace term in $\mathcal{T}$ is irrelevant for collisions of particles with masses much smaller than the LHC energy, our subsequent analysis applies to any number of extra dimensions (larger than 2).

The tree-level exchange of virtual gravitons described by the Lagrangian of eq. (4.31) mediates the processes

$$pp \to \ell^+\ell^-, \qquad pp \to \gamma\gamma, \qquad pp \to jj\,. \tag{4.53}$$

The experimental collaborations concentrated their sensitivity studies on the di-lepton and di-photon final states. However the corresponding cross sections are significantly lower than the $pp \to jj$ cross section, and this is the main factor that determines the observability of these signals even at the initial LHC stage. Indeed requiring final states with invariant mass greater than 1 TeV, jets, leptons and photons with $\eta < 2.5$, and additionally requiring $|\eta_1 - \eta_2| < 1.2$ for the jets, we find for the data we are considering in our example

$$\sigma = \left(\frac{2\,\text{TeV}}{M_T}\right)^8 \times \begin{cases} 12.5\,\text{pb} & \text{for } pp \to jj \\ 10.4\,\text{fb} & \text{for } pp \to \mu^+\mu^- \\ 21.3\,\text{fb} & \text{for } pp \to \gamma\gamma \end{cases} . \tag{4.54}$$

This large difference in cross sections is due partly to trivial flavor and color factors, and partly to the fact that the processes are mediated by the operator of dimension 8 in eq. (4.31), which gives larger rates for the channels with more energetic initial states. In particular $pp \to jj$ benefits from the high energy of the initial partons uu in the t-channel process.

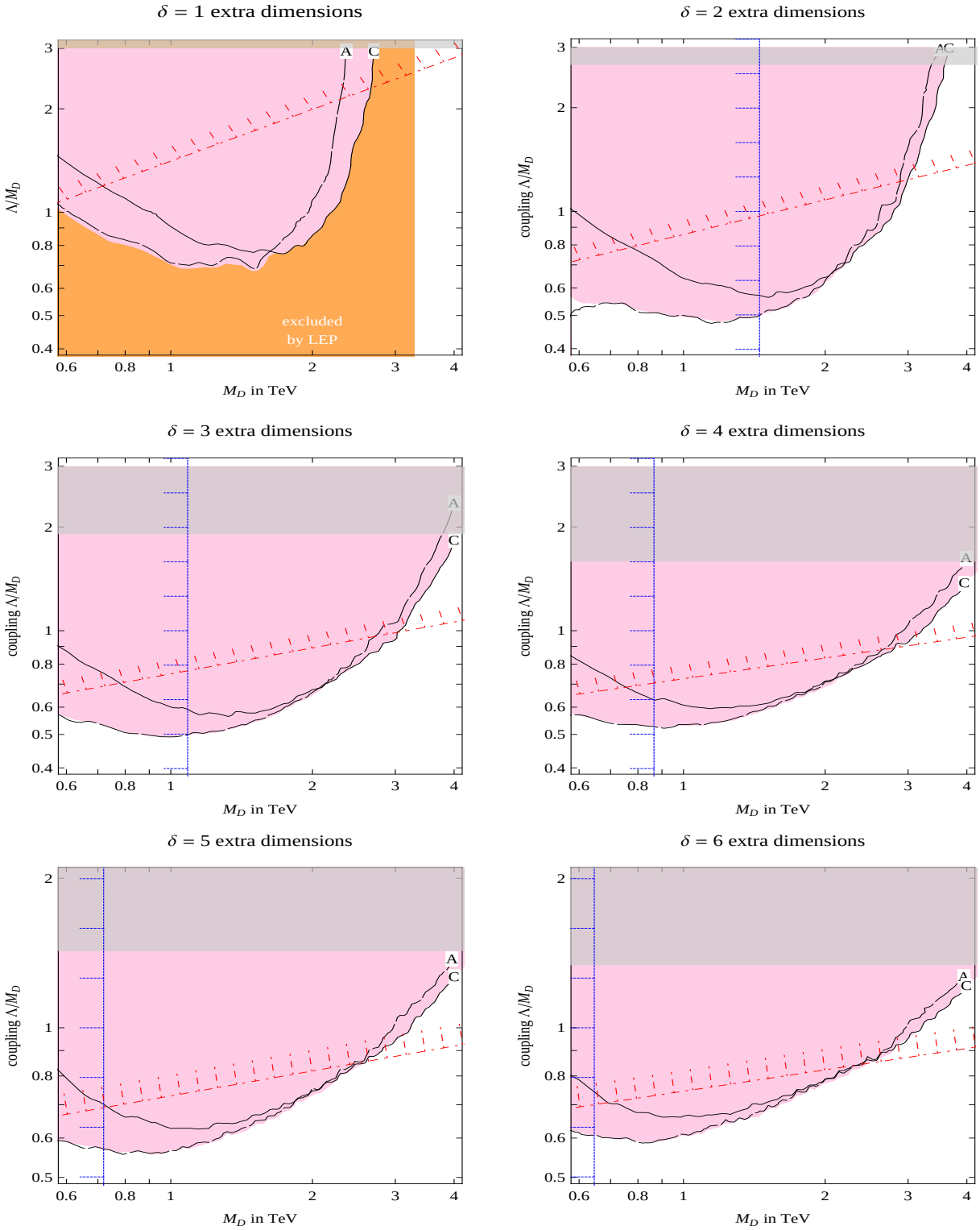

Figure 4.3: *The shaded area is the bound from virtual graviton exchange at CMS (continuous line denoted as 'C', data after* 36/pb*), ATLAS (long-dashed line denoted as 'A', data after* 36/pb*). Vertical blue line: bound from graviton emission (as summarized in table 1 of [7]). Red line: Naive Dimensional Analysis estimate of LEP bound from loop graviton exchange. Upper shading: NDA estimate of the non-perturbative region.*

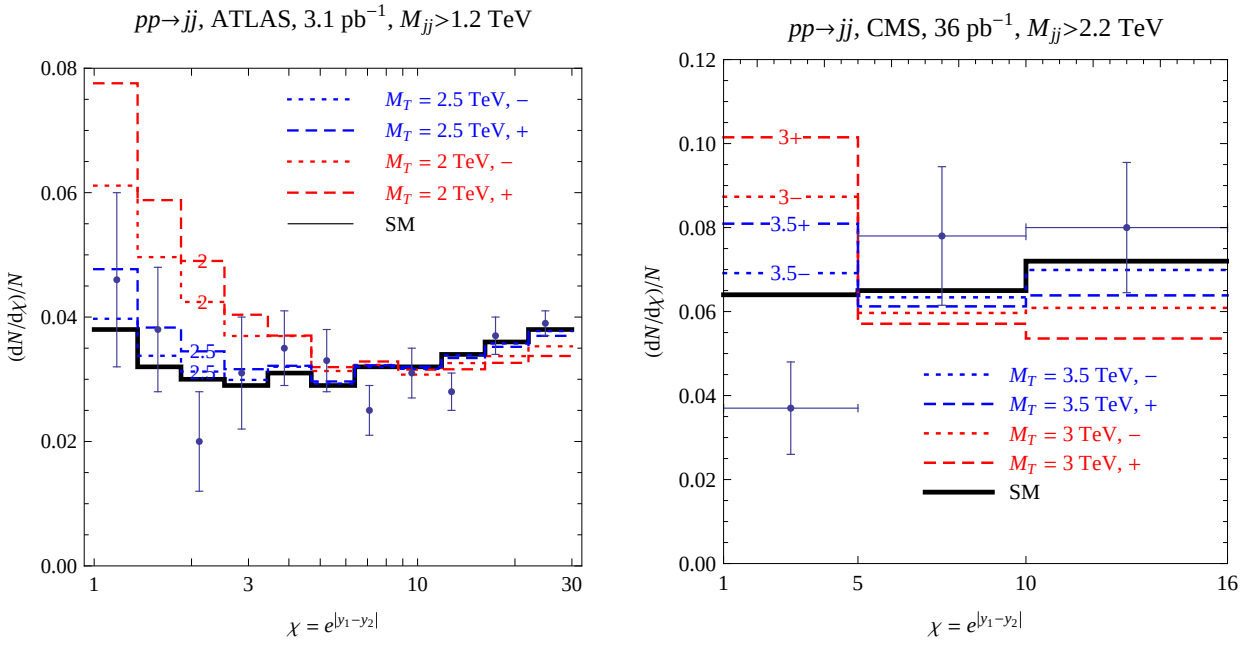

Figure 4.4: *Left (right): $pp \to jj$ angular distribution at ATLAS with $M_{jj} > 1.2\,\text{TeV}$ (at CMS with $M_{jj} > 2.2\,\text{TeV}$) binned as a function of the angular distance χ. The experimental data (crosses) are compared to the SM prediction (black histogram) and to the expectation including virtual graviton effects at tree level.*

In the following we shall show that, from the angular distribution of the jets, even with only 3.1 pb^{-1} of integrated luminosity it was possible to obtain the dominant limit on the operator $\mathcal{T}$.

We study the effect of graviton-mediated amplitudes in the differential and in the total cross section, including interference effects between the SM and the new contributions. Both the total and the differential cross section are affected by NLO effects. However this sensitivity to higher order effects can be reduced by choosing a suitable kinematical quantity and restricting the analysis to certain kinematical regions.

In the data we took in considerations the ATLAS [24] and CMS [19,25] collaborations have searched for the effect of contact interactions in the angular distribution of dijet events. Both collaborations have studied the centrality ratio distribution, and ATLAS also released the normalized distribution in several ranges of invariant mass of the jets on the variable

$$\chi \equiv \exp|y_1 - y_2|\,,$$

where $y_{1,2}$ are the two jet rapidities. Due to the dominance of Coulomb-like scattering in the SM, these distributions are expected to be almost flat in the case of QCD, which helps to reduce the impact of smearing effects. Contact interactions, especially those in eq. (4.31) being mediated by a spin-2 particle, have a different angular distribution with respect to QCD and result in a deviation from a flat distribution.

Data for the χ distribution from ATLAS are reported in fig. 4.4a together with the SM expectation at next-to-leading order [24]. Fig. 4.4a shows also the effect of the graviton operator $\mathcal{T}$ for $M_T = 2$ and 2.5 TeV for both positive or negative interference with the SM.

The prediction of the effect of the operator $\mathcal{T}$ has been obtained simulating the effect of this

operator at the partonic level with MadGraph [26] and CTEQ6L parton distribution functions. We checked that showering and detector effects do not alter significantly the prediction. In particular we checked that with the uncertainties on the data the limit on the contact interaction studied by ATLAS [24] is reproduced at the partonic level within 20%.

We compare data with the theoretical expectation and we compute the 95% CL bound on the coefficient of the $\mathcal{T}$ operator by imposing

$$\chi^2 = \sum_i^{\text{bins}} \frac{(t_i(c_\mathcal{T}) - \mu_i)^2}{\sigma_{i\ \text{stat}}^2 + \sigma_{\text{syst}}^2} < \chi^2_{\text{min}} + 3.84\,, \tag{4.55}$$

where μ_i are the experimental central values, $\sigma_{i\ \text{stat}}$ the statistical errors, $\sigma_{\text{syst}} \approx 0.003$ estimates the systematic uncertainties (we ignore possible correlations between different bins) which are presently subdominant and $t_i(c_\mathcal{T})$ are the theoretical predictions, computed for some values of $c_\mathcal{T}$ and fitted in each bin as a quadratic function of $c_\mathcal{T} = 8/M_T^4$. We find the bound $M_T > 2.1\,\text{TeV}$ reported in table 4.1. This significantly exceeds all previous bounds.

CMS $pp \to jj$ data after 36 pb^{-1} [19] are here plotted in fig. 4.4b. We can reliably estimate the resulting bound, $M_T > 3.4\,\text{TeV}$, as reported in table 4.1. This is comparable to the sensitivity, 3.2 TeV, despite the apparent mild statistical fluctuation in the first bin. From ATLAS $pp \to jj$ data after 36 pb^{-1} [29] we estimate $M_T > 3.2\,\text{TeV}$.

We can compare the sensitivity of the dijet channel to those of the $pp \to \ell^+\ell^-$ and $pp \to \gamma\gamma$ channels considered by the experimental collaborations. CMS [27] found $M_T > 1.8\,\text{TeV}$ from $pp \to \gamma\gamma$ after 36/pb of integrated luminosity. Ref. [27] reported a 95% C.L. sensitivity in the $\gamma\gamma$ channel to $M_T \simeq 3\,\text{TeV}$ for more than 150 pb^{-1} at 10 TeV center of mass energy and [28] claims a sensitivity of the leptonic channel to $M_T \simeq 3\,\text{TeV}$ with 100 pb^{-1} of 14 TeV data. The proposed measurements essentially consist in counting events with large invariant mass, as in eq.(4.54). The $pp \to jj$ signal already reached the same sensitivity with a center of mass energy of 7 TeV and 36 pb^{-1} of integrated luminosity.

Finally, we computed the bound on the dimension-6 operator Υ of eq.(4.32) generated by graviton exchange at loop level. The result is shown in table 4.2 together the other existing bounds. With the published data we find a bound from dijets at LHC that is comparable to the bound from Tevatron and strongly subdominant with respect to the bound from LEP. With 36 pb^{-1} of integrated luminosity we get a bound subdominant with respect to LEP, although significantly larger that existing limits from Tevatron.

4.2.3 Fit to the full graviton-exchange amplitude

Formulæ for the cross sections from tree-level graviton effects in any number of extra dimensions can be found in the appendix of ref. [3]. We implement them in Pythia8 [30] and verify that in the effective-operator approximation ($\mathcal{S} = 8/M_T^4$) the various distributions reproduce the ones previously obtained with MadGraph and that hadronization and jet reconstruction negligibly affect the observables we consider.

We can now compare the data with the full graviton-exchange amplitude, computed in terms of the cut-off Λ, defined to be the maximal KK graviton mass. Even for $\delta = 1$ the correct treatment of $|\mathcal{S}|^2$ in the s-channel is numerically irrelevant here. Indeed we consider the $pp \to jj$ signal which is dominated by the uu initial state which has no s-channel.

Fig. 4.2a shows how the theoretical prediction changes with the cut-off Λ keeping fixed the coefficient of the effective operator $\mathcal{T}$ to be $M_T = 2\,\text{TeV}$, around the present bound: the full amplitude

must be used unless $\Lambda \gg M_D$. Fig. 4.2b shows how the theoretical prediction changes with δ keeping fixed M_D and Λ.

The results of our fit are shown in fig. 4.3, as functions of M_D and of the ratio Λ/M_D. The 95% CL bound is defined as $\chi^2 < \chi^2_{\rm SM}+3.84$. As previously discussed, the ratio Λ/M_D effectively parameterizes the unknown strength of the full quantum-gravity theory. The gray area at larger Λ/M_D covers the region estimated to be non-perturbative according to naive dimensional analysis [7].

The shaded area covers the region excluded by the angular distribution at $M_{jj} > 1.2\,\text{TeV}$.

For comparison, the other two lines show:

- the combined Tevatron-LEP bound from graviton emission (vertical blue lines; computed ignoring the dependence on Λ).
- the LEP bound on loop graviton exchange (red line), estimated according to naive dimensional analysis.

For $\delta = 1$ the LHC bound $M_D \gtrsim 1.5\,\text{TeV}$ remains subdominant with respect to the bound from $e^- e^+ \to f\bar{f}$ scatterings at LEP2, that we estimate to be $M_D \gtrsim 3.4\,\text{TeV}$. For $\delta > 1$ already the first ATLAS data at 3.1 pb$^-$1 explore new regions of the parameters space of gravity in extra dimensions. Those at 36 pb$^-$1 provide stronger bounds.

Bibliography

[1] N. Arkani-Hamed, S. Dimopoulos and G. R. Dvali, Phys. Lett. B 429 (1998) 263 [hep-ph/9803315].

[2] L. Randall and R. Sundrum, Phys. Rev. Lett. 83 (1999) 3370 [hep-ph/9905221].

[3] G. F. Giudice, T. Plehn, A. Strumia, Nucl. Phys. B706 (2005) 455 [arXiv:hep-ph/0408320].

[4] G. F. Giudice, R. Rattazzi and J. D. Wells, Nucl. Phys. B 544, 3 (1999) [hep-ph/9811291].

[5] T. Han, J.D. Lykken and R. Zhang, Phys. Rev. D59 (1999) 105006 [arXiv:hep-ph/9811350].

[6] J.L. Hewett, Phys. Rev. Lett. 82 (1999) 4765 [arXiv:hep-ph/9811356].

[7] G. F. Giudice and A. Strumia, Nucl. Phys. B 663 (2003) 377 [hep-ph/0301232].

[8] G. F. Giudice, R. Rattazzi, J. D. Wells, Nucl. Phys. B630 (2002) 293-325 [hep-ph/0112161].

[9] S. B. Giddings, S. D. Thomas, Phys. Rev. D65, 056010 (2002) [hep-ph/0106219]. S. Dimopoulos, G. L. Landsberg, Phys. Rev. Lett. 87, 161602 (2001). [hep-ph/0106295]. See also T. Banks, W. Fischler, hep-th/9906038.

[10] P. Creminelli, A. Strumia, Nucl. Phys. B596 (125) 2001 [arXiv:hep-ph/0007267].

[11] A. V. Kisselev, Eur. Phys. J. C42 (2005) 217-225. [hep-ph/0412376]. A. V. Kisselev, JHEP 0809, 039 (2008). [arXiv:0804.3941].

[12] The LEP-II Diphoton Working Group, LEP2FF/02-02.

[13] ALEPH 2001-019 CONF 2001-016; DELPHI 2001-094 CONF 522; L3 Note 2759; OPAL Physics Note PN471.

[14] H1 Collaboration, ICHEP02, abstract 979.

[15] ZEUS Collaboration, EPS 2001, abstract 602.

[16] G. Landsberg, for the D0 and CDF collaborations, arXiv:hep-ex/0412028.

[17] D0 collaboration, Phys. Rev. Lett. 103 (2009) 191803 [arXiv:0906.4819].

[18] CMS collaboration, http://cdsweb.cern.ch/record/1335097/files/EXO-10-020-pas.pdf.

[19] CMS collaboration, arXiv:1102.2020. See also the talk by G. Landsberg, "Quest for New Physics with the First LHC data at CMS", 24/1/2011.

[20] LEP Working Group LEP2FF/02-03.

[21] J.A. Green, for the CDF and D0 Collaborations, arXiv:hep-ex/0004035.

[22] K.S. McFarland *et al.* [NuTeV Collaboration], arXiv:hep-ex/9806013.

[23] R. Franceschini, G. F. Giudice, P. P. Giardino, P. Lodone and A. Strumia, JHEP 05 (2011) 092 [arXiv:hep-ph/1101.4919] .

[24] ATLAS collaboration, Phys. Lett. B694 (2011) 327 [arXiv:1009.5069].

[25] CMS collaboration, Phys. Rev. Lett. 105 (2010) 262001 [arXiv:1010.0203].

[26] MadGraph: J. Alwall, P. Demin, S. de Visscher, R. Frederix, M. Herquet, F. Maltoni, T. Plehn, D.L. Rainwater, T. Stelzer, JHEP 0709 (2007) 028 [arXiv:0706.2334]. N.D. Christensen et al., arXiv:0906.2474.

[27] CMS collaboration, arXiv:1103.4279. See also: CMS-PAS-EXO-09-004, "Search for Large Extra Dimensions in the Diphoton Final State".

[28] CMS-NOTE-2006-076, "Search for ADD Extra Dimensional Gravity in Dimuon Channel with the CMS Detector".

[29] ATLAS collaboration, arXiv:1103.3864.

[30] Pythia: T. Sjostrand, S. Mrenna, P. Skands, Comput. Phys. Com. 178, 852 (2008) [arXiv:0710.3820].

Conclusions

The LHC physics program has been successful: with $\approx 25/\text{fb}$ of data per experiment the Higgs boson has been discovered and several of its properties determined within $\approx \pm 20\%$ precision.

We are now entering into the era of precision Higgs physics: deviations from the SM due to new physics no longer can dominate the data. This observation allowed us to propose a 'universal' form in which we assume that the new physics is approximated as a first-order perturbation around the Standard Model predictions. We think that this form could be an useful way for the experiments to report their results, allowing theorists to easily test any desired model. While we present our own global combination in 'universal' form in equation (1.10), we stress that only the experimental collaborations can perform a fully precise analysis.

Using this assumption, we investigated many Beyond Standard Model scenarios, such as supersymmetry or composite Higgs. From our analysis we can not exclude any new physics at TeV scale, but we find that the data currently support a standard Higgs.

For this reason, we supposed that the Standard Model was valid up to the Planck scale. Indeed, in spite of the absence of any signal of new physics, the LHC has provided valuable information for theoretical speculations about physics at very short distances. In that respect, one of the most interesting aspect of the measured value of M_h is its near-criticality: it corresponds to the fact that the electro-weak vacuum is in a meta-stable configuration, on the border between stability and instability.

The special coincidence found in the value of M_h warrants a refined calculation of the high-energy extrapolation of λ.

For this purpose, we performed a NNLO calculation of the Standard Model parameters by means of computer algebra; in particular we used the recurrence relations between two-loops integrals implemented in the Mathematica code Tarcer, part of the FeynCalc package. These relations permit to reduce a dimensional regularized two-loops two-points integral in terms of a complete basis of scalar integrals. In this way we were able to compute the necessary one thousand two-points two-loops and two thousands zero-point two-loops diagrams. The renormalization of the constants was done in the OS scheme, then we shifted the poles in order to obtain $\overline{\text{MS}}$ quantities as functions of the measured constants.

We extracted the fundamental SM parameters λ (quartic Higgs coupling), m (Higgs mass term), y_t (top quark Yukawa coupling) from the precisely measured values of the Higgs, top, W and Z masses and from the Fermi constant at full NNLO. However, because of the present experimental uncertainties on the SM parameters (mostly the top quark mass), we cannot conclusively establish the fate of the EW vacuum, although metastability is now preferred at 99.3% CL.

Then we extrapolated all the couplings to large energies using the RGE equations, now known at NNLO order (3 loop). Thus we investigated the significance of the measured value of M_h, in view of its high-energy extrapolation. A first observation is that λ, together with all other SM coupling constants, remains perturbative in the entire energy domain between the Fermi and the Planck scales. This gives an indirect indication that EW-breaking dynamics is probably weakly interacting. Of

course, strongly-interacting dynamics is not excluded, but there is simply no need for introducing it at any intermediate energy scale.

We have also thoroughly studied the condition of near-criticality in terms of the SM parameters at a high scale, which we identified with the Planck mass. This procedure is more appropriate than a study in terms of physical particle masses, since it is more likely that special features are exhibited by high-energy parameters, just like in the case of gauge coupling unification.

We have found that near-criticality is manifest also when we explore the phase diagram as a function of high-energy SM couplings. Moreover, we found evidence for multiple near-critical conditions. Indeed, the measured SM parameters roughly correspond to the minimum values of Higgs quartic coupling $\lambda(M_{\rm Pl})$ and of the top Yukawa coupling $y_t(M_{\rm Pl})$ (at fixed gauge couplings) that allow for the existence of a sufficiently long-lived EW vacuum. Moreover, at fixed top Yukawa coupling, the maximum possible values of the gauge couplings $g(M_{\rm Pl})$ are preferred. Incidentally, we have also obtained an upper bound on the Higgs mass parameter m from the requirement of vacuum stability, although this bound is too weak to be useful in practice.

These peculiar values of the couplings at very-high energies led us to questioning whether this situation is a coincidence or the results of a high energy dynamics. An intriguing possibility is that the point in which lambda cross zero and becomes negative is due to a matching condition with some kind of new physics, for example high-energy supersymmetry. Another possibility is that the current value of the couplings is the result of a multiverse dynamics that "prefer" a near-critical solution.

We conclude with a possible scenario, in which there exist other extra dimensions in which only the gravity can propagate. We propose a way to study these large extra dimensions at LHC. Indeed the amplitude $pp \to jj$ is modified due to the exchange of gravitons. As example, we show that even with a very low statistics our techniques can thoroughly investigate the existence of extra dimensions.